
[All ETDs from UAB](#)

[UAB Theses & Dissertations](#)

2007

Development of a Sdof Model for an Aluminum Arch Subjected to Impulse Loads

David P. Ray
University of Alabama at Birmingham

Follow this and additional works at: <https://digitalcommons.library.uab.edu/etd-collection>

Recommended Citation

Ray, David P., "Development of a Sdof Model for an Aluminum Arch Subjected to Impulse Loads" (2007).
All ETDs from UAB. 6699.
<https://digitalcommons.library.uab.edu/etd-collection/6699>

This content has been accepted for inclusion by an authorized administrator of the UAB Digital Commons, and is provided as a free open access item. All inquiries regarding this item or the UAB Digital Commons should be directed to the [UAB Libraries Office of Scholarly Communication](#).

DEVELOPMENT OF A SDOF MODEL FOR AN ALUMINUM ARCH
SUBJECTED TO IMPULSE LOADS

by

DAVID P. RAY

A THESIS

Submitted to the graduate faculty of The University of Alabama at Birmingham,
in partial fulfillment of the requirements for the degree of
Master of Science in Civil Engineering

BIRMINGHAM, ALABAMA

2007

DEVELOPMENT OF A SDOF MODEL FOR AN ALUMINUM ARCH SUBJECTED TO IMPULSE LOADS

DAVID P. RAY

CIVIL ENGINEERING

ABSTRACT

Quick and accurate prediction of damage to structures from impulse loading resulting from blasts could provide a useful tool in situations where deployment of non-permanent structures for housing of personnel and equipment is required. The ability to predict the required protected area for shelters in relation to the potential threat of blast loads would provide planners and personnel a valuable tool for use in the protection of life and property. Prediction curves can be developed through the testing of each type of structure using multiple charge sizes and standoff distances. However, this approach is inefficient in that it must be performed for each type of desired structure and in addition, only provides a few data points, which must then be extrapolated to encompass the myriad of potential combinations of charge size and standoff distance. A better tool would be an analytical model that is quick and simple to use, can be modified for multiple shelter types and, most importantly, is accurate across multiple shelter types.

This document was prepared to report the results of analysis performed to develop a static resistance definition for an aluminum arch similar to that used in soft-walled shelter frames. The static resistance curve was developed using a NASA STRuctural ANalysis (NASTRAN) Finite Element Model of a single bay of the shelter system. Pressure loads were input to the model as a distributed load over the surface of the structure facing the impulse load within a nonlinear static NASTRAN analysis. The displacement resulting from the analysis was then used to develop the static resistance

function. The resulting resistance function was then used in a single-degree-of-freedom (SDOF) model to predict the displacement of the system when subjected to impulse loads. This displacement was then compared to empirical results obtained from full-scale testing. In addition to the test impulse conditions, additional cases that simulate various charge sizes and standoff distances were input into the SDOF model. These conditions were chosen to simulate points on the pressure-impulse diagram that showed minor damage to the structure and failure of the structure when using the pressure-impulse diagram developed for the shelter through the test program.

Additional analyses of the frame were then performed using LS-DYNA finite element software to predict damage from impulse loading. The same load cases used within the test program and the SDOF model were simulated within LS-DYNA. In addition to reporting the results of the static resistance curve for the arch frame, this document serves to document the correlation between test results, SDOF analysis results, and LS-DYNA analysis results.

TABLE OF CONTENTS

	<i>Page</i>
ABSTRACT.....	ii
LIST OF TABLES.....	vii
LIST OF FIGURES.....	ix
CHAPTER	
1 INTRODUCTION AND BACKGROUND.....	1
1.1 Shelter Description.....	1
1.2 Test Results.....	3
2 FINITE ELEMENT MODELING METHODOLOGY.....	7
2.1 Model Description.....	7
2.2 Model Verification.....	8
2.3 Model Static Analysis.....	10
2.4 NASTRAN Static Analysis Methods.....	10
2.5 LS-DYNA Impulse Analysis Methods.....	11
3 DEVELOPMENT OF STATIC NONLINEAR RESISTANCE FUNCTION.....	12
3.1 Load Distribution.....	12
3.2 Analysis Method.....	20
3.3 Analysis Results.....	21
3.3.1 2400 lb Load Case Results.....	21
3.3.2 4800 lb Load Case Results.....	26
3.3.3 7200 lb Load Case Results.....	31
3.4 Analysis Parametric Study.....	36
3.4.1 2400 lb Load Case Results Simply Supported.....	36
3.5 Static Resistance Function.....	39
3.5.1 Elastic Static Resistance Function.....	39
3.5.2 Plastic Static Resistance Function.....	40
3.5.3 Static Resistance Function Development.....	42

TABLE OF CONTENTS (Continued)

CHAPTER	<i>Page</i>
4	LS-DYNA IMPULSE LOAD SIMULATION RESULTS 43
4.1	81.1 psi-ms Results 45
4.2	55.7 psi-ms Results 46
4.3	30.5 psi-ms Results 48
4.4	94.8 psi-ms Results 50
4.5	76.4 psi-ms Results 52
4.6	55.0 psi-ms Results 54
4.7	32.2 psi-ms Results 56
4.8	111.0 psi-ms Results 58
4.9	24.7 psi-ms Results 60
4.10	116.8 psi-ms Results 62
4.11	33.1 psi-ms Results 64
5	SDOF MODEL VERIFICATION 67
5.1	SDOF Analytical Development 67
5.2	SDOF Model Term Definition and Calculation 72
5.2.1	Applied Force (F_t) 73
5.2.2	Adjusted Time 74
5.2.3	Load Mass Factor (K_{LM}) 74
5.2.4	System Mass (M_t) 74
6	ANALYSIS CHARTS 75
6.1	81.1 psi-ms 76
6.2	55.7 psi-ms 79
6.3	30.5 psi-ms 81
6.4	94.8 psi-ms 83
6.5	76.4 psi-ms 85
6.6	55.0 psi-ms 87
6.7	32.2 psi-ms 89
6.8	111.0 psi-ms 91
6.9	24.7 psi-ms 93
6.10	116.8 psi-ms 95
6.11	33.1 psi-ms 97
7	SUMMARY AND CONCLUSIONS 99
8	REFERENCES 100

TABLE OF CONTENTS (Continued)

CHAPTER	<i>Page</i>
9 LIST OF ACRONYMS	101

LIST OF TABLES

<i>Table</i>	<i>Page</i>
1.2-1 Test Loads	4
1.2-2 Damage Level	4
3.1-1 Load Calculation for NASTRAN 2400 lb Nonlinear Load Application	14
3.1-2 Load Calculation for NASTRAN 4800 lb Nonlinear Load Application	15
3.1-3 Load Calculation for NASTRAN 7200 lb Nonlinear Load Application	16
3.3.1-1 2400 lb Load Case Deflection with no Large Displacements	22
3.3.1-2 2400 lb Load Case Deflection Large Displacements Included	22
3.3.2-1 4800 lb Load Case Deflection with no Large Displacements	26
3.3.2-2 4800 lb Load Case Deflection Large Displacements Included	27
3.3.3-1 7200 lb Load Case Deflection with no Large Displacements	32
3.3.3-2 7200 lb Load Case Deflection Large Displacements Included	32
3.4.1-1 2400 lbs load Case Deflection No Large Displacements Included, Simply Supported Base	37
3.4.1-2 2400 lbs load Case Deflection Large Displacements Included, Simply Supported Base	38
3.5.1-1 Elastic Stiffness Summary	40
3.5.2-1 Initial Plastic Stiffness Summary	41

LIST OF TABLES (Continued)

<i>Table</i>		<i>Page</i>
3.5.2-2	Second Plastic Stiffness Summary.....	41
4.0-1	Model Impulse Analysis Results.....	44
6.0-1	SDOF Input Parameters.....	75
6.0-2	LS-DYNA/SDOF Results Comparison.....	76

LIST OF FIGURES

<i>Figure</i>		<i>Page</i>
1.1-1	Assembled Shelter.....	2
1.1-2	Shelter Interior View.....	3
1.2-1	Large Impulse.....	5
1.2-2	Medium Impulse.....	5
1.2-3	Small Impulse.....	6
2.0-1	FEM Isometric View.....	7
2.2-1	Mode 1 F _{nz} = 5.9 Hz, Effective Mass Participation = 53%.....	9
2.2-2	Mode 2 F _{nx} = 5.9 Hz, Effective Mass Participation = 47%.....	10
3.1-1	2400 lb NASTRAN Model Load Distribution.....	17
3.1-2	2400 lb NASTRAN Model Load Distribution Section View.....	17
3.1-3	4800 lb NASTRAN Model Load Distribution.....	18
3.1-4	4800 lb NASTRAN Model Load Distribution Section View.....	18
3.1-5	7200 lb NASTRAN Model Load Distribution.....	19
3.1-6	7200 lb NASTRAN Model Load Distribution Section View.....	19
3.2-1	Stress versus Strain Diagram.....	21
3.3.1-1	2400 lb Load Case Deflection versus Load Step.....	23
3.3.1-2	2400 lb Load Case Yield Point.....	24
3.3.1-3	2400 lb Load Case Maximum Deflection.....	25

LIST OF FIGURES (Continued)

<i>Figure</i>		<i>Page</i>
3.3.1-4	2400 lb Load Case Maximum Deflection Section View.....	25
3.3.2-1	4800 lb Load Case Deflection versus Load Step.....	28
3.3.2-2	4800 lb Load Case Yield Point.....	29
3.3.2-3	4800 lb Load Case Maximum Deflection.....	30
3.3.2-4	4800 lb Load Case Maximum Deflection Section View.....	30
3.3.3-1	7200 lb Load Case Deflection versus Load Step.....	33
3.3.3-2	7200 lb Load Case Yield Point.....	34
3.3.3-3	7200 lb Load Case Maximum Deflection.....	35
3.3.3-4	7200 lb Load Case Maximum Deflection Section View.....	35
3.4.1-1	2400 lb Load Case Deflection versus Load Step.....	38
3.5.3-1	Static Resistance Function.....	42
4.0-1	Deflection Recovery Node.....	44
4.1-1	Purlin Translation for 81.1 psi-ms.....	45
4.1-2	Arch Deflected Shape for 81.1 psi-ms.....	46
4.1-3	Arch Stress Distribution for 81.1 psi-ms.....	46
4.2-1	Purlin Translation for 55.7 psi-ms.....	47
4.2-2	Arch Deflected Shape for 55.7 psi-ms.....	47
4.2-3	Arch Stress Distribution for 55.7 psi-ms.....	48
4.3-1	Purlin Translation for 30.5 psi-ms.....	49
4.3-2	Arch Deflected Shape for 30.5 psi-ms.....	49

LIST OF FIGURES (Continued)

<i>Figure</i>		<i>Page</i>
4.3-3	Arch Stress Distribution for 30.5 psi-ms.....	50
4.4-1	Purlin Translation for 94.8 psi-ms.....	51
4.4-2	Arch Deflected Shape for 94.8 psi-ms.....	51
4.4-3	Arch Stress Distribution for 94.8 psi-ms.....	52
4.5-1	Purlin Translation for 76.4 psi-ms.....	53
4.5-2	Arch Deflected Shape for 76.4 psi-ms.....	53
4.5-3	Arch Stress Distribution for 76.4 psi-ms.....	54
4.6-1	Purlin Translation for 55.0 psi-ms.....	55
4.6-2	Arch Deflected Shape for 55.0 psi-ms.....	55
4.6-3	Arch Stress Distribution for 55.0 psi-ms.....	56
4.7-1	Purlin Translation for 32.2 psi-ms.....	57
4.7-2	Arch Deflected Shape for 32.2 psi-ms.....	57
4.7-3	Arch Stress Distribution for 32.2 psi-ms.....	58
4.8-1	Purlin Translation for 111.0 psi-ms.....	59
4.8-2	Arch Deflected Shape for 111.0 psi-ms.....	59
4.8-3	Arch Stress Distribution for 111.0 psi-ms.....	60
4.9-1	Purlin Translation for 24.7 psi-ms.....	61
4.9-2	Arch Deflected Shape for 24.7 psi-ms.....	61
4.9-3	Arch Stress Distribution for 24.7 psi-ms.....	62
4.10-1	Purlin Translation for 116.8 psi-ms.....	63

LIST OF FIGURES (Continued)

<i>Figure</i>		<i>Page</i>
4.10-2	Arch Deflected Shape for 116.8 psi-ms.....	63
4.10-3	Arch Stress Distribution for 116.8 psi-ms.....	64
4.11-1	Purlin Translation for 33.1 psi-ms.....	65
4.11-2	Arch Deflected Shape for 33.1 psi-ms.....	65
4.11-3	Arch Stress Distribution for 33.1 psi-ms.....	66
6.1-1	Initial Conditions.....	76
6.1-2	Load Distribution.....	77
6.1-3	Displacement with Reflected Impulse of 81.1 psi-ms.....	77
6.1-4	SDOF/LS-DYNA Model Displacement Comparison.....	78
6.2-1	Initial Conditions.....	79
6.2-2	Load Distribution.....	79
6.2-3	Displacement with Reflected Impulse of 55.7 psi-ms.....	80
6.2-4	SDOF/LS-DYNA Model Displacement Comparison.....	80
6.3-1	Initial Conditions.....	81
6.3-2	Load Distribution.....	81
6.3-3	Displacement with Reflected Impulse of 30.5 psi-ms.....	82
6.3-4	SDOF/LS-DYNA Model Displacement Comparison.....	82
6.4-1	Initial Conditions.....	83
6.4-2	Load Distribution.....	83
6.4-3	Displacement with Reflected Impulse of 94.8 psi-ms.....	84

LIST OF FIGURES (Continued)

<i>Figure</i>		<i>Page</i>
6.4-4	SDOF/LS-DYNA Model Displacement Comparison.....	84
6.5-1	Initial Conditions.....	85
6.5-2	Load Distribution.....	85
6.5-3	Displacement with Reflected Impulse of 76.4 psi-ms.....	86
6.5-4	SDOF/LS-DYNA Model Displacement Comparison.....	86
6.6-1	Initial Conditions.....	87
6.6-2	Load Distribution.....	87
6.6-3	Displacement with Reflected Impulse of 55.0 psi-ms.....	88
6.6-4	SDOF/LS-DYNA Model Displacement Comparison.....	88
6.7-1	Initial Conditions.....	89
6.7-2	Load Distribution.....	89
6.7-3	Displacement with Reflected Impulse of 32.2 psi-ms.....	90
6.7-4	SDOF/LS-DYNA Model Displacement Comparison.....	90
6.8-1	Initial Conditions.....	91
6.8-2	Load Distribution.....	91
6.8-3	Displacement with Reflected Impulse of 111.0 psi-ms.....	92
6.8-4	SDOF/LS-DYNA Model Displacement Comparison.....	92
6.9-1	Initial Conditions.....	93
6.9-2	Load Distribution.....	93
6.9-3	Displacement with Reflected Impulse of 24.7 psi-ms.....	94
6.9-4	SDOF/LS-DYNA Model Displacement Comparison.....	94

LIST OF FIGURES (Continued)

<i>Figure</i>		<i>Page</i>
6.10-1	Initial Conditions.....	95
6.10-2	Load Distribution.....	95
6.10-3	Displacement with Reflected Impulse of 116.8 psi-ms.....	96
6.10-4	SDOF/LS-DYNA Model Displacement Comparison.....	96
6.11-1	Initial Conditions.....	97
6.11-2	Load Distribution.....	97
6.11-3	Displacement with Reflected Impulse of 33.1 psi-ms.....	98
6.11-4	SDOF/LS-DYNA Model Displacement Comparison.....	98

1.0 INTRODUCTION AND BACKGROUND

A variety of temporary shelters comprised of circular metal arch frames are commercially available and are being used for many purposes. When used for military operations, these shelters may be exposed to external attacks by terrorists or others intent on inflicting harm to personnel and equipment located within the shelter. Full-scale tests have been used to understand the response of shelters to external blast loads. However, conducting full-scale explosive tests of these structures is a costly and time-consuming task. Therefore, it would be advantageous to have proven techniques to simulate impulse loading of the shelters without having to perform full-scale tests and also, the ability to correlate analysis results with test results.

1.1 Shelter Description

A typical metal arch frame shelter, the Alaska Small Shelter System (AKSSS), is shown in Figure 1.1-1. It consists of an aluminum frame covered by a vinyl fabric that is attached to an aluminum base. The structure is formed by attaching five arched bays to the aluminum base. These bays are connected by purlins that span the length of the shelter and attach to each bay. In addition, each bay is attached to the aluminum base on either side of the shelter. The ends of the shelter are enclosed by additional vinyl fabric that provides a reinforced entry way and windows. The sides of the shelter contain flaps that may be opened to provide ventilation to the structure. Figures 1.1-2 below provides an interior view of the subject article.



Figure 1.1-1. Assembled Shelter



Figure 1.1-2. Shelter Interior View

1.2 Test Results

Full-scale explosive tests have been conducted on various shelters including the AKSSS. One test series was conducted in a joint operation between the United States Army Engineer Research and Development Center (ERDC) and the Air Force Research Laboratory (AFRL). This test, named Joint Soldier Protection in Contingency Environments (SPICE), provided test data for shelters exposed to three charge sizes, with multiple shelters used for each charge size. Table 1.2-1 provides a summary of the impulse loads involved in these tests, and Table 1.2-2 provides damage level definitions based on displacement measured at the purlins.

Table 1.2-1. Test Loads

Test	Reflected Impulse (psi-ms)
1B	81.1
1B	55.7
1B	30.5
2	94.8
2	76.4
2	55.0
2	32.2
3	251.0
3	206.4
3	175.3
3	152.2
3	109.0
3	109.0

Table 1.2-2. Damage Level

Level	Damage Level (inches)
Minor	Greater than 4 but less than 14
Severe	Greater than 14 but less than 20
Failure	Greater than 20

Figures 1.2-1, 1.2-2, and 1.2-3 below were taken post test and provide a visual reference to the damage each shelter received in relation to its proximity to the charge. Also included in the test report is a graph of the Conventional Weapons Effect (CONWEP) Predicted Reflected Pressure versus CONWEP Predicted Reflected Impulse with damage predictions overlaid on the graph. This graph presents the test results in a user-friendly format that allows the end user to quickly assess potential shelter damage from anticipated impulse load conditions.



Figure 1.2-1. Large Impulse



Figure 1.2-2. Medium Impulse



Figure 1.2-3. Small Impulse

It should be noted that the Predicted Reflected Impulse was reduced by 45% to 70% due to the flexibility of the shelter not presenting an ideal reflecting surface. The test report provides additional insight into this reduction and the test methods behind the reduction rationale.

2.0 FINITE ELEMENT MODELING METHODOLOGY

The frame was modeled using FEMAP as the preprocessor for model generation, model constraint, and model loading. To simplify the model, only one bay of the frame was included in the Finite Element Model (FEM). Figure 2.0-1 provides an isometric view of the single bay FEM.

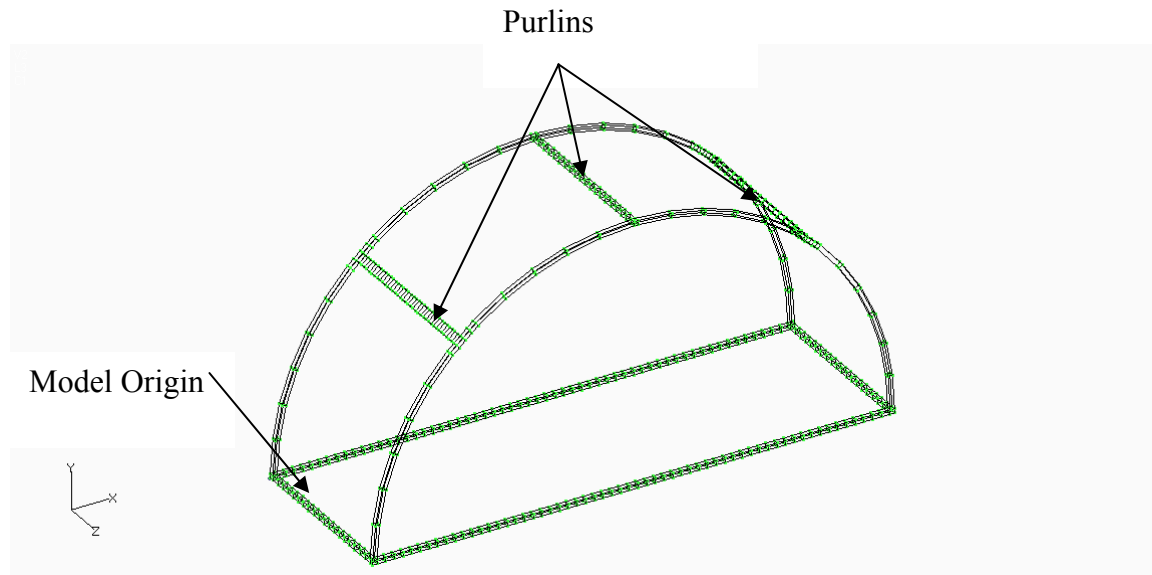


Figure 2.0-1. FEM Isometric View

2.1 Model Description

The frame was modeled using 1132 plate elements to form a four-sided hollow beam element. Each plate element is 2 inches wide by 0.1 inches thick. The plate elements were chosen for the model in anticipation of their use with the LS-DYNA solver which requires plate elements for use with the blast loading card. Figure 2.0-1 above, provides a view of the single bay with the purlins included along the length. The coordinate system for the model was arbitrarily chosen to have the x axis across the arch

with the z axis along the depth of the arch, the y axis out the top of the arch, and the origin as shown in Figure 2.0-1. The FEM includes the weight of the aluminum frame. The mass of the fabric covering the frame was neglected in the model. This assumption was made to simplify the modeling effort so that the attempt to correlate FEM with Single Degree of Freedom (SDOF) modeling could continue in order to determine the feasibility of using a simple SDOF to represent a flexible soft-walled structure. The base restraint was modeled by placing elements on the ground surface and restraining them in all six degrees of freedom. The frame was then attached to these restrained elements. A parametric study was performed for the base restraint to compare the impact of varying restraint conditions on analysis results. This analysis is presented in Section 3.4.

2.2 Model Verification

Before proceeding with the static analysis, the FEM was verified for completeness and accuracy by a series of model verification steps. The first method was to run a rigid-body mode check of the model. The FEMAP model was exported into a NASTRAN data deck, and all external constraints were removed from the model. Once the data deck was appropriately configured for a real eigenvalue analysis, the Nx NASTRAN solver was used to extract the first 10 natural frequencies from the model. Even though only six rigid body modes were expected, 10 natural frequencies were requested to verify that no additional rigid body modes existed. As expected, the analysis returned six zero frequencies. The second verification method was to run a normal modes analysis, once again using Nx NASTRAN, and analyze the mode shapes against the mode shapes intuitively expected from the model. The two predominate

modes returned from the normal modes analysis are shown in Figures 2.2-1 and 2.2-2. These figures also include the mode direction and effective mass participation in the mode as a percentage of total mass as calculated by the NASTRAN model. The final verification was to check the mesh fidelity to ensure that an adequate number of elements were used to accurately represent the behavior of the system. The model fidelity check was performed by constructing a simple beam element model and performing the same analyses that were requested for the shell element model. The results from the beam element model were checked against the results previously obtained from the shell element model and were found to be compatible. Therefore, due to the results from these three verification methods, the model was verified to be correct and of sufficient fidelity to provide accurate results.

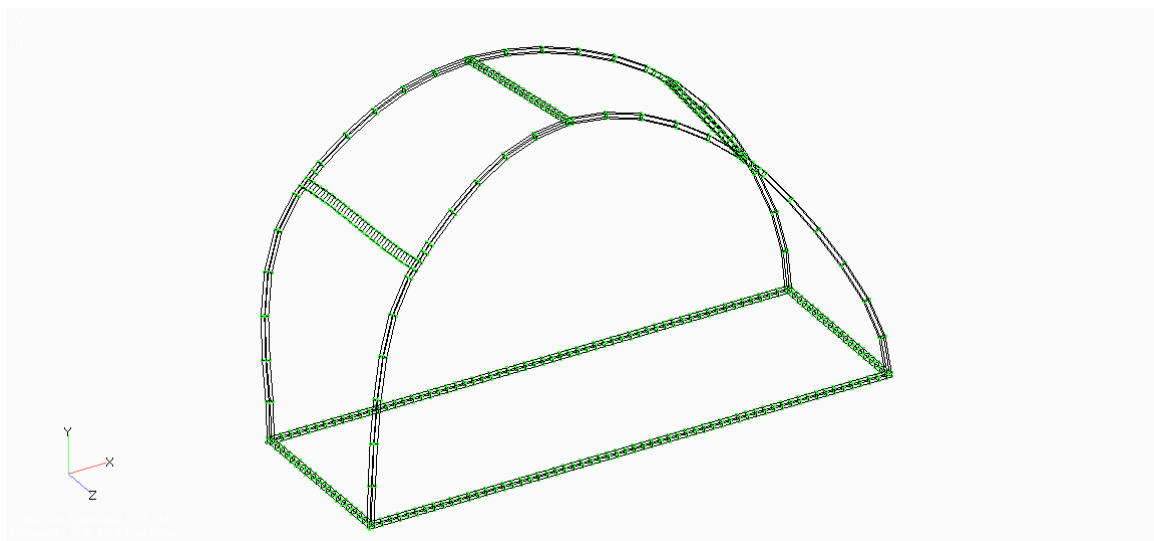


Figure 2.2-1. Mode 1 F_{nz} = 5.9 Hz, Effective Mass Participation = 53%

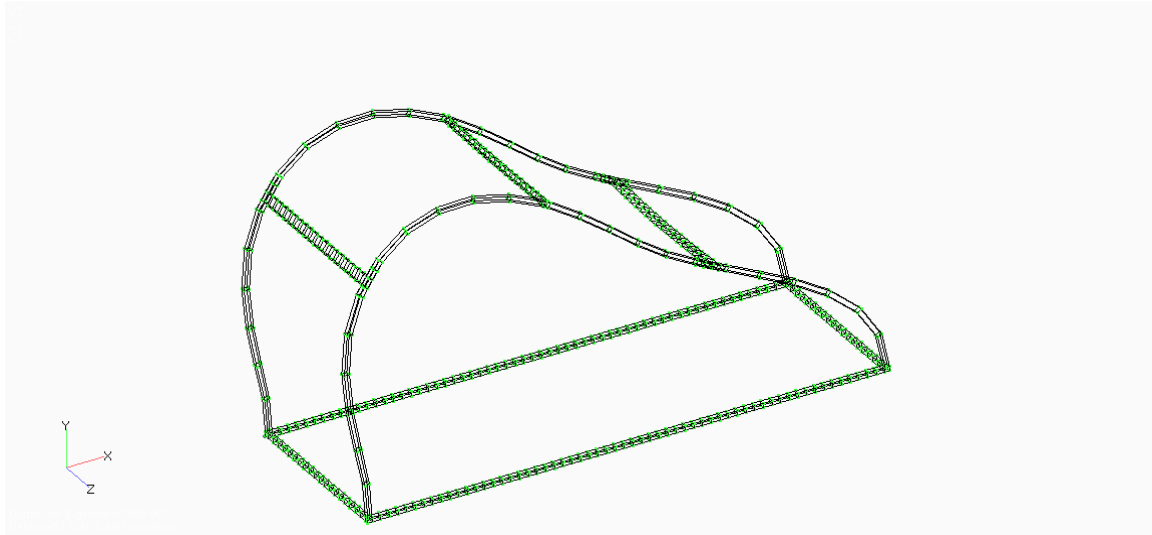


Figure 2.2-2. Mode 2 $F_{nx} = 6.7$ Hz, Effective Mass Participation = 47%

2.3 Model Static Analysis

Test results were obtained by placing the test charge in a position that was normal to the long side of the structure. Therefore, to correlate the test results with the FEM results, all analyses were performed with the load applied parallel to the x axis in the positive x direction. Static analysis consisted of two distinct analyses. The first method was to apply a static load across the face of the shell elements and use NASTRAN to solve for the stresses within the frame. The second method was to export the FEMAP model to LS-DYNA and use the blast load card to simulate the test conditions reported in the test report.

2.4 NASTRAN Static Analysis Methods

Initial NASTRAN runs were made using unit loads applied across the surface of the frame. These solutions, along with additional NASTRAN linear and nonlinear static

solutions will be required to develop the SDOF model for the frame. Additional detail of this analysis is contained in Section 4.0.

2.5 LS-DYNA Impulse Analysis Methods

The FEM was exported into a LS-DYNA format directly from FEMAP. A LOAD_BLAST card was inserted into the LS-DYNA data deck to represent different impulse loading conditions. Multiple impulse loads were analyzed through the model with special attention to impulse loads from the test report. Additional detail of this analysis is contained in Section 4.0.

3.0 DEVELOPMENT OF STATIC NONLINEAR RESISTANCE FUNCTION

In order to develop a single-degree-of-freedom (SDOF) model, it is necessary to understand the deflection behavior of the system. When subjected to an impulse load in the x direction, the arch will have two distinct deflection phases, as it deflects in the elastic mode initially and then transitions to the plastic phase. The development of the static resistance function used the NASTRAN model of the system to perform a geometric and material static nonlinear analysis and establish the static resistance function of the system. Three separate analyses were performed using different load values. The three load values considered were 2400 lbs, 4800 lbs, and 7200 lbs, distributed over the two arches making up the structure. These load values were chosen such that the low end of the load only slightly exceeded the material yield point, while the high end greatly exceeded the material yield point and approached the deflection that was considered severe damage during the test program. The results of these three analyses were compared for consistency of results, especially for the elastic portion of the system. This analysis yielded a stiffness value for both the linear and nonlinear portions of the deflection of the system. The load distribution, analysis methods, and results for this analysis are described in the following sections.

3.1 Load Distribution

The static resistance function development used a load distribution equation to calculate the load that should be applied at multiple discrete points along the frame. This equation recognized that the frame will experience the highest loads on surfaces that are perpendicular to the impulse (base of frame), with the load decreasing to zero on surfaces

that are parallel to the load (top of frame). Therefore, the load used in the NASTRAN analysis was calculated for each point according to the following equation.

$$P = \left[\frac{P_{max}}{\frac{\pi}{2} * x} \right] * \left[\pi * \left(\frac{x}{2} \right) - x \left(\pi + \tan^{-1} \frac{y}{x} \right) \right] \quad 3.1$$

P_{max} = maximum load point

x = x coordinate of load point

y = y coordinate of load point

Equation 3.1 provides an accurate load distribution as long as all points along the curve are equally distributed. If the points are not equally distributed, the load will be higher at the points that are closer together and lower at the points that are spaced farther apart. This load anomaly would occur in the model because the area near the purlin consists of a finer mesh because this is the area where deflection data is desired. The purlin area is broken into five discrete areas that are equivalent to the other eleven areas on each arch. To accommodate this finer mesh and keep the load distribution consistent, the load in the purlin area was averaged and applied over the five nodes in the area. Tables 3.1-1, 3.1-2, and 3.1-3 below provide the load distribution used in the static nonlinear analyses as calculated per equation 3.1. The averaging of the load at points 6-10 can be seen in the column titled “Final Load Distribution.” Also note that the difference between the column titled “P” and the column titled “Final Load Distribution” is not important as long as the load is distributed along the arch according to equation

3.1, because the final total is used in the static resistance calculation, i.e. $K = \text{final load}$ distribution/deflection. The load distributions shown in Tables 3.1-1, 3.1-2, and 3.1-3 were applied to each side of the two arch segments in the model to arrive at the final total load applied to the arch.

Table 3.1-1. Load Calculation for NASTRAN 2400 lb Nonlinear Load Application

Point	Pmax (lbs)	X (in)	Y (in)	P (lbs)	Theta (rad)	Final Load Distribution (lbs)
1	100	0.0	121.0	-0.1	0.00	0.0
2	100	-16.1	117.8	8.6	0.10	8.6
3	100	-31.1	116.8	16.5	0.21	16.5
4	100	-46.2	111.7	24.9	0.31	24.9
5	100	-61.1	104.5	33.7	0.42	33.7
6	100	-74.1	95.6	42.0	0.52	9.2
7	100	-77.1	93.3	43.9	0.63	9.2
8	100	-80.8	90.1	46.5	0.73	9.2
9	100	-82.2	88.8	47.5	0.84	9.2
10	100	-85.9	85.2	50.2	0.94	9.2
11	100	-97.3	71.3	59.7	1.05	59.7
12	100	-103.2	63.1	65.0	1.15	65.0
13	100	-112.9	44.1	76.3	1.26	76.3
14	100	-118.0	29.0	84.7	1.36	84.7
15	100	-119.9	14.4	92.4	1.47	92.4
16	100	-121.0	0.0	100.0	1.57	100.0
Sum				791.9		607.8

Table 3.1-2. Load Calculation for NASTRAN 4800 lb Nonlinear Load Application

Point	Pmax (lbs)	X (in)	Y (in)	P (lbs)	Theta (rad)	Final Load
						Distribution (lbs)
1	200	0.0	121.0	-0.1	0.00	0.0
2	200	-16.1	117.8	17.2	0.10	17.2
3	200	-31.1	116.8	33.0	0.21	33.0
4	200	-46.2	111.7	49.9	0.31	50.0
5	200	-61.1	104.5	67.3	0.42	67.4
6	200	-74.1	95.6	83.9	0.52	18.4
7	200	-77.1	93.3	87.9	0.63	18.4
8	200	-80.8	90.1	93.0	0.73	18.4
9	200	-82.2	88.8	95.1	0.84	18.4
10	200	-85.9	85.2	100.5	0.94	18.4
11	200	-97.3	71.3	119.4	1.05	119.4
12	200	-103.2	63.1	130.1	1.15	130.0
13	200	-112.9	44.1	152.6	1.26	152.6
14	200	-118.0	29.0	169.3	1.36	169.4
15	200	-119.9	14.4	184.8	1.47	184.8
16	200	-121.0	0.0	200.0	1.57	200.0
Sum				1584		1215.8

Table 3.1-3. Load Calculation for NASTRAN 7200 lb Nonlinear Load Application

Point	Pmax (lbs)	X (in)	Y (in)	P (lbs)	Theta (rad)	Final Load
						Distribution (lbs)
1	300	0.0	121.0	-0.2	0.00	0.0
2	300	-16.1	117.8	25.7	0.10	25.8
3	300	-31.1	116.8	49.5	0.21	49.5
4	300	-46.2	111.7	74.8	0.31	74.8
5	300	-61.1	104.5	101.0	0.42	101.0
6	300	-74.1	95.6	125.9	0.52	27.6
7	300	-77.1	93.3	131.8	0.63	27.6
8	300	-80.8	90.1	139.5	0.73	27.6
9	300	-82.2	88.8	142.6	0.84	27.6
10	300	-85.9	85.2	150.7	0.94	27.6
11	300	-97.3	71.3	179.1	1.05	179.1
12	300	-103.2	63.1	195.1	1.15	195.1
13	300	-112.9	44.1	228.8	1.26	228.8
14	300	-118.0	29.0	254.0	1.36	254.0
15	300	-119.9	14.4	277.2	1.47	277.2
16	300	-121.0	0.0	300.0	1.57	300.0
Sum				2375.6		1823.3

The load distribution used in the NASTRAN model is further illustrated in Figures 3.1-1 through 3.1-6 which are taken from the analysis model with the load distribution view turned on. Figures 3.1-1, 3.1-3, and 3.1-5 show the entire model with the load distribution view turned on, while Figures 3.1-2, 3.1-4, and 3.1-6 show a section view of the model so that the actual load numbers are more easily seen. As shown in these figures and discussed previously, the load is applied to nodes comprising each side of the two arches that are used in the model.

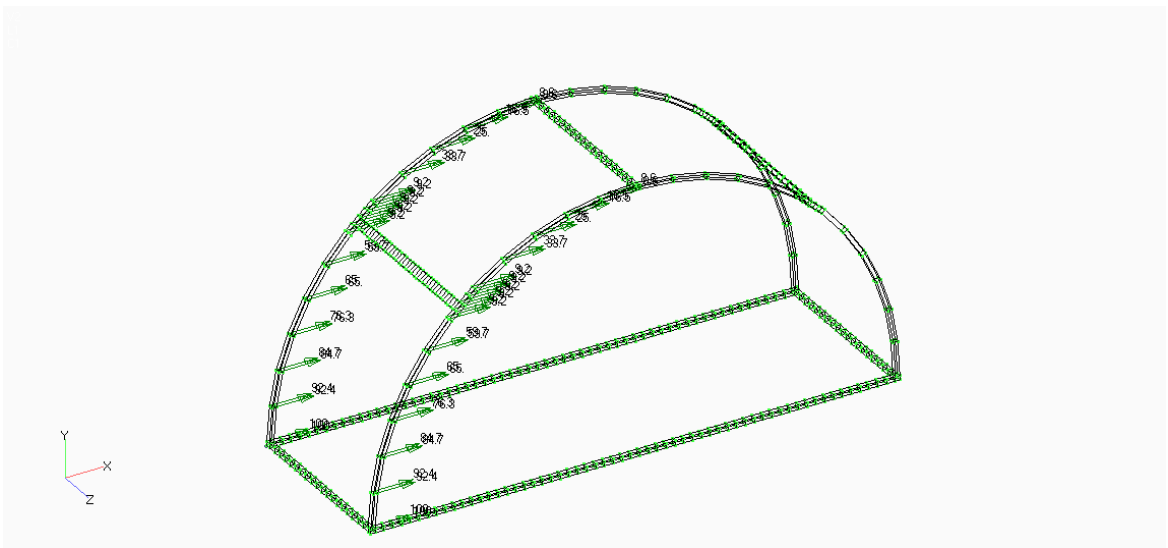


Figure 3.1-1. 2400 lb NASTRAN Model Load Distribution

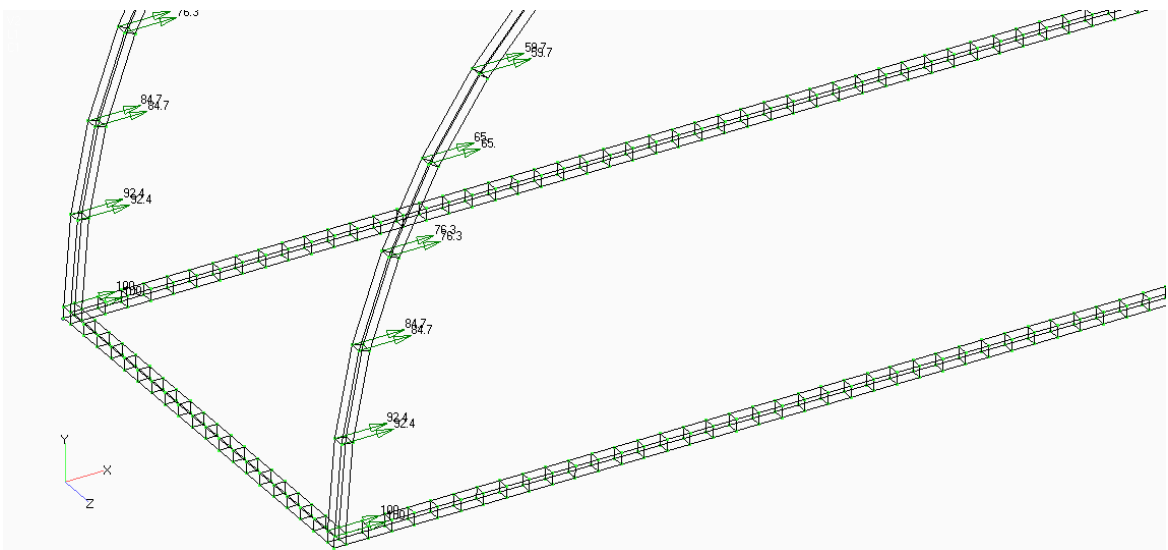


Figure 3.1-2. 2400 lb NASTRAN Model Load Distribution Section View

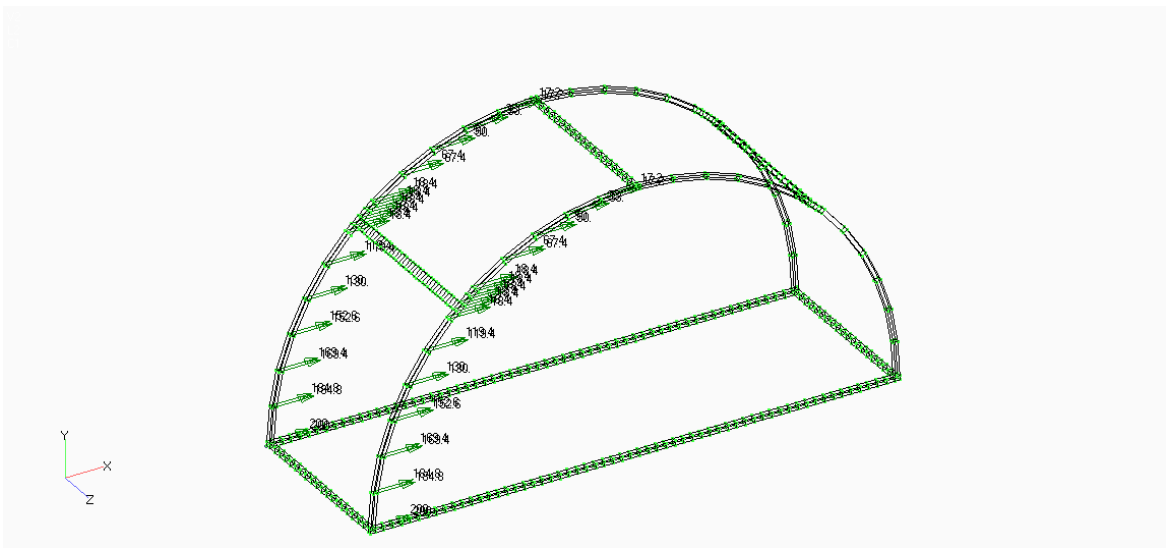


Figure 3.1-3. 4800 lb NASTRAN Model Load Distribution

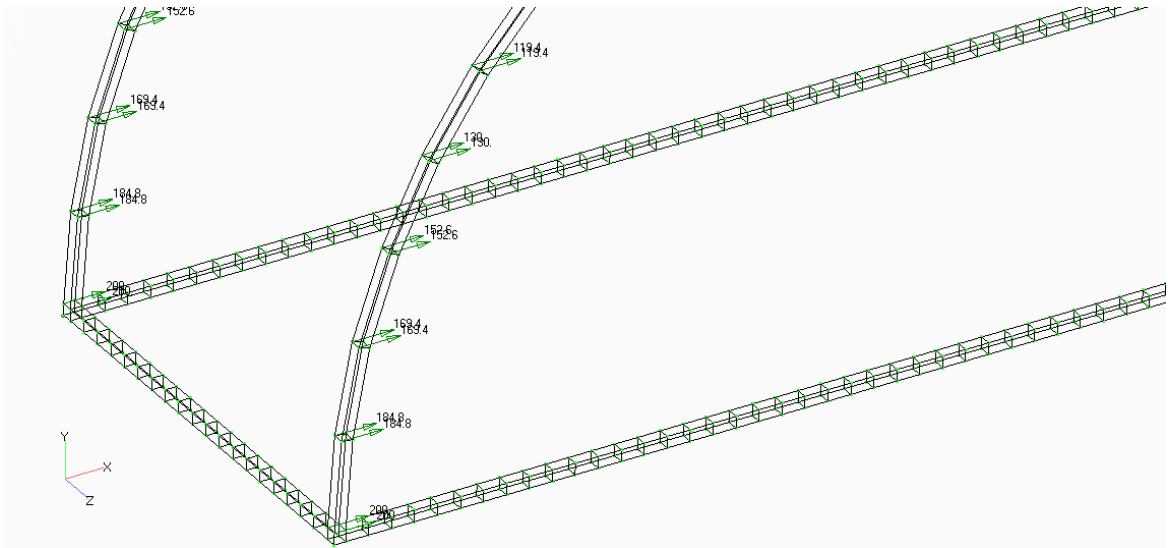


Figure 3.1-4. 4800 lb NASTRAN Model Load Distribution Section View

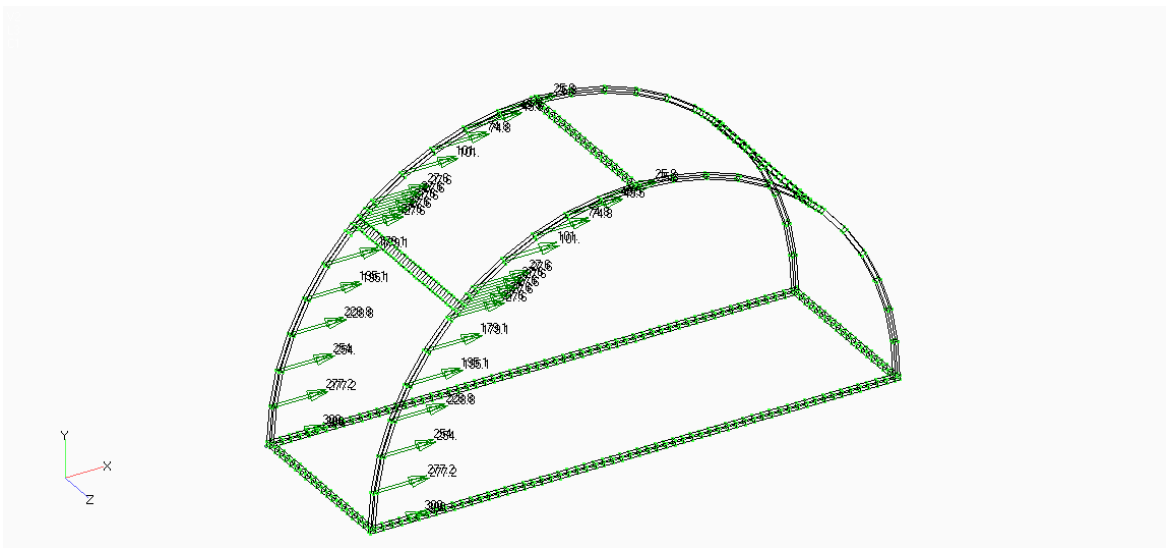


Figure 3.1-5. 7200 lb NASTRAN Model Load Distribution

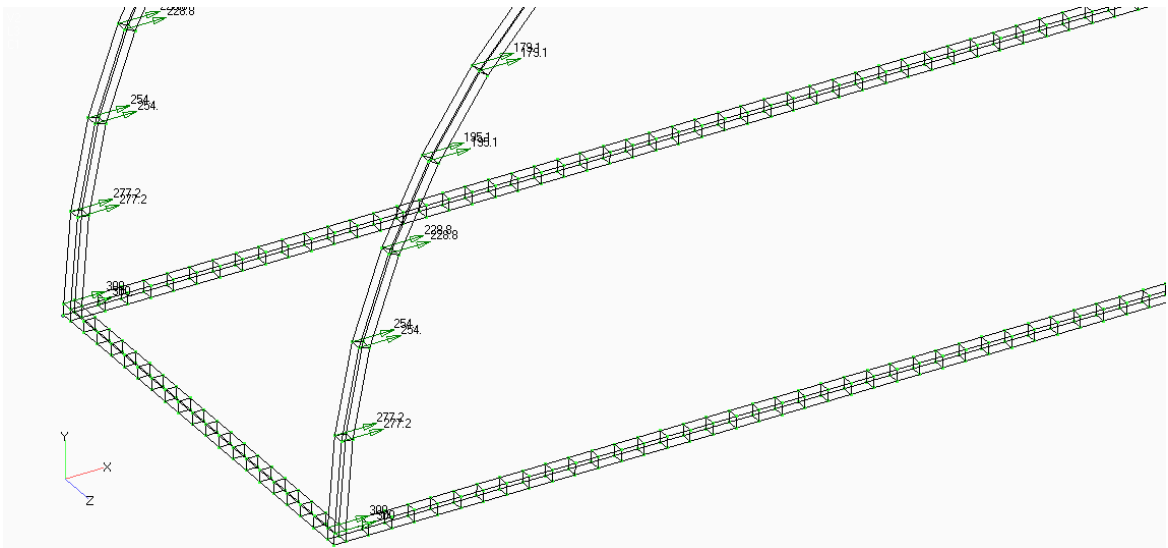


Figure 3.1-6. 7200 lb NASTRAN Model Load Distribution Section View

3.2 Analysis Method

The development of the resistance definition was accomplished using the static nonlinear solution method available in Nx NASTRAN. The load distribution described in Section 3.1 was applied to the model in 16 equally distributed load steps. Both geometric and material nonlinear analysis was conducted for each load distribution. For the material nonlinear analysis, the stress vs. strain diagram taken from the FEMAP pre-processor and shown in Figure 3.2-1 below was used in the model. This function was used to represent the behavior of the material through and beyond the yield point. The stress strain diagram for Aluminum Alloy 6061-T6 as taken from MIL-HDBK-5H was used to represent the material of the frame. As seen in Figure 3.2-1, the material yield point is 35000 psi, with a material ultimate strength of 42000 psi. Geometric nonlinear behavior was modeled by using the PARAM LGDISP command in the NASTRAN Model. This allowed for the inclusion of follower forces and stiffness matrix updates, as the deflection in the model changed with increasing load. All three load distribution cases were run with large displacement effects turned both on and off in order to compare the results, which are discussed in Section 3.3. Deflections discussed in the following paragraph were taken from nodes located near the purlin interface with each arch. These nodes were chosen for their proximity to deflection sensors used in the test program on the actual structure.

Aluminum Alloy 6061-T6 Stress/Strain Curve

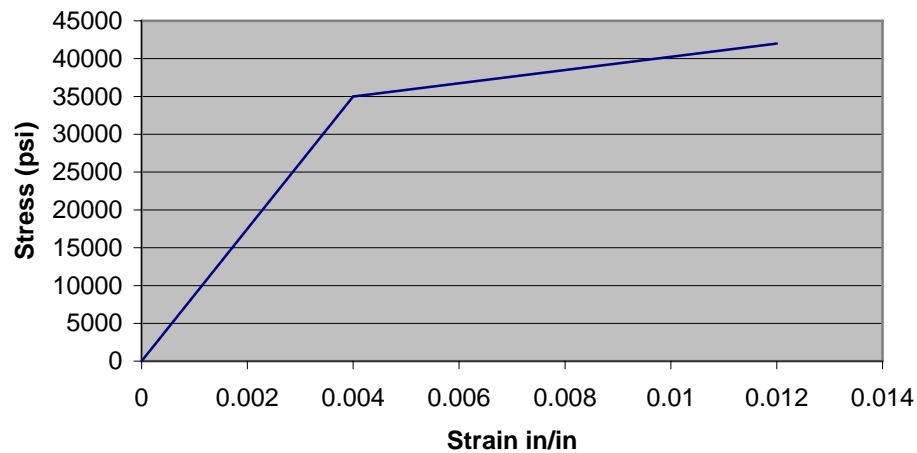


Figure 3.2-1. Stress versus Strain Diagram

3.3 Analysis Results

The results of the two analysis load conditions are presented in this section. Each analysis consisted of running a material nonlinear analysis, then a geometric and material nonlinear analysis, and comparing the results. These results were then used to calculate a static resistance function.

3.3.1 2400 lb Load Case Results

Tables 3.3.1-1 and 3.3.1-2 provide a summary of the maximum deflection at the selected nodes in the model for the 2400 lb load case. As shown in the figures, the difference in deflection due to the inclusion of large displacements is negligible when compared to the overall deflection of the system.

Table 3.3.1-1. 2400 lb Load Case Deflection with no Large Displacements

Load Step	Node	Displacement	
		(in)	Stress (psi)
1	1097	0.29	4319
2	1097	0.58	8638
3	1097	0.87	12957
4	1097	1.16	17276
5	1097	1.45	21596
6	1097	1.74	25915
7	1097	2.03	30235
8	1097	2.32	34554
9	951	2.62	35920
10	951	2.93	36931
11	951	3.24	37947
12	951	3.58	39740
13	951	3.93	41584
14	951	4.28	43453
15	936	4.63	45340

Table 3.3.1-2. 2400 lb Load Case Deflection Large Displacements Included

Load Step	Node	Displacement	
		(in)	Stress (psi)
1	1097	0.29	4324
2	1097	0.58	8658
3	1097	0.87	13001
4	1097	1.16	17353
5	1097	1.45	21714
6	1097	1.75	26084
7	1097	2.04	30462
8	1097	2.32	34859
9	951	2.64	35995
10	951	2.95	37010
11	951	3.26	38094
12	951	3.61	39913
13	951	3.97	41763
14	951	4.32	43650
15	951	4.68	45546

As shown previously, there is no difference in deflection until the material yield point is reached. Once the material yields, however, the deflection is greater for the analysis that includes large deflection effects. This difference is negligible as it is only an increase of 0.9%. Figure 3.3.1-1 provides a graph of the deflection versus load step overlaid for the analysis, with large displacements turned both on and off.

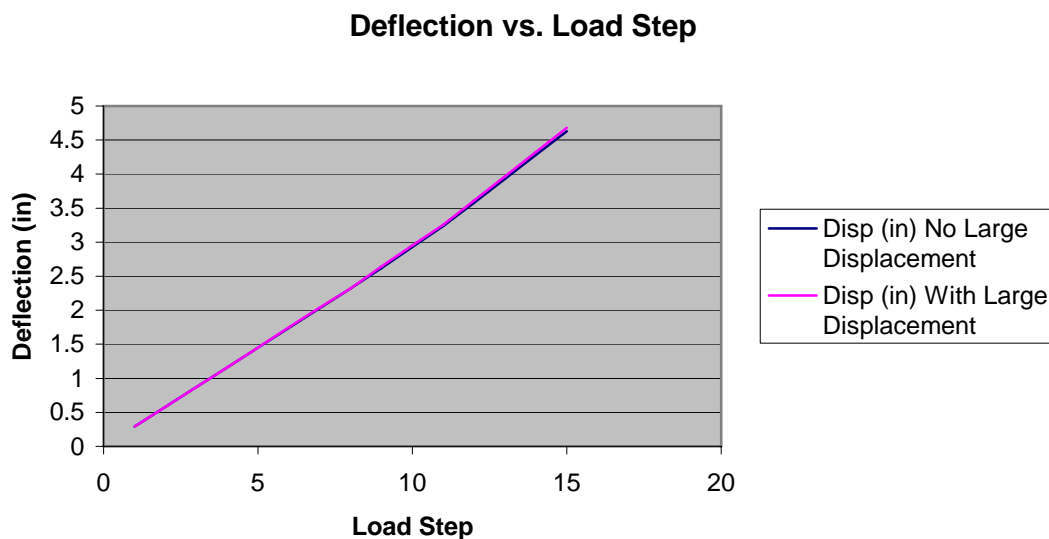


Figure 3.3.1-1. 2400 lb Load Case Deflection versus Load Step

As can be seen from the above tables and graphs, yielding of the material begins at approximately load step 8 when the material stress reaches 34859 psi and a deflection of 2.32 inches. Load step eight is equivalent to an applied load of $8/15(2400 \text{ lbs}) = 1280 \text{ lbs}$. This yields an equivalent spring constant of $K = 1280 \text{ lbs}/2.32 \text{ inches} = 552 \text{ lbs/in}$. for the elastic portion of the deflection. Once the material begins to yield, the structure begins to deflect at a higher rate. The spring constant calculation for this portion of the deflection is calculated as $K = (2400 \text{ lbs} - 1280 \text{ lbs})/(4.63 \text{ inches} - 2.32 \text{ inches}) = 485$

lbs/in. For the 2400 lb load case, the decrease in static resistance is only 13%. Figures 3.3.1-2 and 3.3.1-3 show the stress distribution as the frame first approaches the yield point in step 8, and as the frame approaches maximum deflection in step 15, while Figure 3.3.1-4 provides a section view of the stress distribution at the base of the frame at maximum deflection.

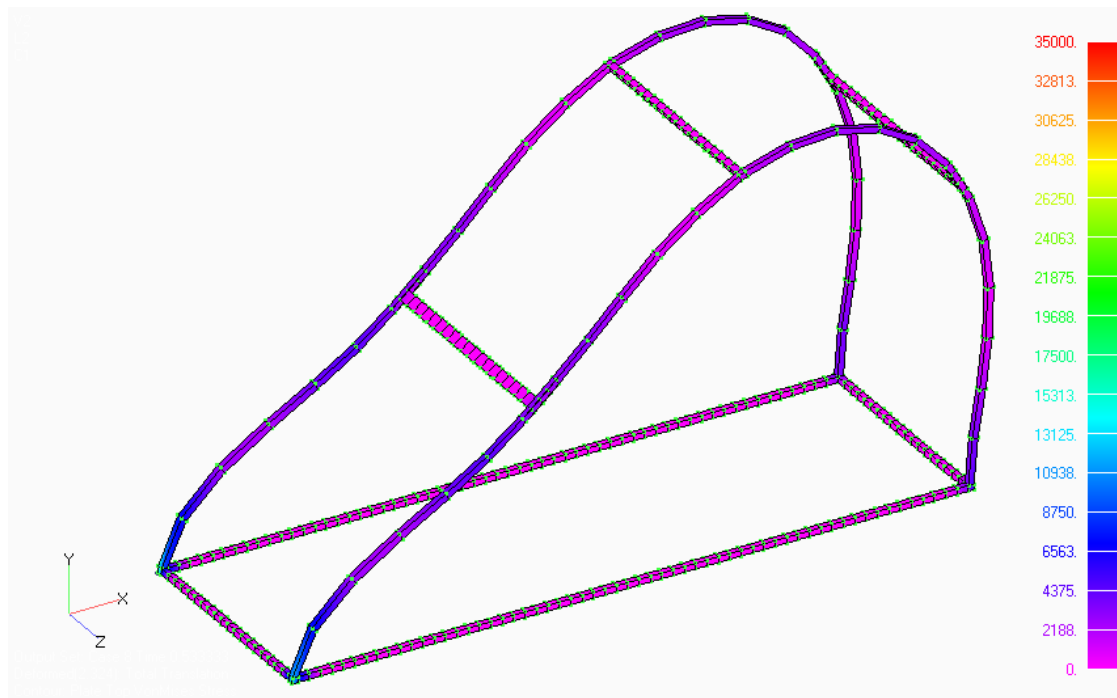


Figure 3.3.1-2. 2400 lb Load Case Yield Point

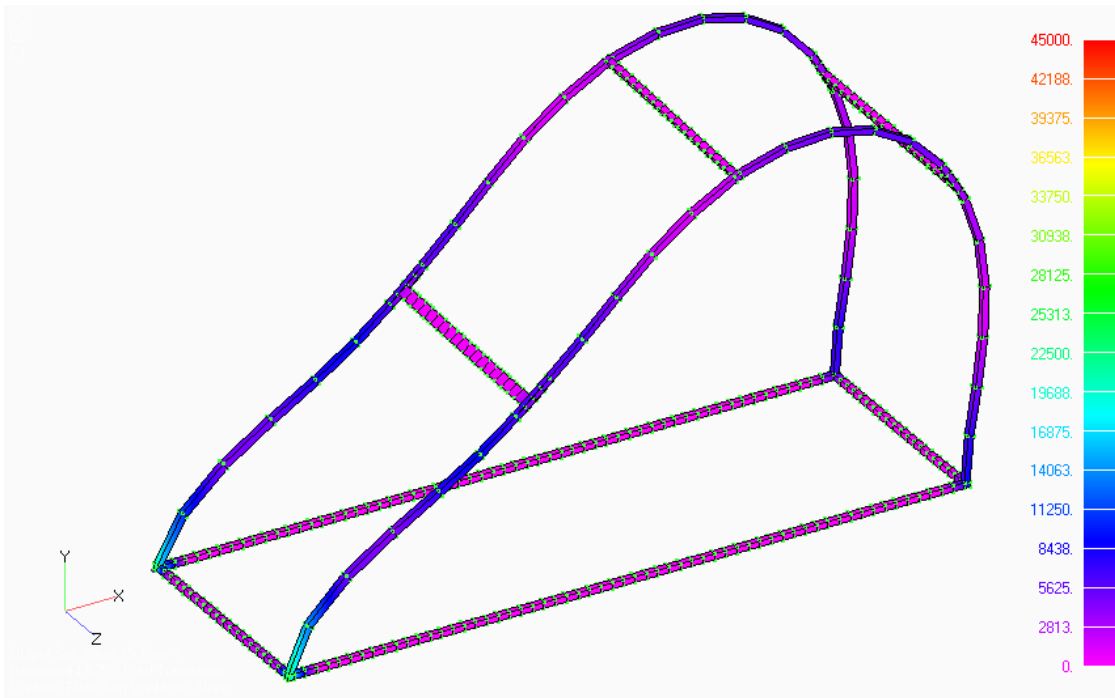


Figure 3.3.1-3. 2400 lb Load Case Maximum Deflection

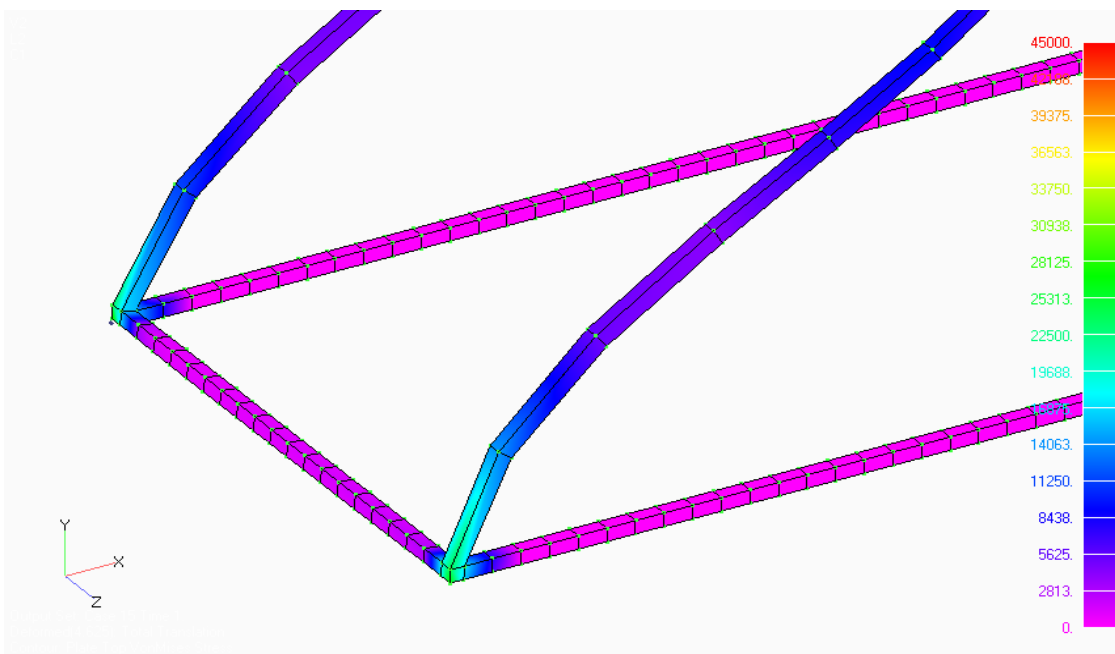


Figure 3.3.1-4. 2400 lb Load Case Maximum Deflection Section View

3.3.2 4800 lb Load Case Results

Tables 3.3.2-1 and 3.3.2-2 provide a summary of the maximum deflection at the selected nodes in the model for the 4800 lb load case. As shown in the figures and discussed previously for the 2400 lb load case, the difference in deflection due to the inclusion of large displacements is negligible when compared to the overall deflection of the system.

Table 3.3.2-1. 4800 lb Load Case Deflection with no Large Displacements

Load Step	Node	Displacement	
		(in)	Stress (psi)
1	1097	0.58	8643
2	1097	1.16	17288
3	1097	1.74	25932
4	1097	2.32	34576
5	951	2.93	36938
6	951	3.59	39757
7	951	4.28	43473
8	936	4.98	47276
9	936	5.73	51370
10	936	6.50	55566
11	936	7.28	59706
12	936	8.09	63467
13	936	8.92	67034
14	936	9.78	70672
15	936	10.83	74780

Table 3.3.2-2. 4800 lb Load Case Deflection Large Displacements Included

Load Step	Node	Displacement	
		(in)	Stress (psi)
1	1097	0.58	8663
2	1097	1.16	17364
3	1097	1.75	26100
4	1097	2.33	34890
5	951	2.95	37016
6	951	3.62	39930
7	951	4.33	43671
8	951	5.04	47485
9	951	5.80	51533
10	951	6.58	55702
11	951	7.37	59881
12	951	8.18	63796
13	936	9.00	67533
14	936	9.83	71163
15	936	10.73	75002

As shown in the previously, there is no difference in deflection until the material yield point is reached. Once the material yields, however, the deflection is greater for the analysis that includes large deflection effects, except for the last load step. The difference is once again negligible as it is only a change of 0.9%. Figure 3.3.2-1 provides a graph of the deflection versus load step overlaid for the analysis with large displacements turned both on and off.

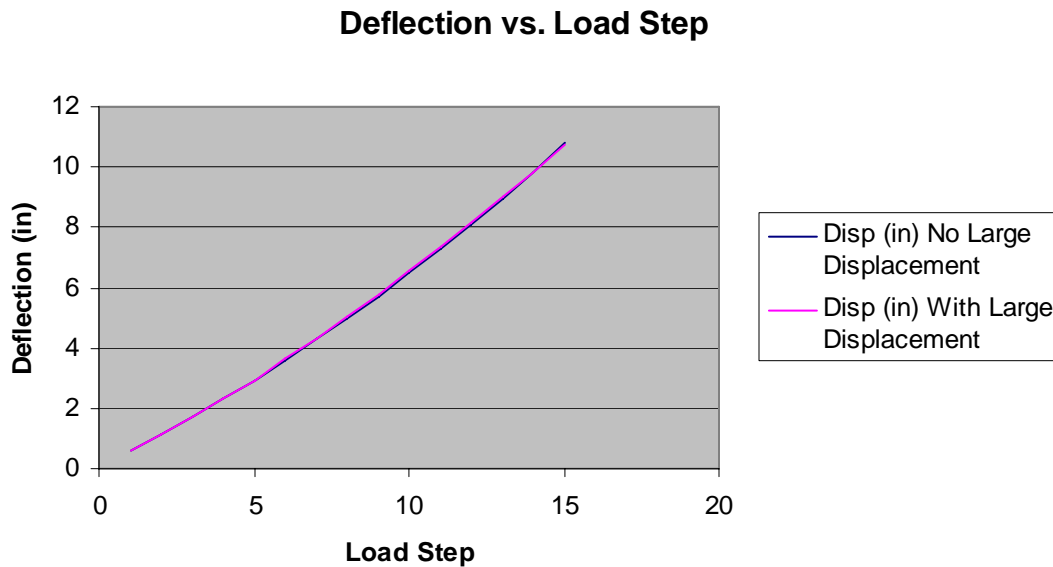


Figure 3.3.2-1. 4800 lb Load Case Deflection versus Load Step

As can be seen from the above tables and graphs, yielding of the material begins at approximately load step 4 when the material stress reaches 34576 psi and a deflection of 2.32 inches. Load step four is equivalent to an applied load of $4/15(4800 \text{ lbs}) = 1280 \text{ lbs}$. This yields an equivalent spring constant of $K = 1280 \text{ lbs}/2.32 \text{ inches} = 552 \text{ lbs/in.}$ for the elastic portion of the deflection. Once the material begins to yield, the structure begins to deflect at a higher rate. The spring constant calculation for this portion of the deflection is calculated as $K = (4800 \text{ lbs} - 1280 \text{ lbs})/(10.83 \text{ inches} - 2.32 \text{ inches}) = 414 \text{ lbs/in.}$ For the 4800 lb load case, the decrease in static resistance is 25%. Figures 3.3.2-2 and 3.3.2-3 show the stress distribution as the frame first approaches the yield point in step 4 and as the frame approaches maximum deflection in step 15. Figure 3.3.2-4 provides a section view of the stress distribution in step 15. This view provides a more detailed view of the stress distribution that clearly shows the maximum stress at the base

of the frame, with varying stress levels as the structure deflects in response to the distributed load.

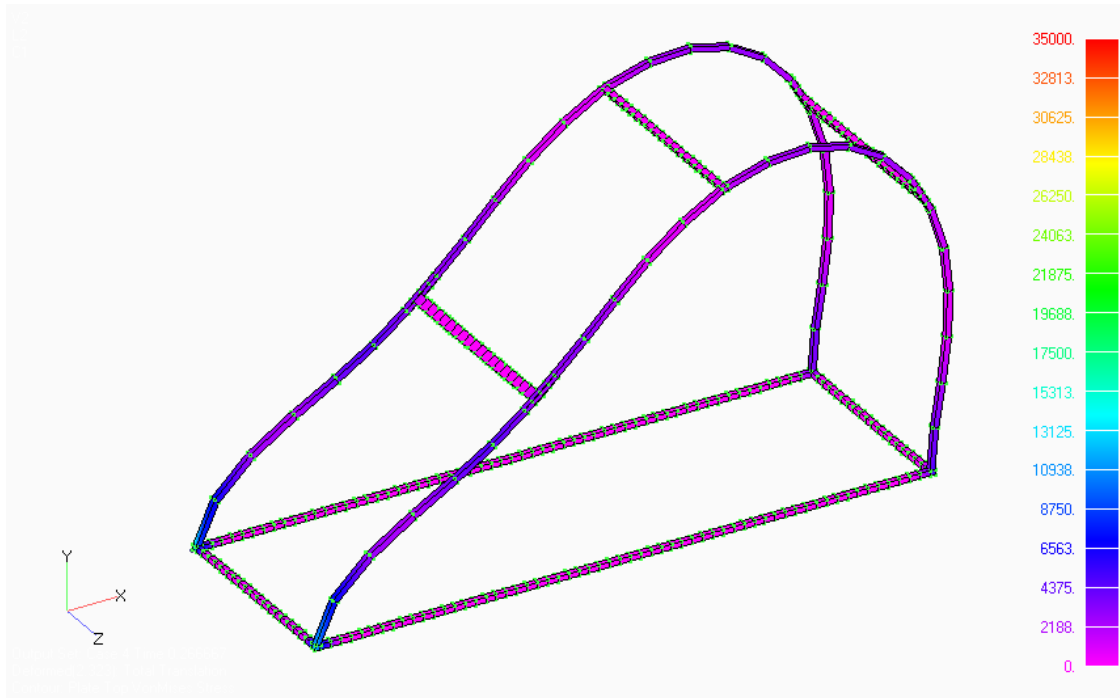


Figure 3.3.2-2. 4800 lb Load Case Yield Point

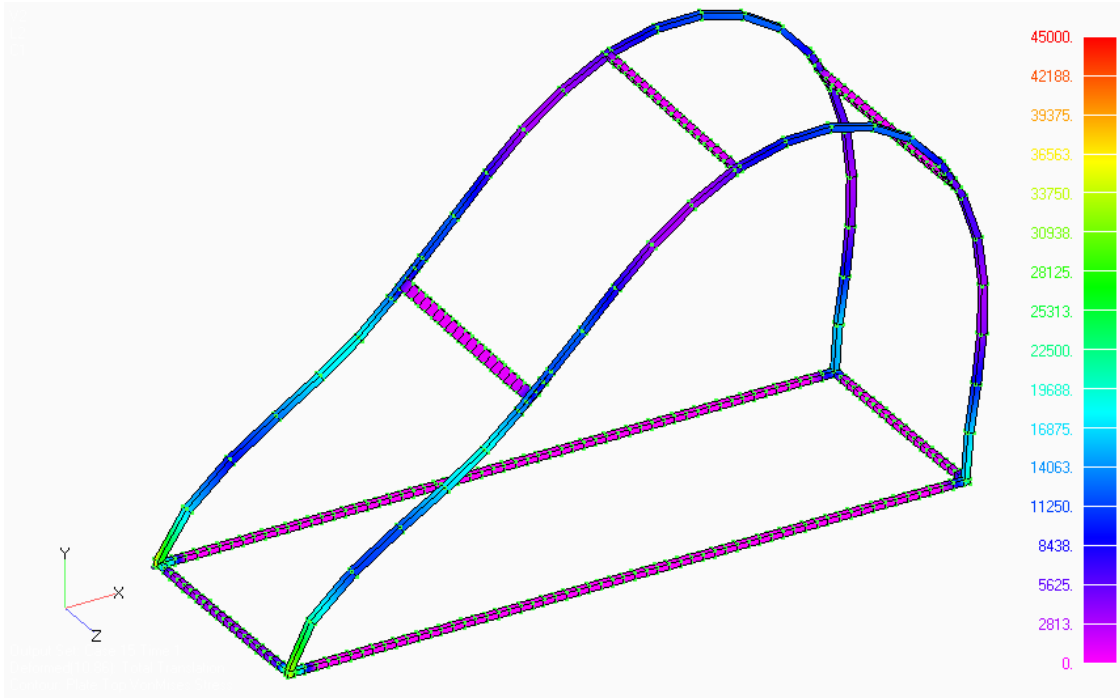


Figure 3.3.2-3. 4800 lb Load Case Maximum Deflection

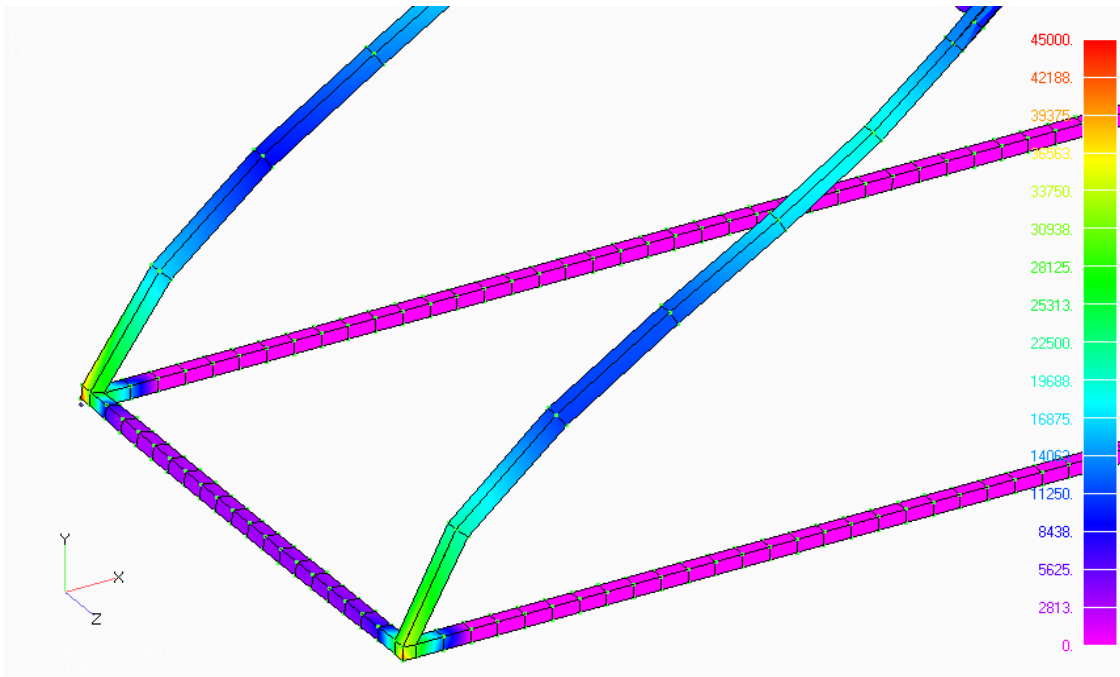


Figure 3.3.2-4. 4800 lb Load Case Maximum Deflection Section View

3.3.3 7200 lb Load Case Results

Tables 3.3.3-1 and 3.3.3-2 below provide a summary of the maximum deflection at the selected nodes in the model for the 7200 lb load case. As shown in the figures and discussed previously for the 2400 lb and 4800 lb load cases, the difference in deflection due to the inclusion of large displacements is negligible when compared to the overall deflection of the system. There is no difference in deflection until the material yield point is reached. Once the material yields, however, the deflection is greater for the analysis that includes large deflection effects until approximately 10 inches of deflection is reached, after that point, the analysis with no large displacement effects, i.e. no follower forces, produces the greater deflection. The difference is more noticeable for the 7200 lb analysis with a 5% difference in deflection. This large differential is attributed to the larger overall deflection, allowing for more impact due to change in the applied force direction. Figure 3.3.3-1 provides a graph of the deflection versus load step overlaid for the analysis with large displacements turned both on and off.

Table 3.3.3-1. 7200 lb Load Case Deflection with no Large Displacements

Load Step	Node	Displacement	
		(in)	Stress (psi)
1	1097	0.87	12956
2	1097	1.74	25913
3	951	2.62	35922
4	951	3.58	39746
5	936	4.62	45347
6	936	5.73	51351
7	936	6.88	57649
8	936	8.09	63443
9	936	9.33	68786
10	936	10.82	74745
11	936	12.60	81311
12	936	14.43	88269
13	936	16.29	95388
14	936	18.27	102927
15	936	20.49	111034

Table 3.3.3-2. 7200 lb Load Case Deflection Large Displacements Included

Load Step	Node	Displacement	
		(in)	Stress (psi)
1	1097	0.87	12999
2	1097	1.75	26081
3	951	2.64	35997
4	951	3.61	39920
5	951	4.68	45554
6	951	5.79	51514
7	951	6.96	57783
8	951	8.17	63771
9	936	9.40	69325
10	936	10.72	74965
11	936	12.34	81314
12	936	14.01	87828
13	936	15.66	94506
14	936	17.41	101532
15	936	19.37	108937

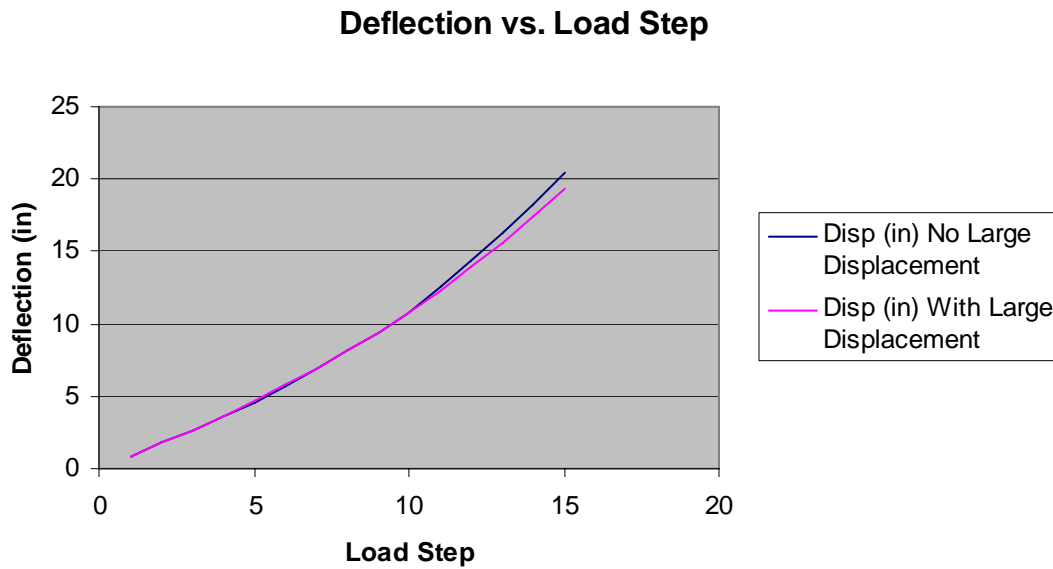


Figure 3.3.3-1. 4800 lb Load Case Deflection versus Load Step

As can be seen from the above tables and graphs, yielding of the material begins at approximately load step 3 when the material stress reaches 35922 psi and a deflection of 2.62 inches. Load step 3 is equivalent to an applied load of $3/15(7200 \text{ lbs}) = 1440 \text{ lbs}$. This yields an equivalent spring constant of $K = 1440 \text{ lbs}/2.62 \text{ inches} = 550 \text{ lbs/in}$. for the elastic portion of the deflection. Once the material begins to yield, the structure begins to deflect at a higher rate. The spring constant calculation for this portion of the deflection is calculated as $K = (7200 \text{ lbs} - 1440 \text{ lbs})/(20.49 \text{ inches} - 2.62 \text{ inches}) = 322 \text{ lbs/in}$. For the 7200 lb load case, the decrease in static resistance is 41%. Figures 3.3.3-2 and 3.3.3-3 show the stress distribution as the frame first approaches the yield point in step 4, and as the frame approaches maximum deflection in step 15. Figure 3.3.3-4 also provides a section view of the stress distribution in step 15. This provides a more detailed view of the stress distribution that clearly shows the maximum stress at the base of the

frame, with varying stress levels as the structure deflects in response to the distributed load.

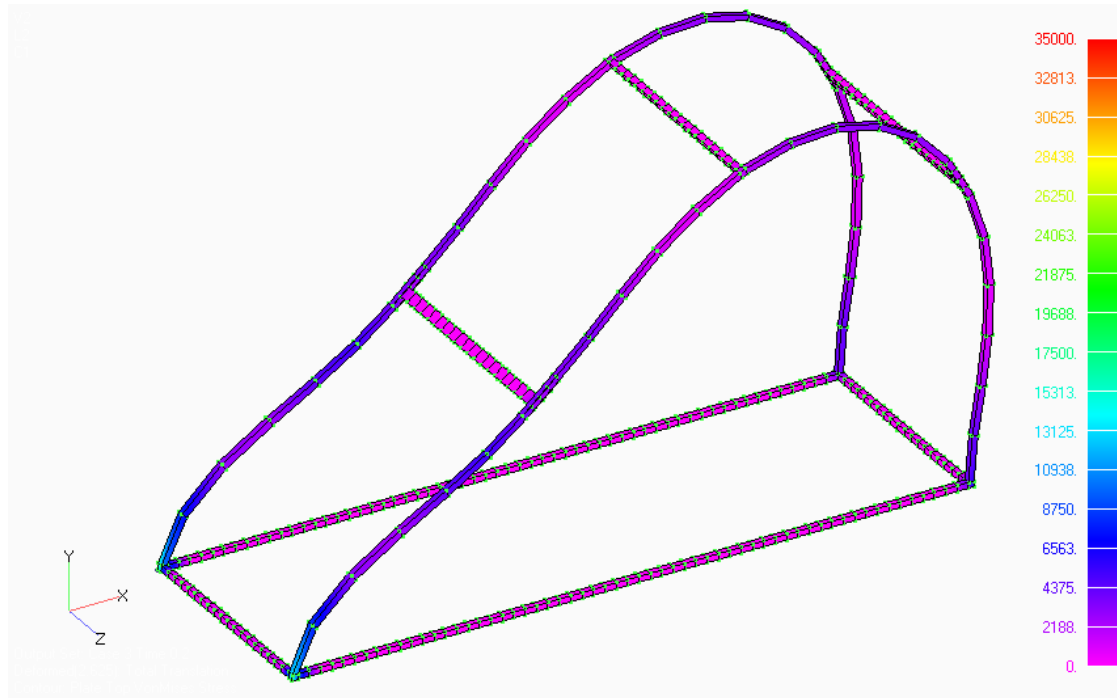


Figure 3.3.3-2. 7200 lb Load Case Yield Point

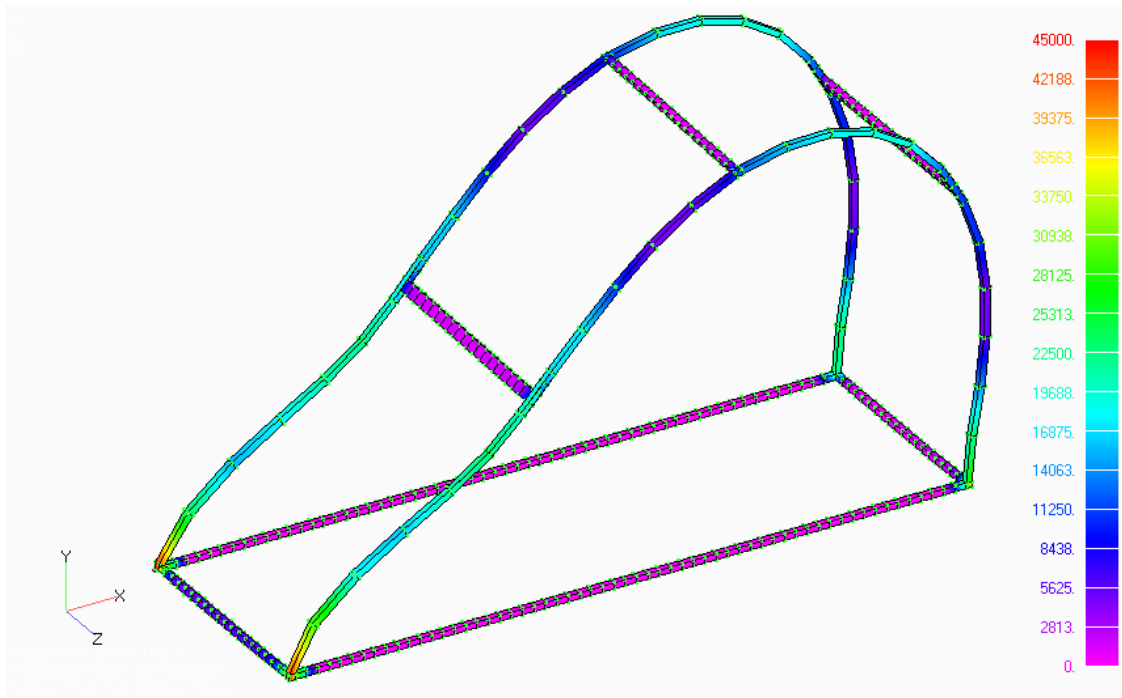


Figure 3.3.3-3. 7200 lb Load Case Maximum Deflection

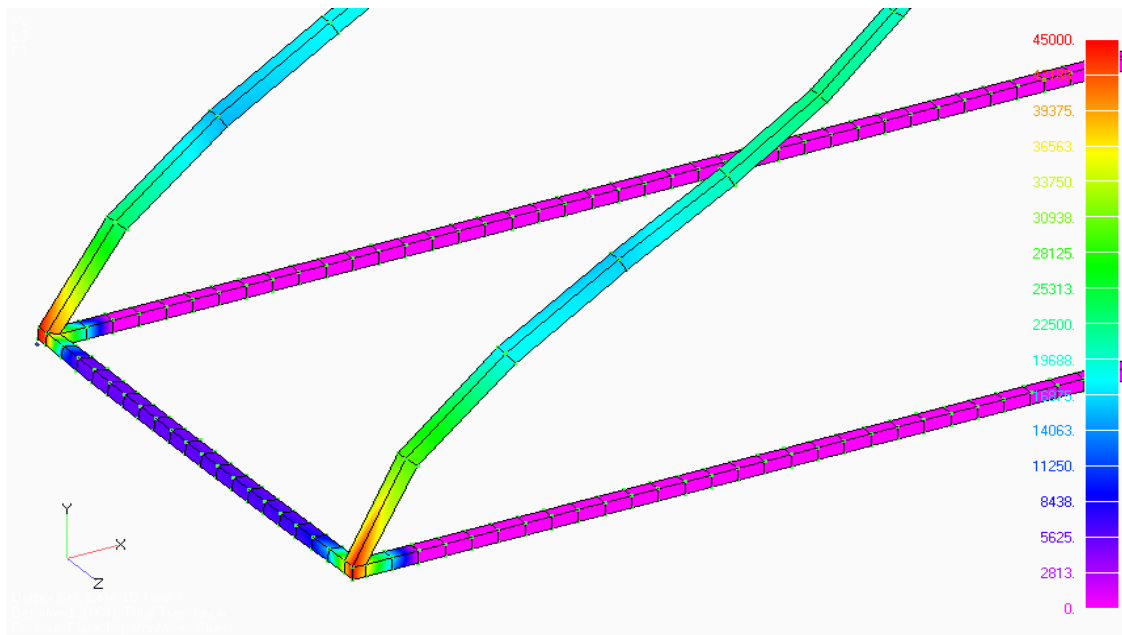


Figure 3.3.3-4. 7200 lb Load Case Maximum Deflection Section View

3.4 Analysis Parametric Study

The shelter field assembly provides a base support that is realistically somewhere between simply supported and fixed. All analysis in Section 3.3 assumed a fixed support. This section will repeat the analysis of the 2400 lb load case using a simply supported base to determine the impact of base restraint on the resistance function of the frame.

3.4.1 2400 lb Load Case Results Simply Supported

Tables 3.4.1-1 and 3.4.1-2 provide a summary of the maximum deflection at the selected nodes in the model for the 2400 lb load case with a simply supported base. As in the fixed base condition, the difference in deflection due to the inclusion of large displacements is negligible when compared to the overall deflection of the system. Figure 3.4.1-1 provides a graph that includes an overlay of the displacements due to a 2400 lb load case with a fixed base and with a simply supported base. Large displacement effects were not included in these runs.

**Table 3.4.1-1. 2400 lb Load Case Deflection No Large Displacements Included,
Simply Supported Base**

Load Step	Node	Displacement (in)	Stress (psi)
1	1097	0.29	4330
2	1097	0.58	8661
3	1097	0.87	12991
4	1097	1.16	17321
5	1097	1.45	21652
6	1097	1.74	25982
7	1097	2.03	30313
8	1097	2.32	34643
9	951	2.62	35953
10	951	2.93	36970
11	951	3.24	38003
12	951	3.59	39827
13	951	3.94	41691
14	951	4.28	43581
15	936	4.63	45489

Table 3.4.1-2. 2400 lb Load Case Deflection, Large Displacements Included, Simply Supported Base

Load Step	Node	Displacement	
		(in)	Stress (psi)
1	1097	0.29	4335
2	1097	0.58	8680
3	1097	0.87	13034
4	1097	1.16	17397
5	1097	1.45	21769
6	1097	1.75	26150
7	1097	2.04	30540
8	1097	2.33	35009
9	951	2.64	36027
10	951	2.95	37048
11	951	3.27	38163
12	951	3.62	40001
13	951	3.97	41878
14	951	4.33	43779
15	951	4.68	45695

Deflection vs. Load Step

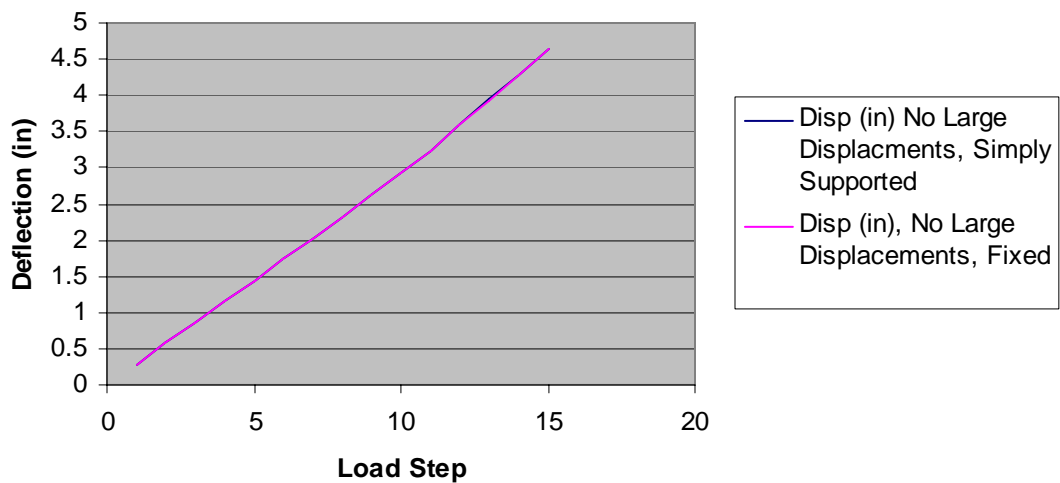


Figure 3.4.1-1. 2400 lb Load Case Deflection versus Load Step

As seen in Figure 3.4.1-1, the base support condition has no appreciable impact on the deflection and stress distribution; therefore, the static resistance function developed using the fixed base condition is valid even when considering the uncertainty of the actual base restraint condition.

3.5 Static Resistance Function

The three load cases discussed in the previous sections provide a foundation to develop a static resistance function that could be used in a SDOF Model to predict the deflection of the frame subjected to impulse loading. The function will need to consist of a piecewise linear representation of the frame stiffness with the curve defining the stiffness through the elastic and plastic material phase as well as accounting for the effects of large displacement.

3.5.1 Elastic Static Resistance Function

The elastic portion of the curve was consistent among the three load case analysis performed. Each load case showed that the material begins to yield at approximately 1300 lbs of applied force. Table 3.5.1-1 provides a summary of the three load cases, along with maximum material stress, displacement, and the resulting stiffness calculation.

Table 3.5.1-1. Elastic Stiffness Summary

Load Case	Load Step	Stress (psi)	Load at Yield (lbs)	Displacement (inches)	Stiffness (lb/in)
2400 lbs	8	34554	1280	2.32	552
4800 lbs	4	34576	1280	2.32	552
7200 lbs	3	35922	1440	2.62	550

The above cases show good correlation among the three load cases analyzed and provide an elastic stiffness of 550 lbs/in until a deflection of 2.3 inches is reached.

3.5.2 Plastic Static Resistance Function

Analysis of the frame model at the material yield point and beyond shows that the stiffness of the structure continues to decrease as the deflection increases. Even though the material stress versus strain curve is linear before and after the yield point, the apparent stiffness continues to decrease due to the deflection of the structure and the resulting recalculation of the stiffness matrix in the NASTRAN model based on the updated geometry. Therefore, two plastic stiffness numbers will be used for the plastic portion of the curve. The first portion will be based on the deflection of all three load cases and will encompass the stiffness up to a deflection of approximately 4.6 inches, which is the maximum deflection found in the 2400 lb load case. Table 3.5.2-1 provides a summary for all three load cases up to the 4.6 inch deflection. Data from all three load cases is included in the table, even though interpolation is required to correlate the data for the 4800 lb load case, since the nearest deflections are at 4.3 inches and 5.0 inches.

Table 3.5.2-1. Initial Plastic Stiffness Summary

Load Case	Load Step	Stress (psi)	Load (lbs)	Displacement (inches)	Stiffness (lb/in)
2400 lbs	15	45340	2400	4.63	485
4800 lbs	7 and 8	45374	2400	4.65	481
7200 lbs	5	45374	2400	4.62	480

The calculation of the stiffness using the data above is shown in the following equations.

$$2400 \text{ lb load case } K = (2400 \text{ lbs} - 1280 \text{ lbs}) / (4.63 \text{ inches} - 2.32 \text{ inches})$$

$$4800 \text{ lb load case } K = (2400 \text{ lbs} - 1280 \text{ lbs}) / (4.65 \text{ inches} - 2.32 \text{ inches})$$

$$7200 \text{ lb load case } K = (2400 \text{ lbs} - 1440 \text{ lbs}) / (4.62 \text{ inches} - 2.62 \text{ inches})$$

Table 3.5.2-1 shows that the minor variations in the point at which the material yield point is assumed to be reached do not influence the calculation.

The second portion of the plastic stiffness calculation will be based on deflection data from the 4800 lb and 7200 lb load cases. This calculation will encompass the stiffness up to a deflection of 10.83 inches, which is the maximum deflection found in the 4800 lb load case. Table 3.5.2-2 provides a summary of data for the stiffness calculation for the second portion of the plastic curve.

Table 3.5.2-2. Second Plastic Stiffness Summary

Load Case	Load Step	Stress (psi)	Load (lbs)	Displacement (inches)	Stiffness (lb/in)
4800 lbs	15	74780	4800	10.83	387
7200 lbs	10	74745	4800	10.82	387

The calculation of the stiffness using the data above is shown in the following equations.

$$4800 \text{ lb load case } K = (4800 \text{ lbs} - 2400 \text{ lbs}) / (10.83 \text{ inches} - 4.63 \text{ inches})$$

$$7200 \text{ lb load case } K = (4800 \text{ lbs} - 2400 \text{ lbs}) / (10.82 \text{ inches} - 4.63 \text{ inches})$$

3.5.3 Static Resistance Function Development

The three stiffness values for the various deflections are assembled into one curve, shown in Figure 3.5.3-1, which represents the static resistance function for the frame. This curve is incorporated into a SDOF model of the frame that represents the applied load, stiffness, and mass of the structure.

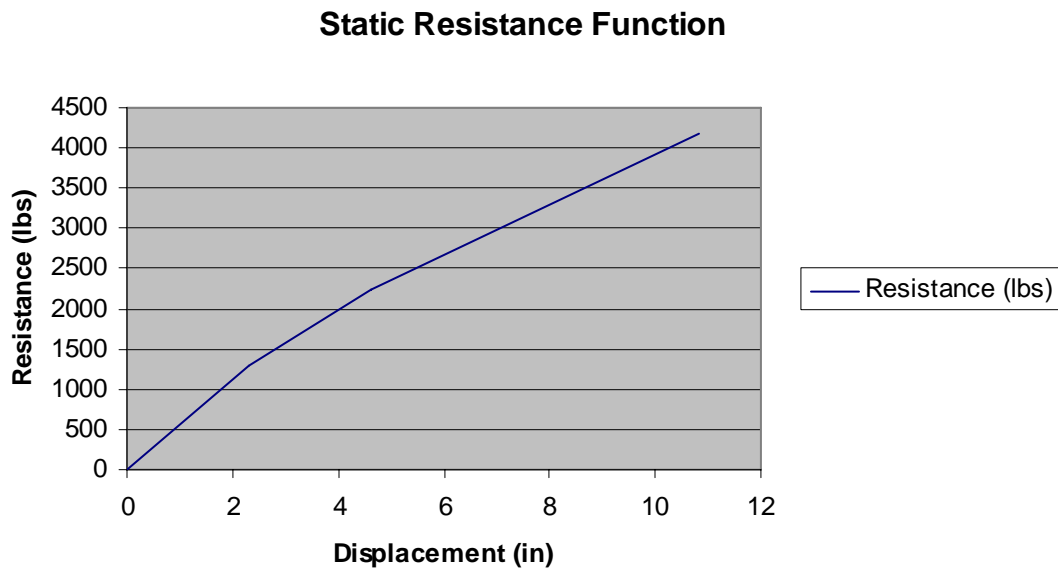


Figure 3.5.3-1. Static Resistance Function

4.0 LS-DYNA IMPULSE LOAD SIMULATION RESULTS

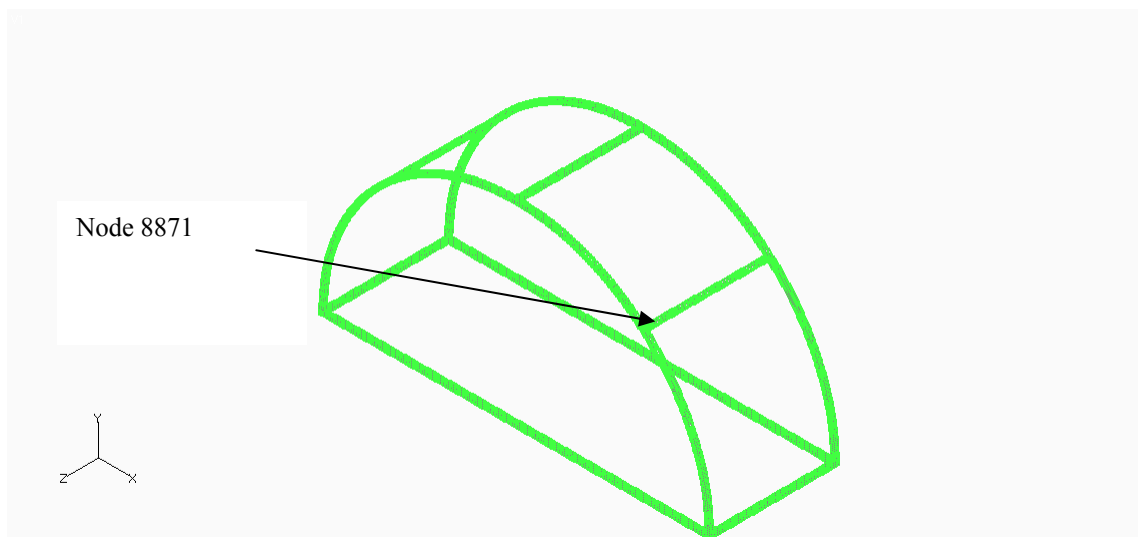
The results of the effort to validate the predictive capability of LS-DYNA impulse load modeling applied to the aluminum arch frames are summarized in Table 4.0-1. The correlation between the model results and test data shows a significant lack of agreement between the test results and the model results. The lack of correlation is primarily due to two significant differences between the test cases and the analytical models. The first difference is the load application that in the test cases is applied to the entire shelter structure including fabric while in the analytical models; only the exposed aluminum structure is considered for load application. The second difference is the lack of the fabric weight and stiffness in the analytical models.

In addition to the test case results, four additional cases were modeled to simulate points along the pressure-impulse diagram that is documented in the test report. The correlation for these cases showed the same lack of agreement between the predicted results and the model results for the four conditions chosen. The four conditions were chosen to follow the pressure-impulse diagram, with two cases falling on the minor to no damage portion of the curve, and the other two cases falling on the severe to failure portion of the curve. As described in Section 3.0, all deflections were taken from the interface of the purlin to the arch on the side facing the impulse load. The model recovery point is shown in Figure 4.0-1 below. The deflections for this point are typical for purlin deflections on either side of the frame. The following sections present the results of each analysis including graphs of deflection versus time for each load case and maximum stress within the aluminum arch.

Table 4.0-1. Model Impulse Analysis Results

Reflected Impulse (psi-ms)	Displacement (inches)	Model Predicted Result	Test Damage Level	Prediction Curve **
81.1	4.3	Minor	Severe	Failure
55.7	3.5	None	Minor	Moderate
30.5	3.5	None	None	Minor
94.8	10.1	Minor	Severe	Failure
76.4	8.5	Minor	Severe	Severe
55.0	6.0	Minor	Minor	Minor
32.2	3.4	None	None	Threshold
111.0	6.8	Minor	N/A	Failure
24.7	3.1	None	N/A	Minor
116.8	8.0	Minor	N/A	Failure
33.1	4.0	Minor	N/A	Minor

**Utilizing the reduced impulse curve presented in the test report

**Figure 4.0-1. Deflection Recovery Node**

4.1 81.1 psi-ms Results

Results for this load case are shown in Figures 4.1-1 and 4.1-2. As seen in Figure 4.1-1, maximum deflection was approximately 4.3 inches, which falls on the threshold of minor damage. The model was terminated after two complete cycles of the frame. In addition, as shown in Figure 4.1-3, the maximum stress at the base of the arch did not exceed the yield stress of the arch material. The lack of material yield with the 4.6 inch deflection is a lack of correlation with the resistance function that can be seen in several of the following load cases. This difference is primarily due to the deflected shape providing higher deflections at the purlin for some blast cases.

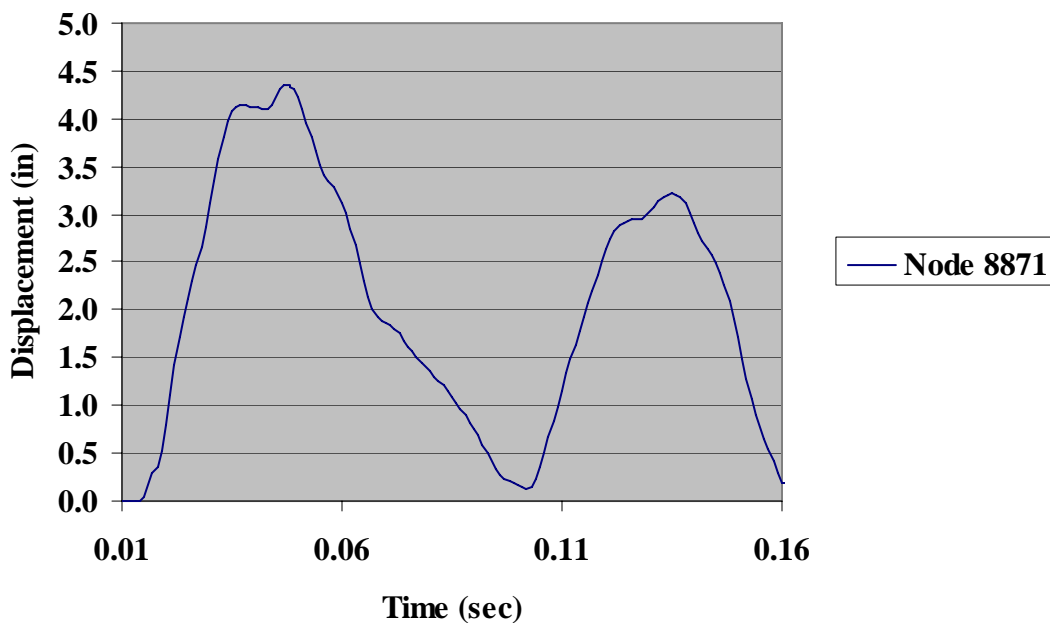


Figure 4.1-1. Purlin Translation for 81.1 psi-ms

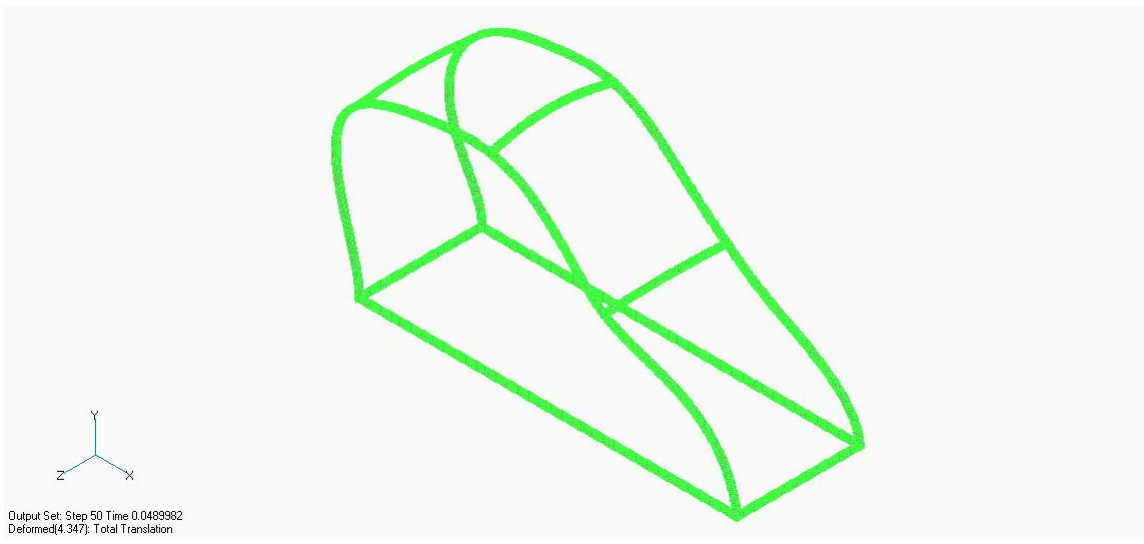


Figure 4.1-2. Arch Deflected Shape for 81.1 psi-ms

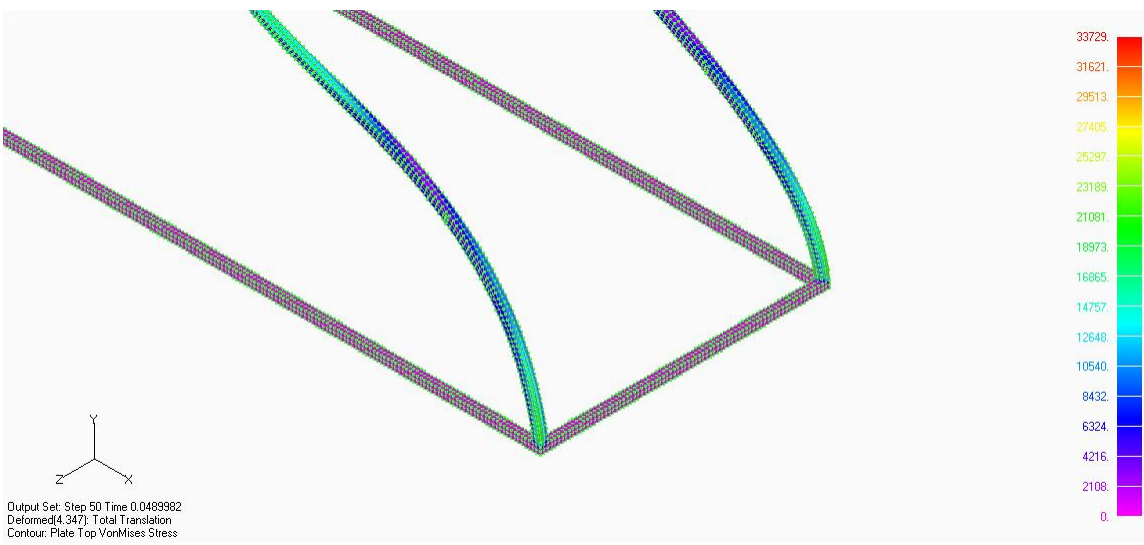


Figure 4.1-3. Arch Stress Distribution for 81.1 psi-ms

4.2 55.7 psi-ms Results

Results for this load case are shown in Figures 4.2-1 and 4.2-2. As seen in Figure 4.2-1, maximum deflection was approximately 3.5 inches, which falls in the minor/no

damage category. Figure 4.2-2 provides a deformed view of the structure. In addition, the maximum stress did not exceed the material yield stress, as shown in Figure 4.2-3.

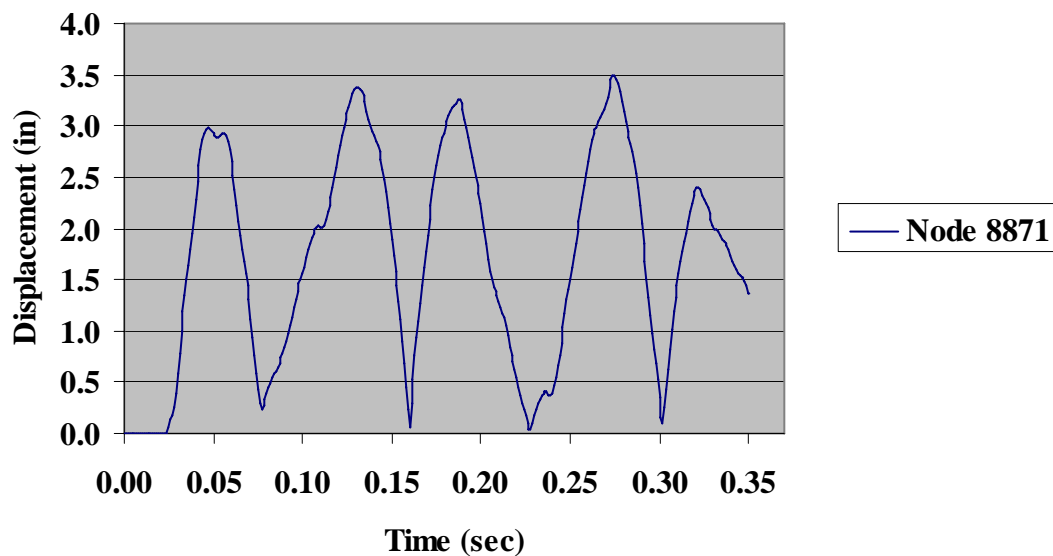


Figure 4.2-1. Purlin Translation for 55.7 psi-ms

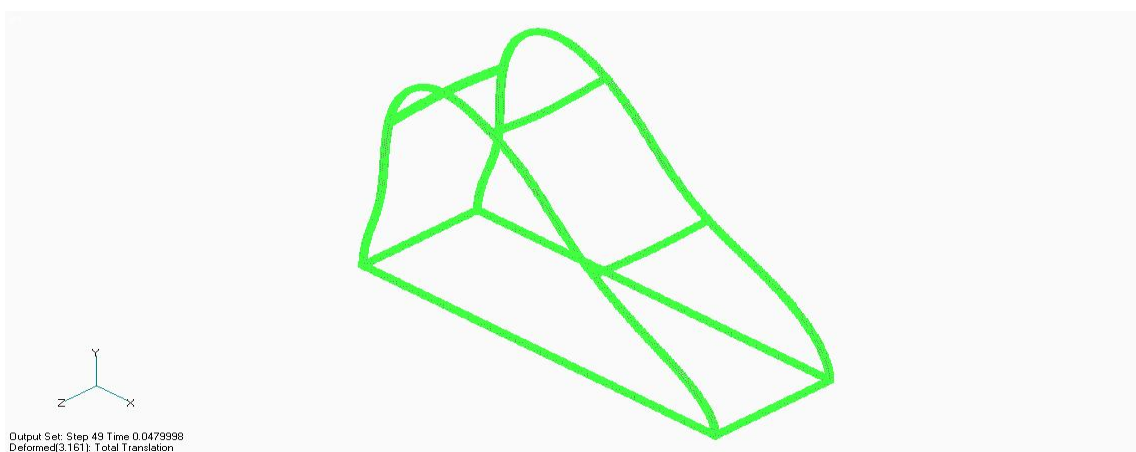


Figure 4.2-2. Arch Deflected Shape for 55.7 psi-ms

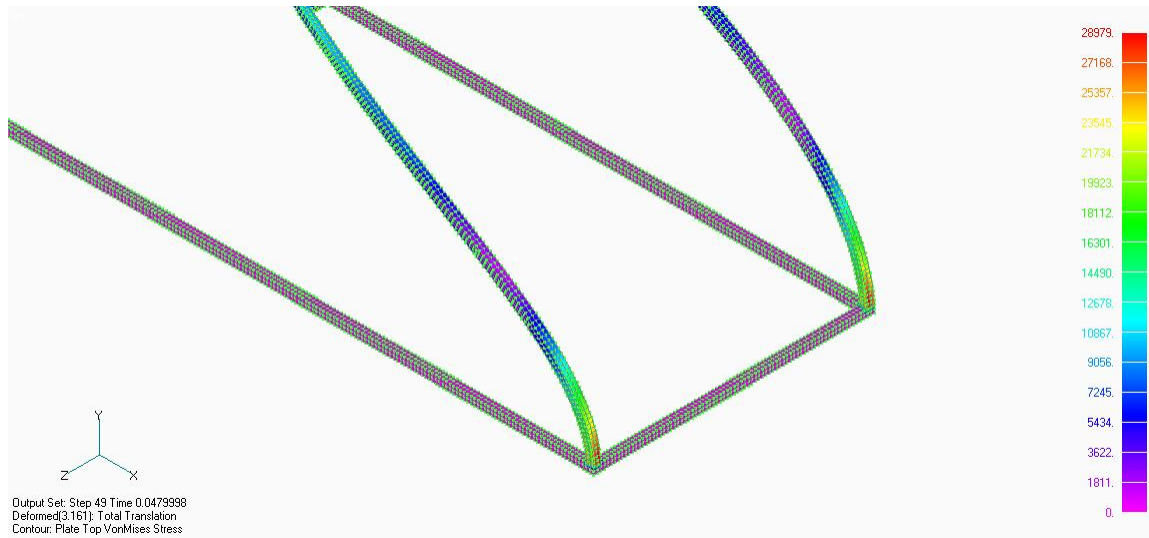


Figure 4.2-3. Arch Stress Distribution for 55.7 psi-ms

4.3 30.5 psi-ms Results

Results for this load case are shown in Figures 4.3-1 and 4.3-2. As seen in Figure 4.3-1, maximum deflection was approximately 3.5 inches, which falls in the minor/no damage category and correlates with the damage that was reported from the actual test result. Figure 4.3-2 provides an image of the deformed shape of the structure at approximately 1.8 inches of purlin deflection, while Figure 4.3-3 provides a stress contour of the structure at approximately 1.8 inches of deflection, which corresponds to the maximum deflection for the first peak of the deflection curve. As seen in Figure 4.3-3, the maximum stress at the base of the structure did not exceed the material yield stress.

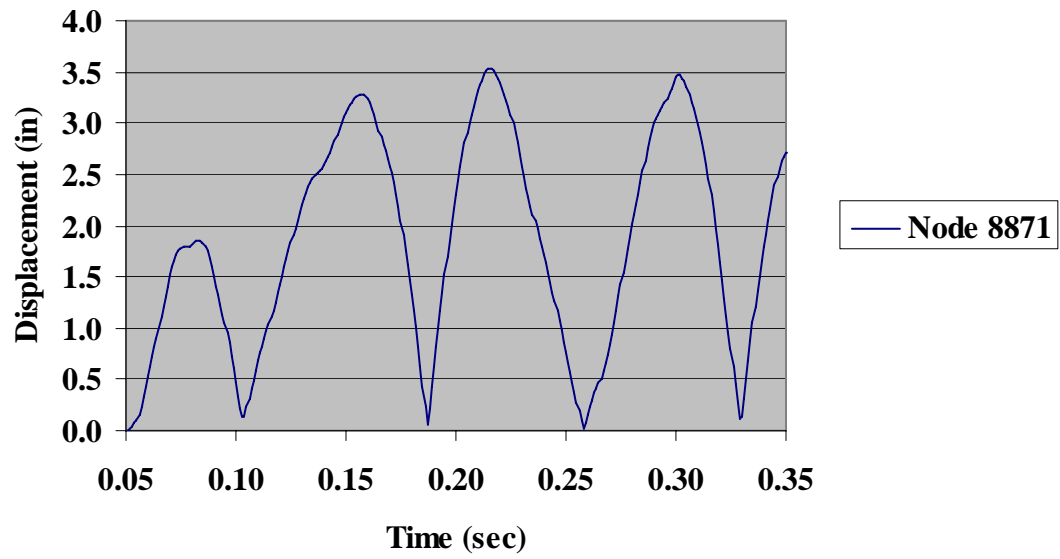


Figure 4.3-1. Purlin Translation 30.5 psi-ms

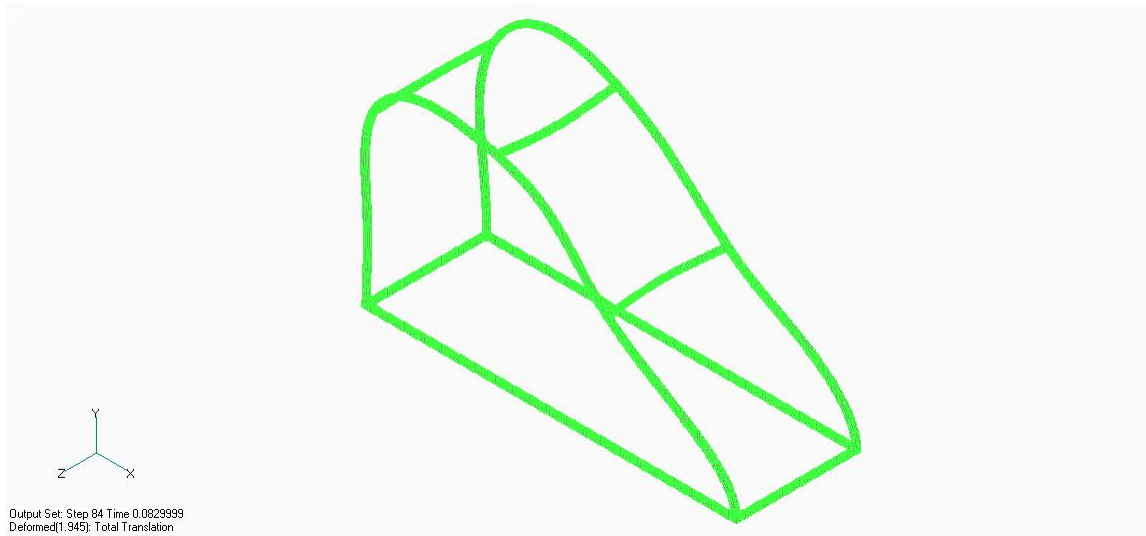


Figure 4.3-2. Arch Deflected Shape for 30.5 psi-ms

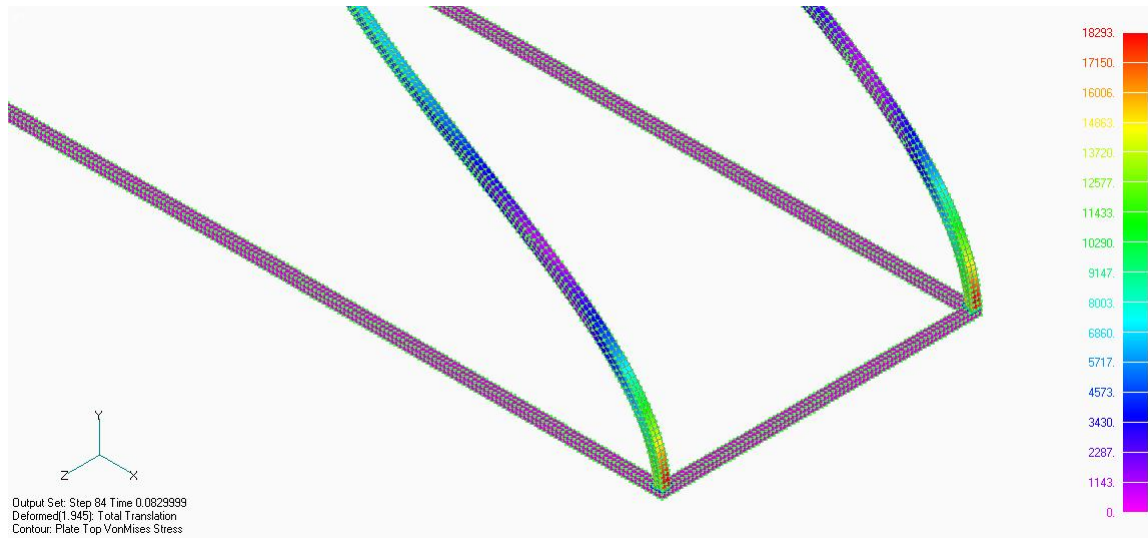


Figure 4.3-3. Arch Stress Distribution for 30.5 psi-ms

4.4 94.8 psi-ms Results

Results for this load case are shown in Figures 4.4-1 and 4.4-2. As seen in Figure 4.4-1, maximum deflection in the structure was 10.1 inches, which falls in the minor damage category and does not agree with the test report prediction curve. However, the predicted damage for this case is high in the minor category and is nearing the severe category. Figure 4.4-2 provides an image of the deformed shape of the structure at approximately 6.8 inches of purlin deflection while Figure 4.4-3 provides a stress contour of the structure at approximately 6.8 inches of deflection, which corresponds to the maximum deflection for the first peak of the deflection curve. As seen in Figure 4.4-3, the maximum stress at the base of the structure exceeds the material yield stress.

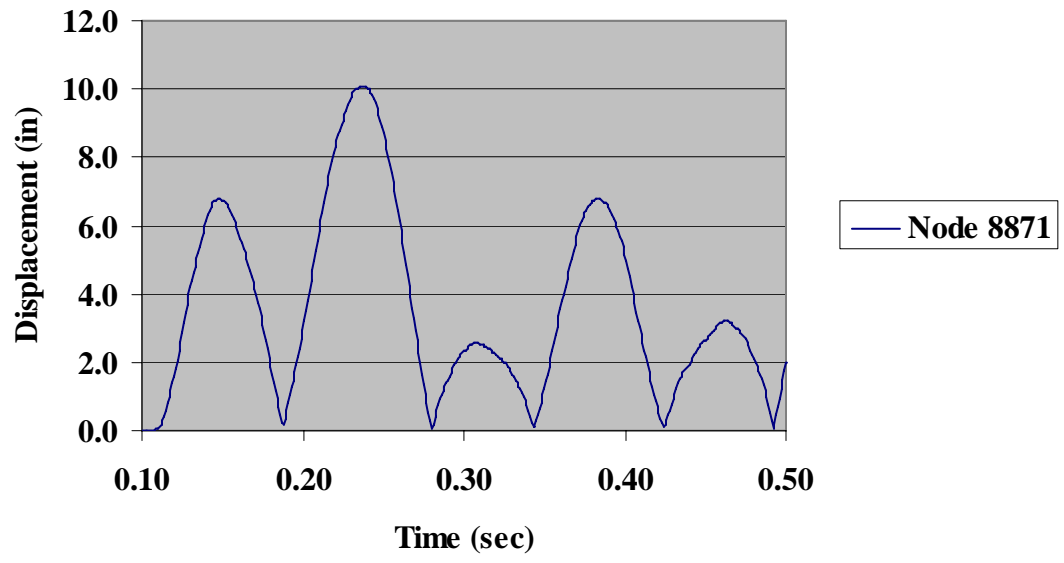


Figure 4.4-1. Purlin Translation for 94.8 psi-ms

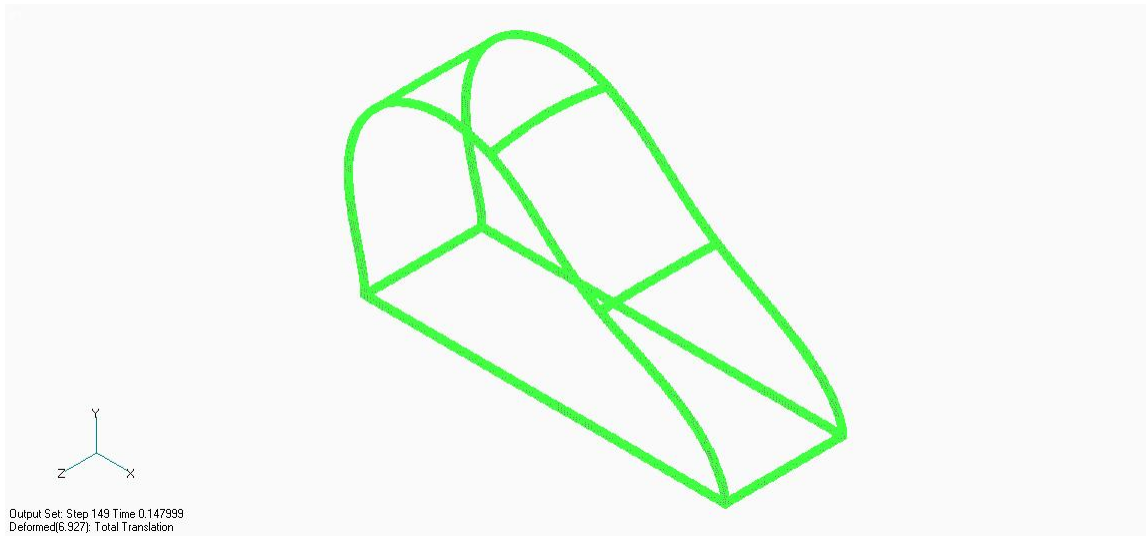


Figure 4.4-2. Arch Deflected Shape for 94.8 psi-ms

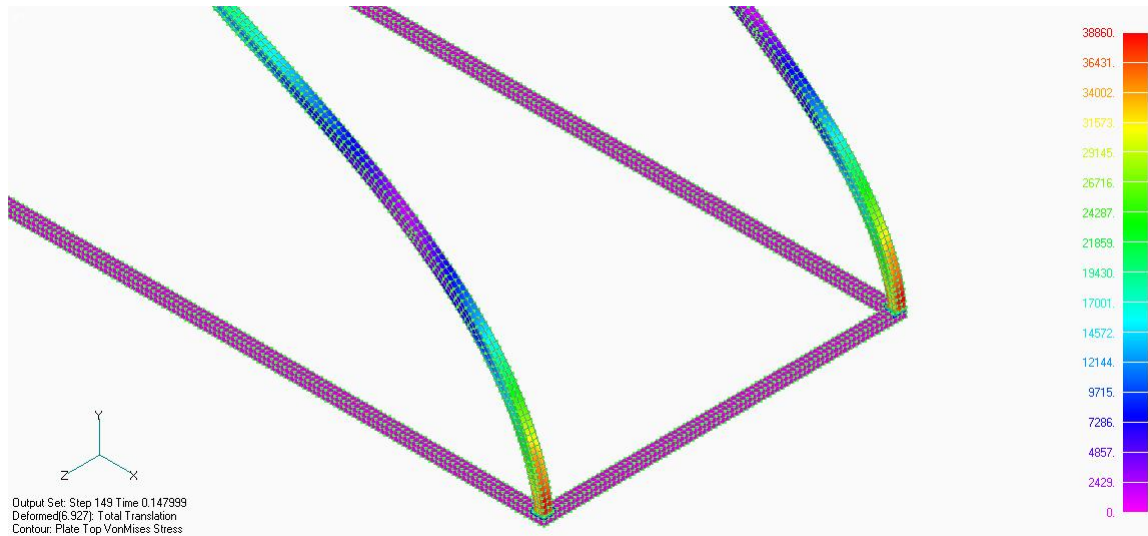


Figure 4.4-3. Arch Stress Distribution for 94.8 psi-ms

4.5 76.4 psi-ms Results

Results for this load case are shown in Figures 4.5-1 and 4.5-2. As seen in Figure 4.5-1, maximum deflection in the structure was approximately 8.5 inches, which falls in the minor damage category and is below the damage predicted by the test report curve. Figure 4.5-2 provides an image of the deformed shape of the structure at approximately 5.4 inches of purlin deflection, while Figure 4.5-3 provides a stress contour of the structure at approximately 5.4 inches of deflection, which corresponds to the maximum deflection for the first peak of the deflection curve. As can be seen in Figure 4.5-3, the maximum stress at the base of the structure equals the material yield stress.

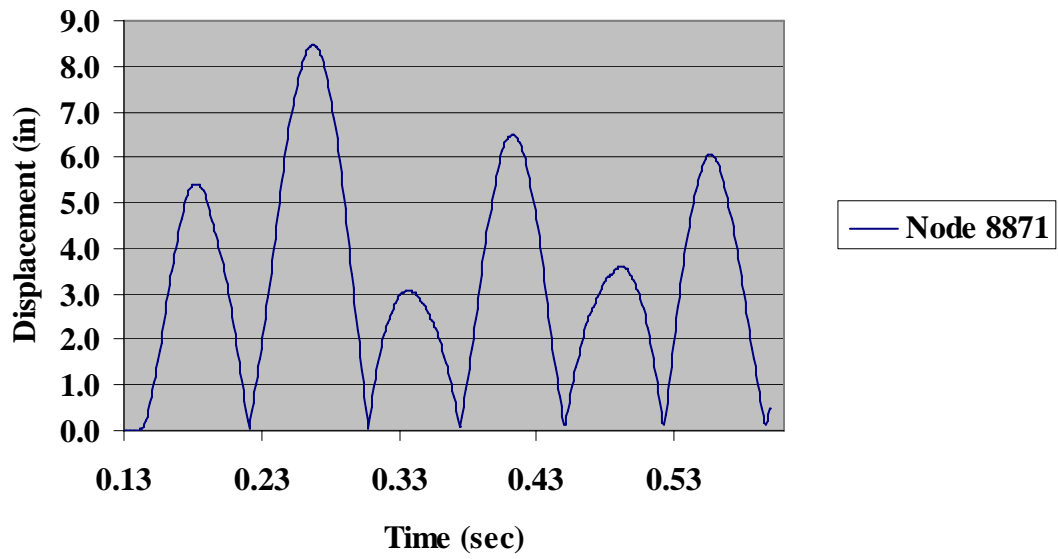


Figure 4.5-1. Purlin Translation for 76.4 psi-ms

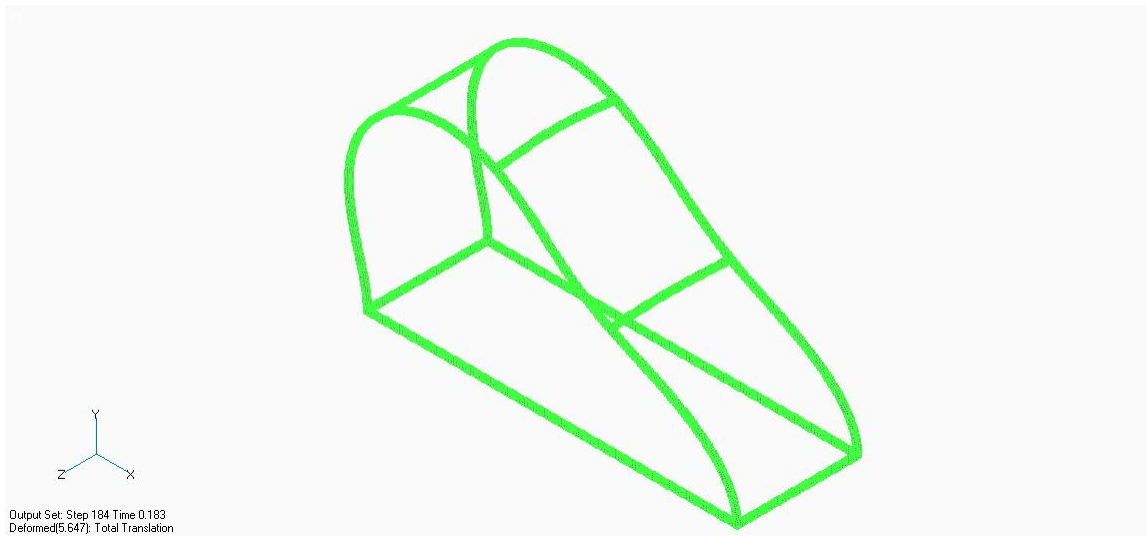


Figure 4.5-2. Arch Deflected Shape for 76.4 psi-ms

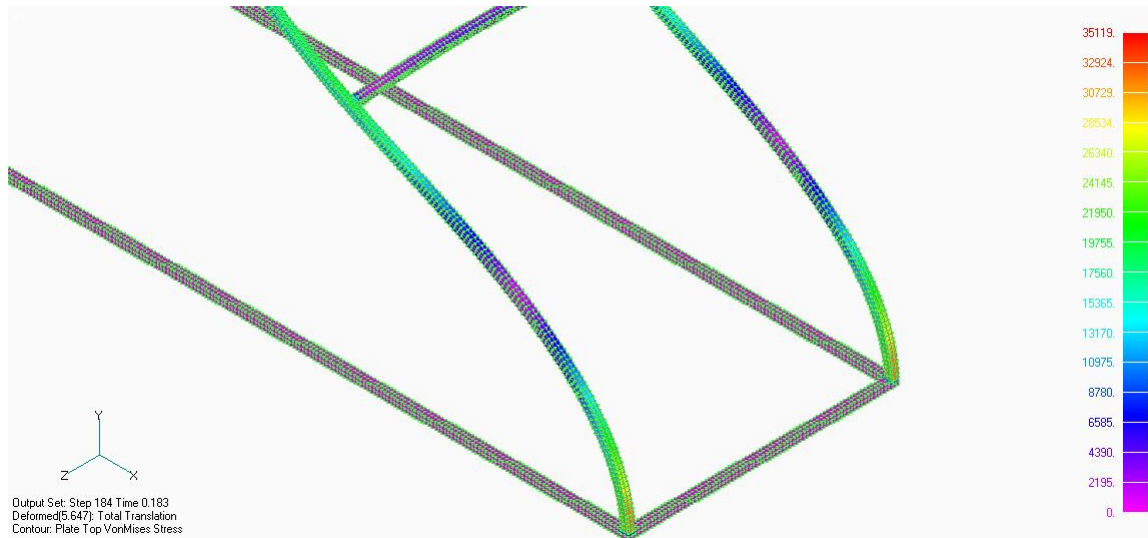


Figure 4.5-3. Arch Stress Distribution for 76.4 psi-ms

4.6 55.0 psi-ms Results ft

Results for this load case are shown in Figures 4.6-1 and 4.6-2. As seen in Figure 4.6-1, maximum deflection in the structure was approximately 6.0 inches, which falls in the minor damage category and correlates to the damage predicted by the test report curve. Figure 4.6-2 provides an image of the deformed shape of the structure at approximately 3.9 inches of purlin deflection, while Figure 4.6-3 provides a stress contour of the structure at approximately 3.9 inches of deflection, which corresponds to the maximum deflection for the first peak of the deflection curve. As can be seen in Figure 4.6-3, the maximum stress at the base of the structure is less than the material yield stress.

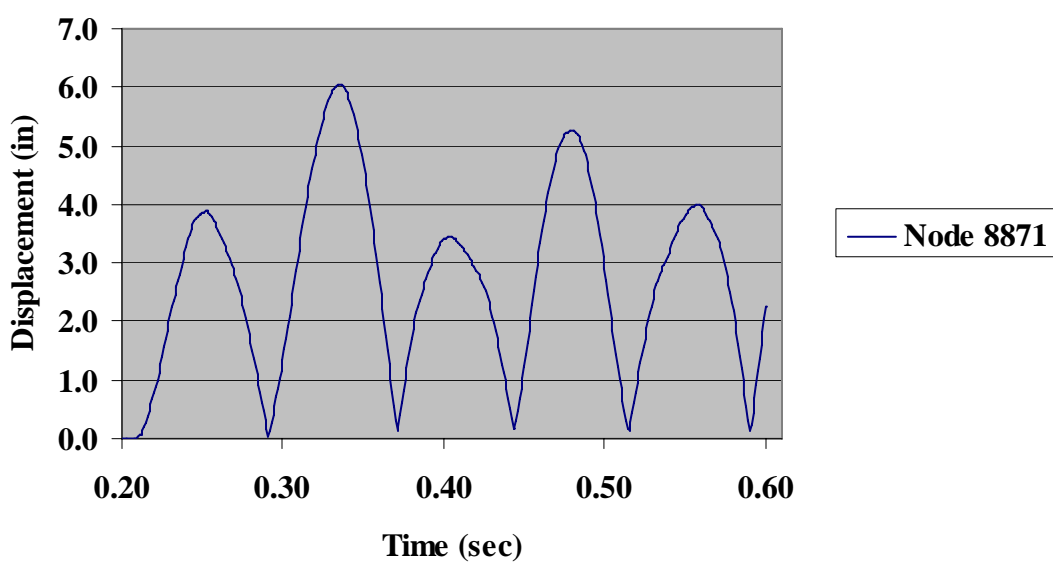


Figure 4.6-1. Purlin Translation for 55.0 psi-ms

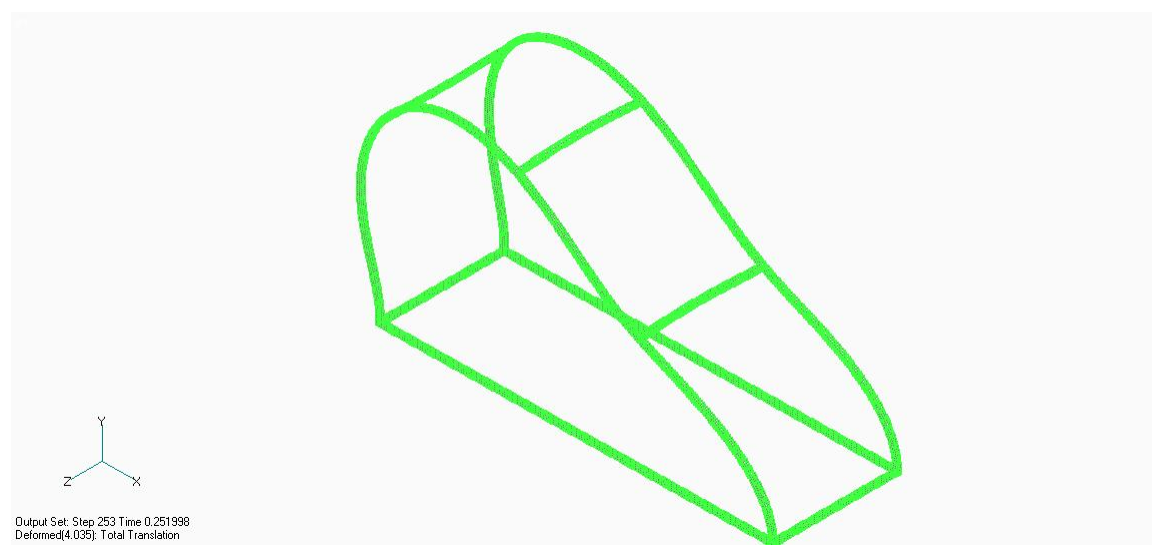


Figure 4.6-2. Arch Deflected Shape for 55.0 psi-ms

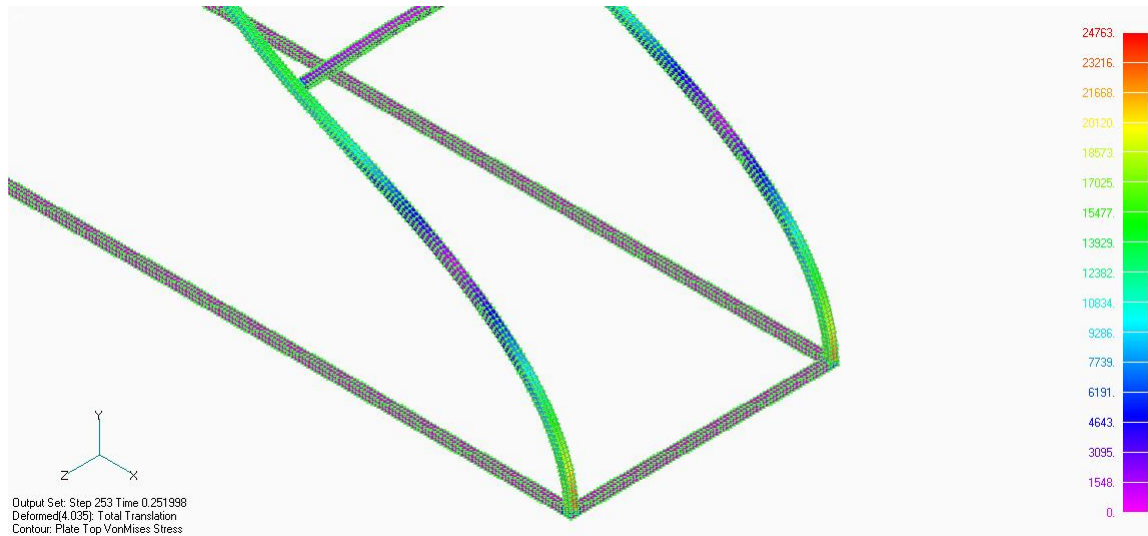


Figure 4.6-3. Arch Stress Distribution for 55.0 psi-ms

4.7 32.2 psi-ms Results

Results for this load case are shown in Figures 4.7-1 and 4.7-2. As seen in Figure 4.7-1, maximum deflection in the structure was approximately 3.4 inches, which falls in the no damage category and is slightly below the result presented in the test report and in line with the damage predicted by the test report curve presented. Figure 4.7-2 provides an image of the deformed shape of the structure at approximately 2.2 inches of purlin deflection, while Figure 4.7-3 provides a stress contour of the structure at approximately 2.2 inches of deflection, which corresponds to the maximum deflection for the first peak of the deflection curve. As seen in Figure 4.7-3, the maximum stress at the base of the structure is less than the material yield stress.

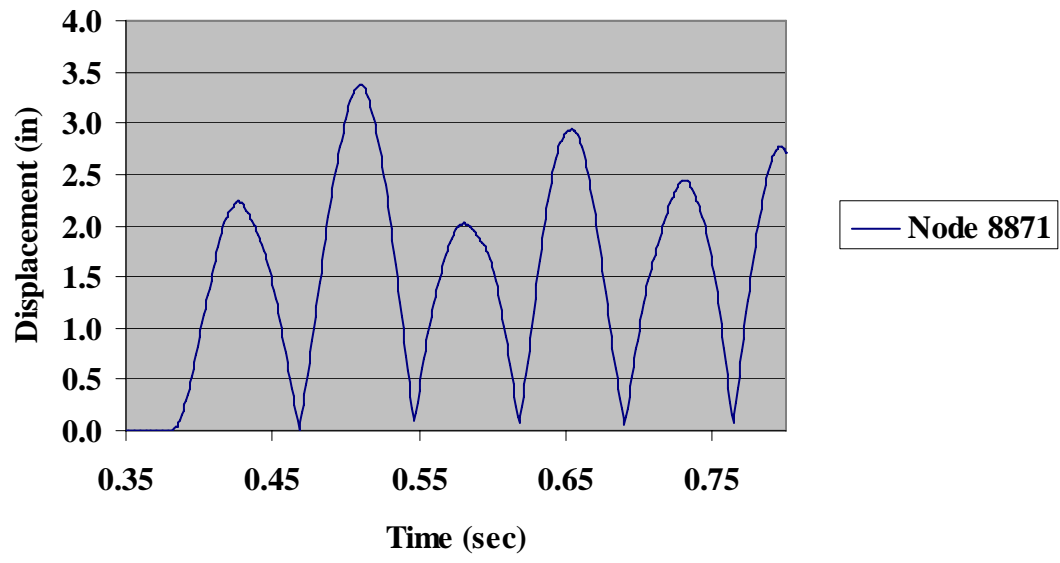


Figure 4.7-1. Purlin Translation for 32.2 psi-ms

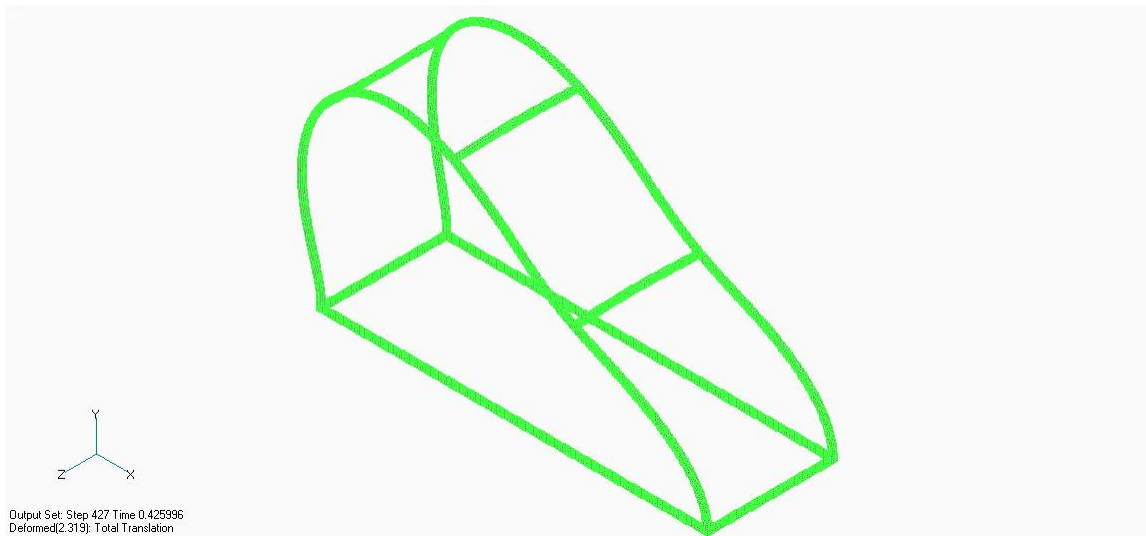


Figure 4.7-2. Arch Deflected Shape for 32.2 psi-ms

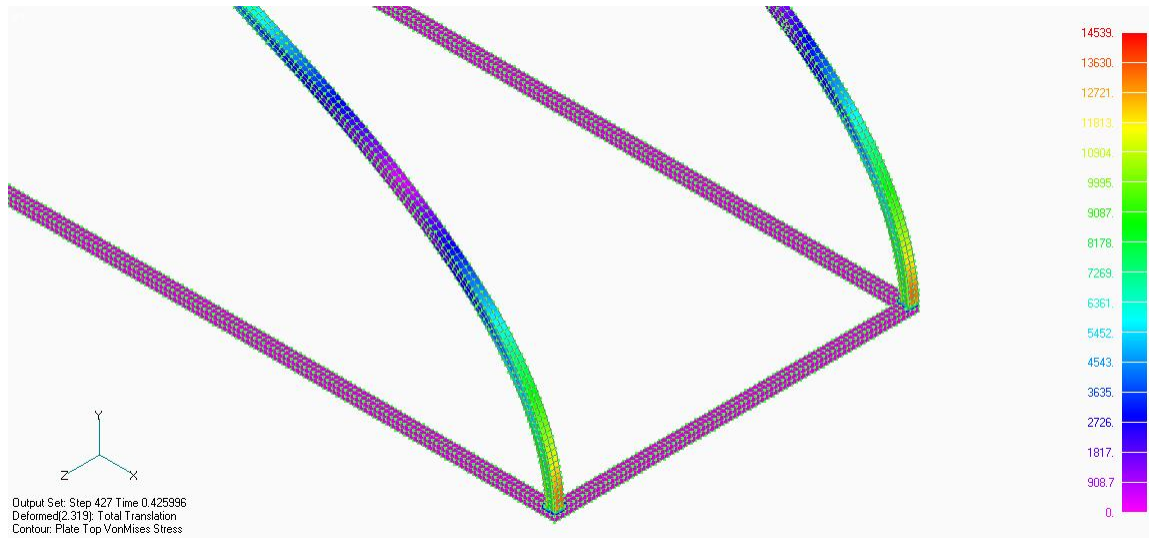


Figure 4.7-3. Arch Stress Distribution for 32.2 psi-ms

4.8 111.0 psi-ms Results

Results for this load case are shown in Figures 4.8-1 and 4.8-2. This load was chosen to represent an impulse load that should fall into the failure mode when one uses the test report prediction curve. As seen in Figure 4.8-1, maximum deflection in the structure was approximately 6.8 inches, which falls in the minor damage category and is below the damage predicted by the test report curve. Figure 4.8-2 provides an image of the deformed structure at maximum deflection, while Figure 4.8-3 provides a stress contour of the base of the structure at maximum deflection. As shown in Figure 4.8-3, the maximum stress in the structure does exceed the material yield stress.

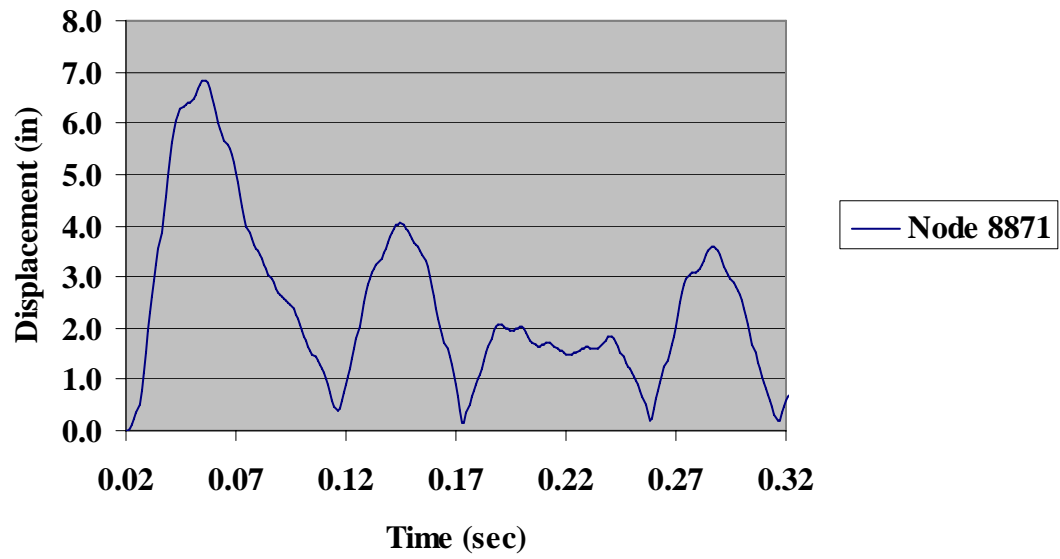


Figure 4.8-1. Purlin Translation for 111.0 psi-ms

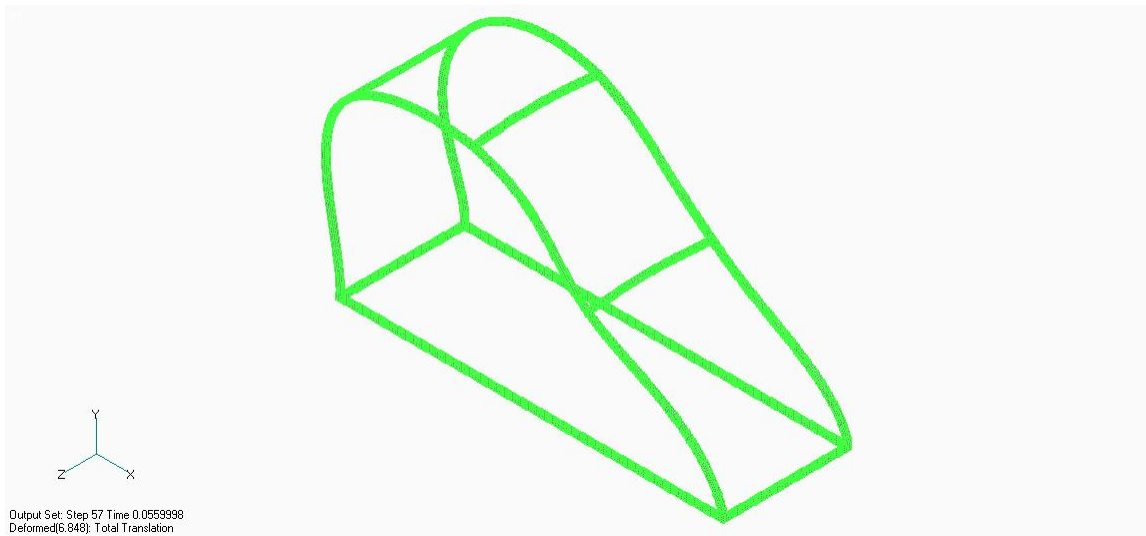


Figure 4.8-2. Arch Deflected Shape for 111.0 psi-ms

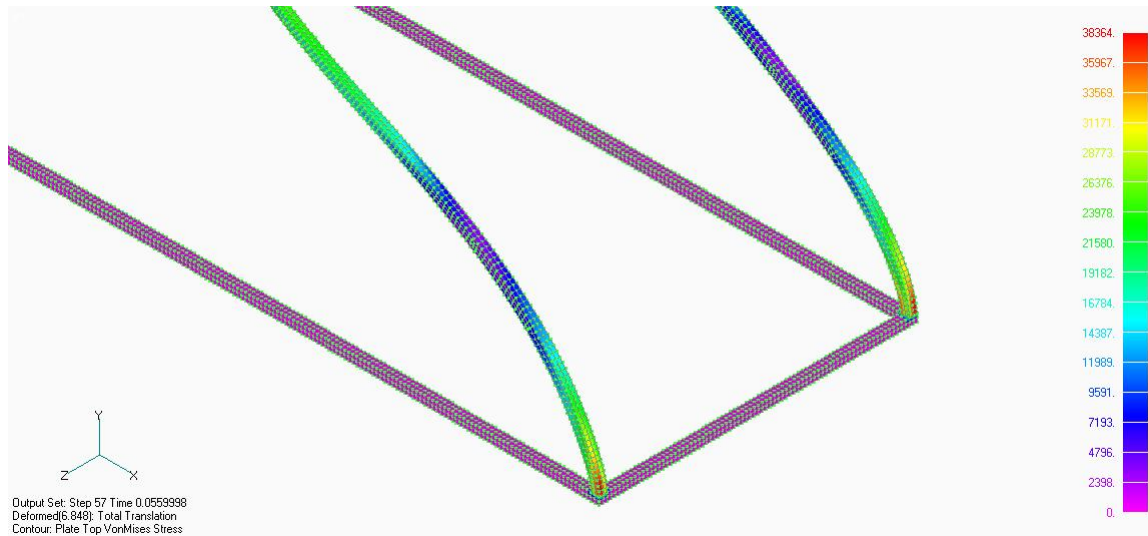


Figure 4.8-3. Arch Stress Distribution for 111.0 psi-ms

4.9 24.7 psi-ms Results

Results for this load case are shown in Figures 4.8-1 and 4.8-2. This load was chosen to represent an impulse load that should fall into the minor damage region when using the test report prediction curve. As shown in Figure 4.9-1, maximum deflection in the structure was approximately 3.1 inches, which falls in the no damage category and is in line with the damage predicted by the test report curve, since the cutoff between no damage and minor damage is 4.0 inches. Figure 4.9-2 provides an image of the deformed shape of the structure at approximately 1.7 inches of purlin deflection, while Figure 4.9-3 provides a stress contour of the structure at approximately 1.7 inches of deflection, which corresponds to the maximum deflection for the first peak of the deflection curve. As can be seen in Figure 4.9-3, the maximum stress at the base of the structure is less than the material yield stress.

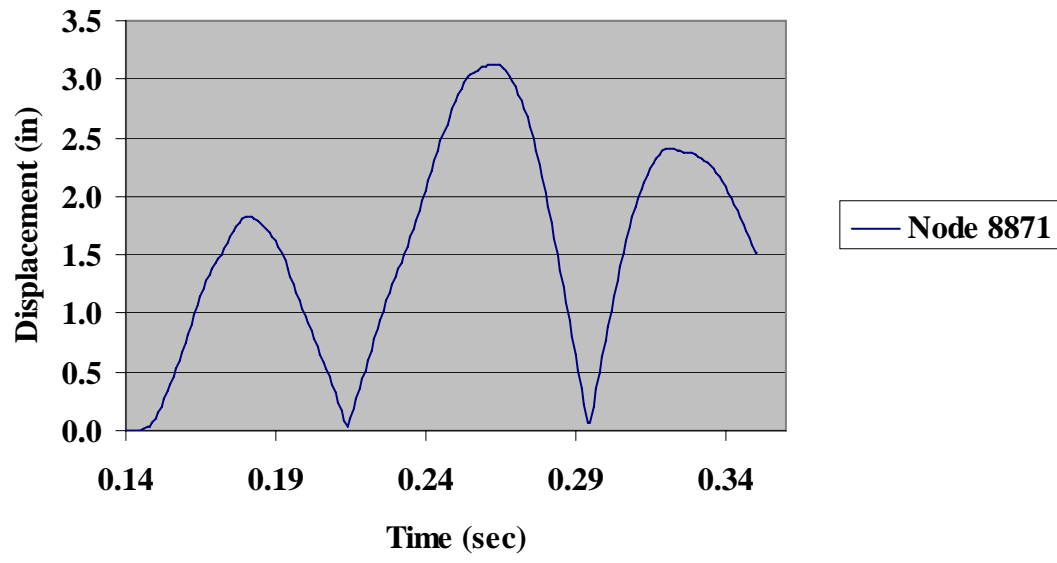


Figure 4.9-1. Purlin Translation for 24.7 psi-ms

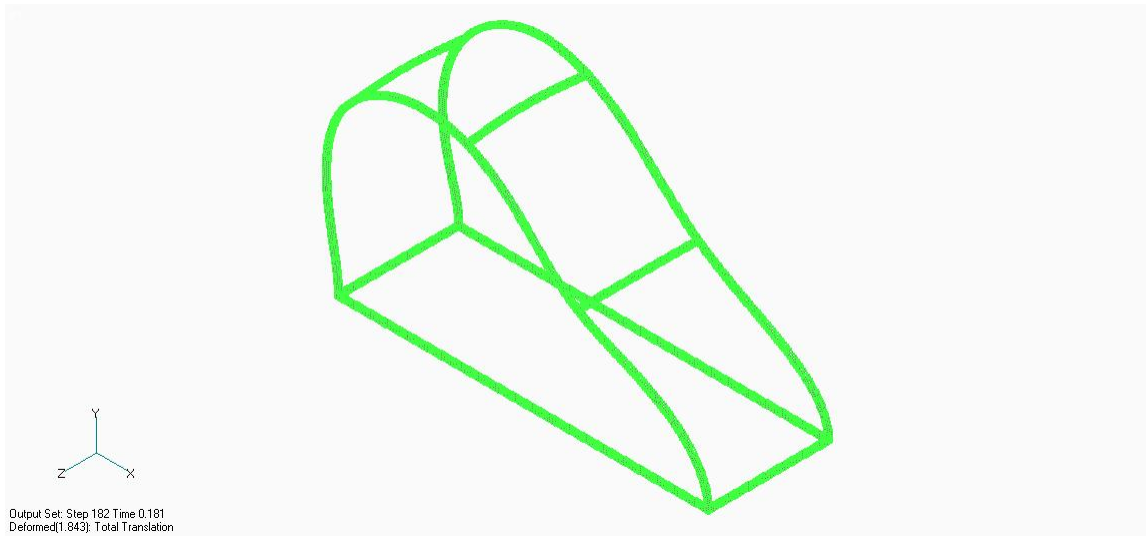


Figure 4.9-2. Arch Deflected Shape for 24.7 psi-ms

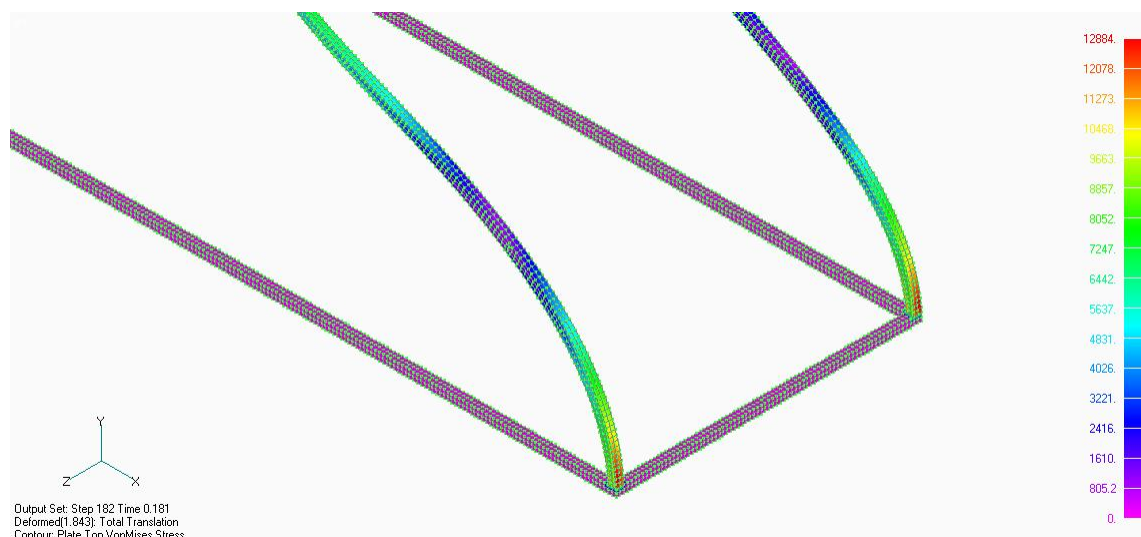


Figure 4.9-3. Arch Stress Distribution for 24.7 psi-ms

4.10 116.8 psi-ms Results

Results for this load case are shown in Figures 4.10-1 and 4.10-2. This load was chosen to represent an impulse load that should fall into the failure mode when utilizing the test report prediction curve. As shown in Figure 4.10-1, maximum deflection in the structure was approximately 8.0 inches, which falls in the minor damage category and is less than the damage predicted by the test report curve. Figure 4.10-2 provides an image of the deformed structure at maximum deflection, while Figure 4.10-3 provides a stress contour of the base of the structure at maximum deflection. As shown in Figure 4.10-3, the maximum stress in the structure does exceed the material yield stress.

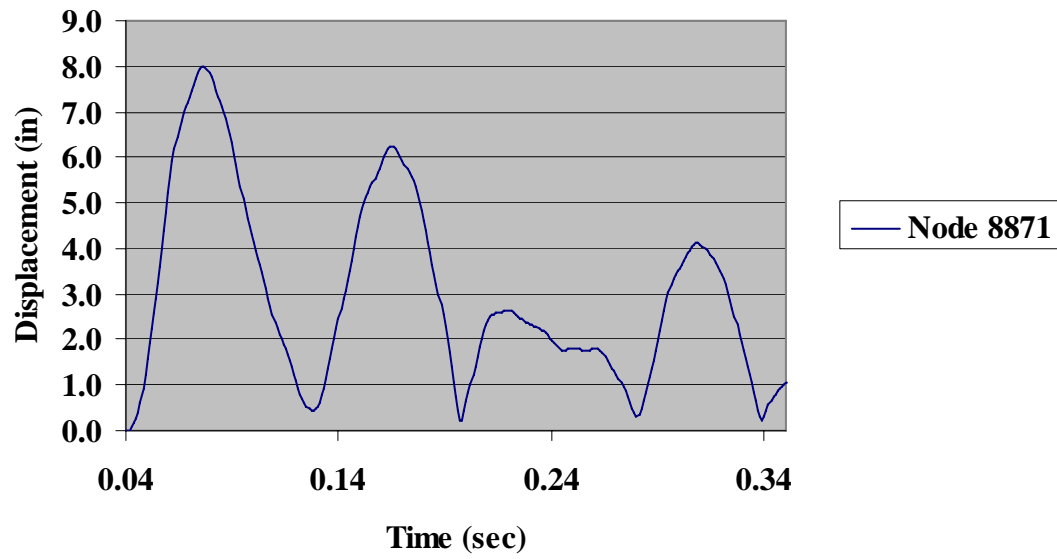


Figure 4.10-1. Purlin Translation for 116.8 psi-ms

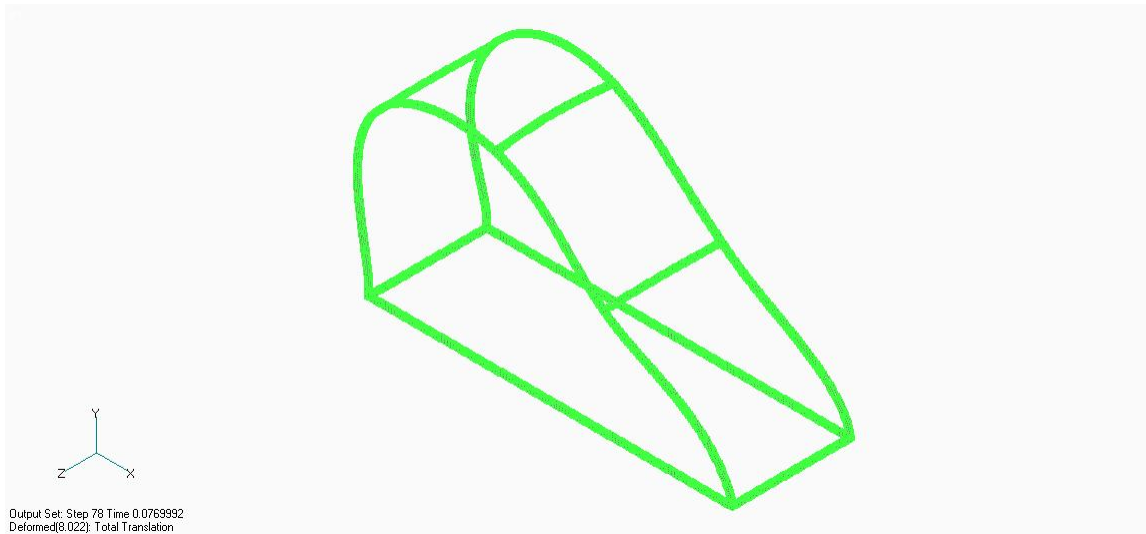


Figure 4.10-2. Arch Deflected Shape for 116.8 psi-ms

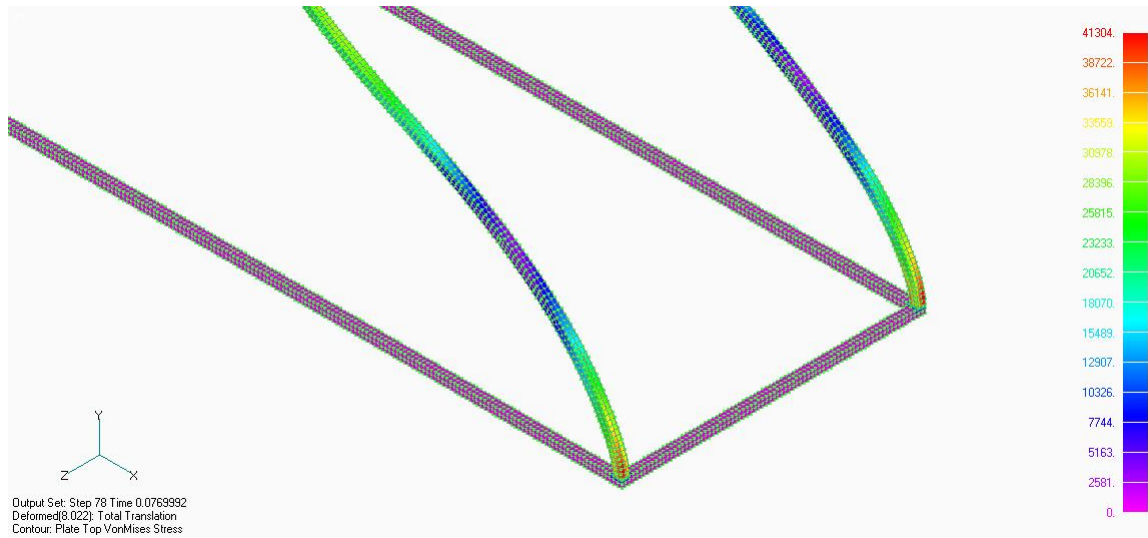


Figure 4.10-3. Arch Stress Distribution for 116.8 psi-ms

4.11 33.1 psi-ms Results

Results for this load case are shown in Figures 4.11-1 and 4.11-2. This load was chosen to represent an impulse load that should fall into the minor damage region when using the test report prediction curve. As shown in Figure 4.11-1, maximum deflection in the structure was approximately 4.0 inches, which falls in the minor damage category and is in line with the damage predicted by the test report curve. Figure 4.11-2 provides an image of the deformed shape of the structure at approximately 2.4 inches of purlin deflection, while Figure 4.11-3 provides a stress contour of the structure at approximately 2.4 inches of deflection, which corresponds to the maximum deflection for the first peak of the deflection curve. As shown in Figure 4.11-3, the maximum stress at the base of the structure is less than the material yield stress.

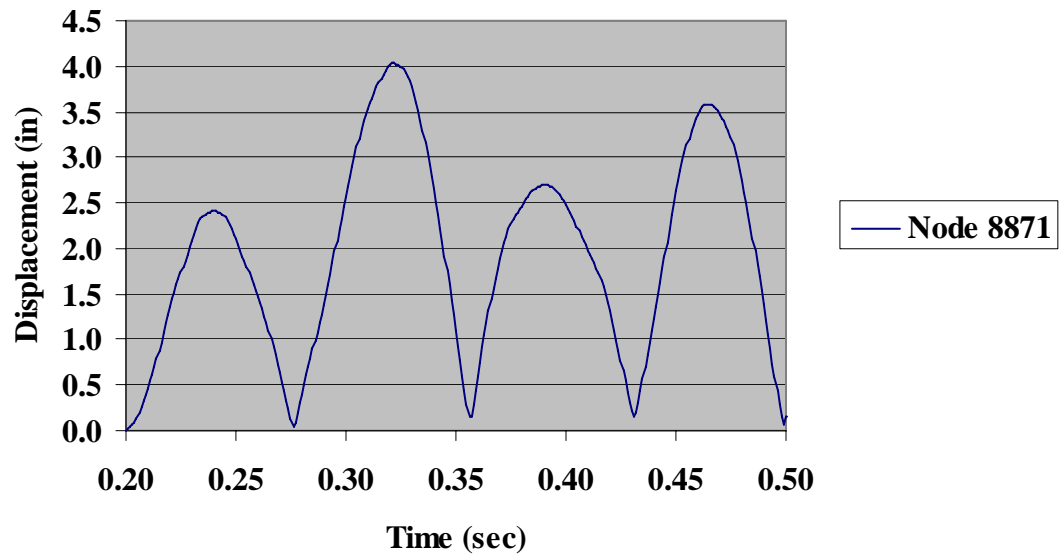


Figure 4.11-1. Purlin Translation for 33.1 psi-ms

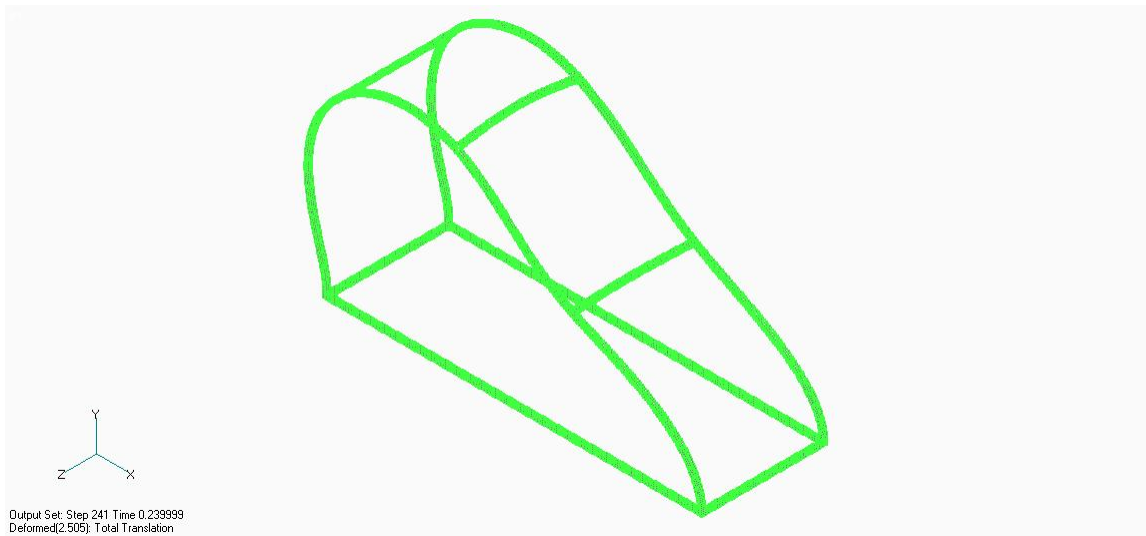


Figure 4.11-2. Arch Deflected Shape for 33.1 psi-ms

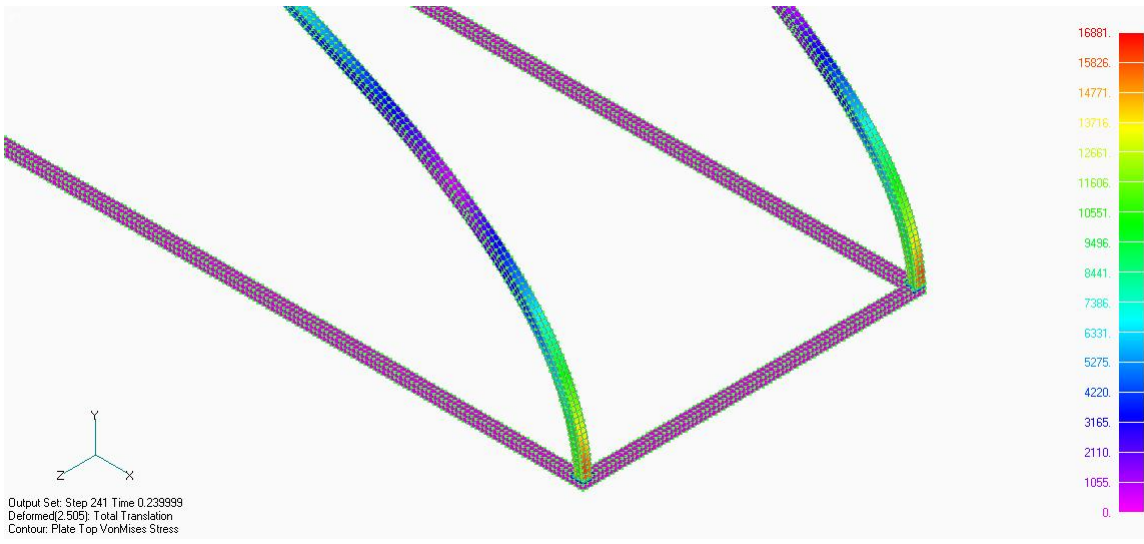


Figure 4.11-3. Arch Stress Distribution for 33.1 psi-ms

5.0 SDOF MODEL VERIFICATION

The goal of this analysis was to develop a simplified model that may be used to predict deflection of the structure under various impulse loadings. A single-degree-of-freedom dynamic model will be used in this effort. Section 5.1 provides an analytical development of the SDOF model.

5.1 SDOF Analytical Development

Equation 5.1.1 provides the basic equation of motion for a single-degree-of-freedom system with the included terms defined.

$$M_e \ddot{y}(t) + C_e \dot{y} + K_e y(t) = F_e(t) \quad 5.1.1$$

M_e = equivalent mass of the SDOF model

$\ddot{y}(t)$ = acceleration of the system

C_e = equivalent damping of the system

$\dot{y}(t)$ = velocity of the system

K_e = equivalent stiffness of the system

$y(t)$ = displacement of the system

$F_e(t)$ = equivalent load applied to the system as a function of time

The analysis approach is designed to provide a maximum predicted static deflection at the purlin interface of the structure. Damping in this model does play a role

in the initial deflection and will be considered zero for this analysis. Therefore, equation 5.1.1 reduces to equation 5.1.2.

$$M_e \ddot{y}(t) + K_e y(t) = F_e(t) \quad 5.1.2$$

The equivalent mass, M_e , of the SDOF system representing a system with continuous mass distribution, m , is given by Biggs in Equation 5.1.3.

$$M_e = \int^l m \phi^2(x) dx \quad 5.1.3$$

The mass factor K_m is defined as the ratio of the equivalent mass to the actual total mass of the structure.

$$K_m = \frac{M_e}{M_t} \quad 5.1.4$$

In the case of a beam with a constant mass along its length, $M_t = mL$, and M_e is given by equation (5.1.3); therefore, the mass factor is given by equation 5.1.5.

$$K_m = m \int^L m \phi^2(x) \frac{dx}{m(L)} = \frac{1}{L} \int^L m \phi^2(x) dx \quad 5.1.5$$

The equivalent force is given by equation 5.1.6.

$$F_e = \int^L w(x) \phi(x) dx \quad 5.1.6$$

The load factor, K_L , is then defined as the ratio of the equivalent force to the actual force of $F_t = w(x)L$, which for a uniform load becomes $F_t = wL$.

$$K_L = \frac{F_e}{F_t} = \int^L w(x) \phi(x) \frac{dx}{w(L)} = \frac{1}{L} \int^L \phi(x) dx \quad 5.1.7$$

Biggs defines the resistance of an element, R , as the internal force restoring the element to its unloaded static position, and defines it in terms of the load distribution for which the analysis is being made (Biggs, 1964). The stiffness of the element is therefore simply the ratio of the rate of resistance to the incremental change in deflection, equation 5.1.8.

$$K = \frac{\Delta R}{\Delta y} \quad \text{and} \quad K_e = \frac{\Delta R_e}{\Delta y} \quad 5.1.8$$

For the beam to be in equilibrium, resistance must always be equal to the force.

$$\frac{F_e}{F_t} = \frac{R_e}{R_t}$$

$$K_L = \frac{K_e}{K_y}(y) \quad 5.1.9$$

Biggs introduces one final factor, which is K_{LM} , the load-mass factor, in order to simplify the equation of motion in terms of that factor alone. K_{LM} is defined as the ratio of the mass factor to the load factor. Equation 5.1.2 may now be written in terms of the real system with transformation factors, Equations (5.1.4), (5.1.7), and (5.1.9).

$$K_m M_t \ddot{y}(t) + K_L K y(t) = K_L F(t)$$

Dividing this equation by K_L we arrive at:

$$\frac{K_m M_t}{K_L} \ddot{y}(t) + K y(t) = F(t) \quad M_t = \text{Total mass of system} = m L$$

By calling K_{LM} (load-mass factor) = $\frac{K_m}{K_L}$, we arrive at our final equation of motion,

Equation (5.1.10).

$$K_{LM} M_t \ddot{y}(t) + K y(t) = F(t) \quad 5.1.10$$

The natural period, T , of the system is given by (Biggs, 1964).

$$T = 2\pi \left[\frac{K_{LM} M_t}{K} \right]^{\frac{1}{2}}$$

Since the resistance of the system $R y = K y$, the equation of motion in terms of the resistance of the system is shown is Equation 5.1.11.

$$K_{LM} M_t \ddot{y}(t) + R [y(t)] = F_t \quad \text{or} \quad \ddot{y}(t) = \frac{F_t}{K_{LM} M_t} - \frac{R[y(t)]}{K_{LM} M_t} \quad 5.1.11$$

Where

K_{LM} = constant that depends on the shape function of the applicable behavior region.

This equation of motion can now be solved numerically for $y(t)$, which gives the total motion-time history of the mass in the idealized system, and is the same as the transverse purlin deflection-time history. The appropriate transformation factors and element stiffness values are applied during the various stages of analysis. The equation of motion can be solved by direct numerical integration. Several numerical integration schemes are described by Biggs (1964), including the constant velocity procedure, the linear acceleration method, the Newmark β method, and several finite difference methods. The Newmark β method is a very versatile method for solving differential equations incrementally. The central difference method corresponds to a Newmark time scheme with parameter values $\beta=0$ and $\gamma = 1/2$. The central difference formula relates the acceleration, \ddot{y}_t at time t to the displacement $y_{t-\Delta t}$, y_t , and $y_{t+\Delta t}$ corresponding to displacement at times $t - \Delta t$, t , and $t + \Delta t$, respectively, according to Equation 5.1.12.

$$\ddot{y} = \frac{[y_{t-\Delta t} - 2y_t + y_{t+\Delta t}]}{\Delta t^2} \quad 5.1.12$$

Substituting Equation (5.1.12) into Equation (5.1.11) and rearranging to solve for $y_{t+\Delta t}$ in terms of $y_{t-\Delta t}$ and y_t yields.

$$y_{t+\Delta t} = \frac{F_t \Delta t^2}{K_{LM} M_t} + \left[\frac{2 - R_y \Delta t^2}{K_{LM} M_t} \right] y_t - y_{t-\Delta t} \quad 5.1.13$$

The central difference method is an explicit time scheme because the unknown \ddot{y}_n is only a function of known values. Equation 5.1.13 allows for the displacement at the next time increment $y_{t+\Delta t}$ to be calculated in terms of system constants and the current and previous displacement values $y_{t-\Delta t}$ and y_t . Note that F_t is non-zero only when load is being applied to the structure and that R_y is a function of the displacement.

5.2 SDOF Model Term Definition and Calculation

Equation 5.1.13 provides the equation of motion for a SDOF model that is used to represent the system. This equation was programmed into the Microsoft spreadsheet program Excel. The terms included in the SDOF are defined and calculated below for inclusion into the SDOF model.

5.2.1 Applied Force (F_t)

F_t is the forcing function applied to the structure as a function of time. The applied force used in the SDOF is derived from the overpressure and time duration calculated by using a spreadsheet program based on the CONWEP Program. This spreadsheet calculated the reflected pressure and time duration based on charge size in pounds of TNT and the distance the charge is located from the structure. The reflected pressure is then multiplied by the exposed area to derive the applied force. Exposed area was calculated as the area of the structure facing the charge with the area reduced by the same function as used to reduce the applied force in the static resistance function calculation.

$$\text{Area of one arch} = r * (\theta) * (2 \text{ inches}) = 120 \text{ inches} (1.57 \text{ rad}) * (2 \text{ inches}) 376.8 \text{ in}^2$$

The distribution of the above area using equation 3.1 yields an effective area of 188.4 in². Therefore, the two arches have a total effective area of 376.8 in². In addition to this area, the area of the two cross members will be added to the exposed area.

$$\text{Cross member area (CMS)} = (2 \text{ members}) (80 \text{ inches})(2 \text{ inches})$$

$$\text{CMA} = 320 \text{ in}^2$$

$$\text{Total exposed area} = 320 \text{ in}^2 + 376.8 \text{ in}^2$$

$$\text{Total exposed area} = 696.8 \text{ in}^2$$

$$F_t = (\text{reflected pressure})(696.8 \text{ in}^2)$$

5.2.1.1

5.2.2 Adjusted Time

The load in the SDOF is applied as a right triangle beginning at the maximum load as calculated in section 5.2.1 and decreasing to zero in a linear manner. Since the area under this right triangle should be equivalent to the reflected impulse (RI), the time duration of the load application is adjusted to create an equivalent area according to equation 5.2.2.1.

$$\text{Adjusted Time} = \left(\frac{2 * RI}{F_t} \right) \quad 5.2.2.1$$

5.2.3 Load Mass Factor (K_{LM})

The load mass factor is a constant that depends on the shape function of the applicable behavior region. For this effort, K_{LM} is assumed to be the mass participation factor in the x direction from the modal analysis of the structure as described in section 2.0. The x axis is the primary axis of movement in the impulse loading simulation, which is why this participation factor was chosen. Therefore, $K_{LM} = 0.47$.

5.2.4 System Mass (M_t)

M_t is simply the total mass of the system. For the subject system, the system weight is 123.5 lbs; therefore, $M_t = 123.5 \text{ lbs} / 386.1 \text{ in/sec}^2 = 0.32 \text{ lb-sec}^2/\text{in}$. This final weight excludes the weight of the base restraints in the model.

6.0 ANALYSIS CHARTS

The SDOF derivation described in Section 5.0 is implemented in the 11 analyses described in this report using the parameters shown in Table 6.0-1.

Table 6.0-1. SDOF Input Parameters

Reflected Pressure (psi)	Reflected Impulse (psi-ms)	Adjusted Time Duration (ms)
33.7	81.1	4.8
15.9	55.7	7.0
6.0	30.5	10.2
7.7	94.8	24.6
5.6	76.4	27.2
3.6	55.0	30.6
1.8	32.2	35.8
30.0	111.0	7.4
2.8	24.7	17.6
18.0	116.8	13.0
2.7	33.1	24.5

The inclusion of these parameters resulted in the SDOF results shown in Table 6.0-2, which provides the results from the SDOF model as well as the LS-DYNA model such that the two may be compared. In addition to the tabular comparison, the following subsections provide graphical comparisons of the results from the two methods.

Table 6.0-2. LS-DYNA/SDOF Results Comparison

Impulse (psi-ms)	LS-DYNA Displacement (in)	SDOF Displacement (in)
81.1	4.3	5.3
55.7	3.5	3.5
30.5	3.5	1.8
94.8	10.1	6.1
76.4	8.5	4.5
55.0	6.0	3.2
32.2	3.4	2.2
111.0	6.8	7.1
24.7	3.1	1.5
116.8	8.0	7.9
33.1	4.0	1.9

6.1 81.1 psi-ms

Initial Conditions	
Area Exposed (in²)	696.8
Reflected Impulse (psi-ms)	81.1
Delta t (sec)	0.0001
Mt (lb.sec²/in)	0.32
KLMe	0.47
KLMP	0.47
Reflected Pressure (psi)	33.7
F₀ (lb)	23,482.00
Adjusted Time (sec)	0.0048
Kelastic (lb/in)	552
K plastic (lb/in)	485
K plastic (lb/in)	387
ye elastic limit (in)	2.32
yp plastic (in)	4.63

Figure 6.1-1. Initial Conditions

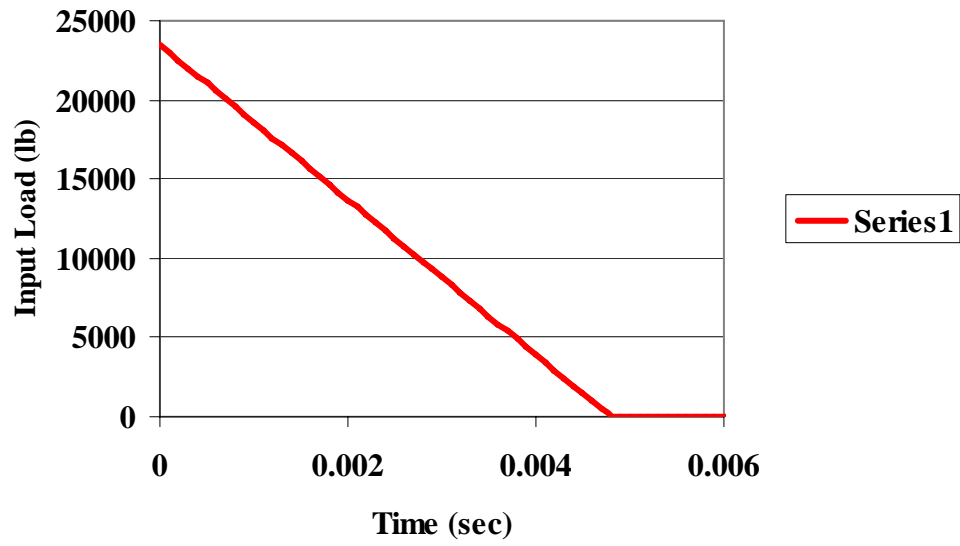


Figure 6.1-2. Load Distribution

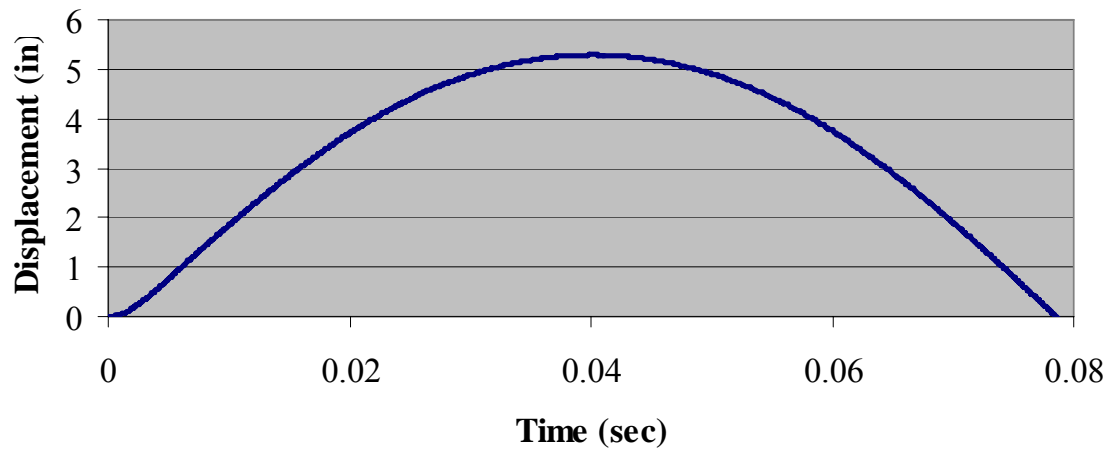


Figure 6.1-3. Displacement with Reflected Impulse of 81.1 psi-ms

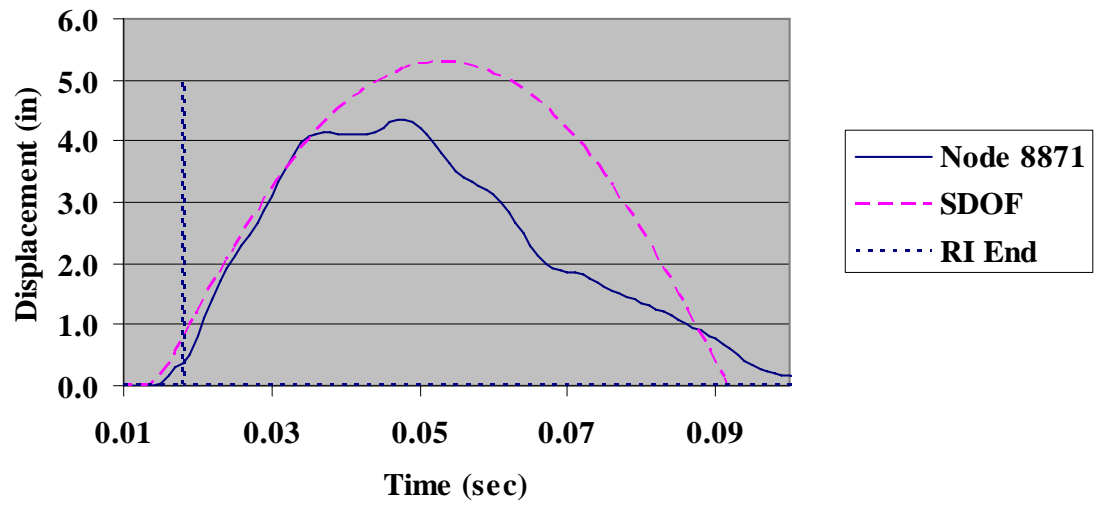


Figure 6.1-4 SDOF/LS-DYNA Model Displacement Comparison

6.2 55.7 psi-ms

Initial Conditions	
Area Exposed (in ²)	696.8
Reflected Impulse (psi-ms)	55.7
Delta t (sec)	0.0001
Mt (lb.sec ² /in)	0.32
KLMe	0.47
KLMp	0.47
Reflected Pressure (psi)	15.9
F ₀ (lb)	11,079.00
Adjusted Time (sec)	0.007
K elastic (lb/in)	552
K plastic (lb/in)	485
K plastic (lb/in)	387
ye elastic limit (in)	2.32
yp plastic (in)	4.63

Figure 6.2-1. Initial Conditions

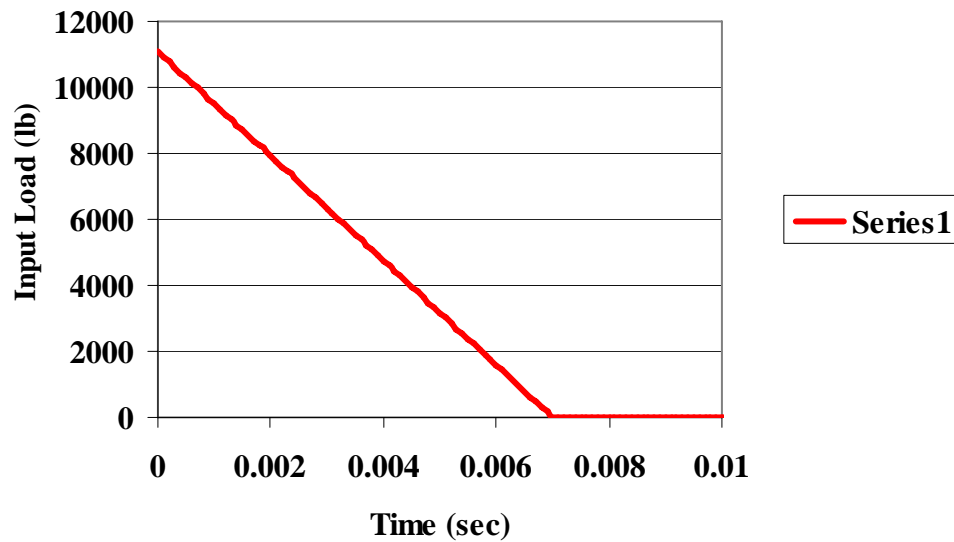


Figure 6.2-2. Load Distribution

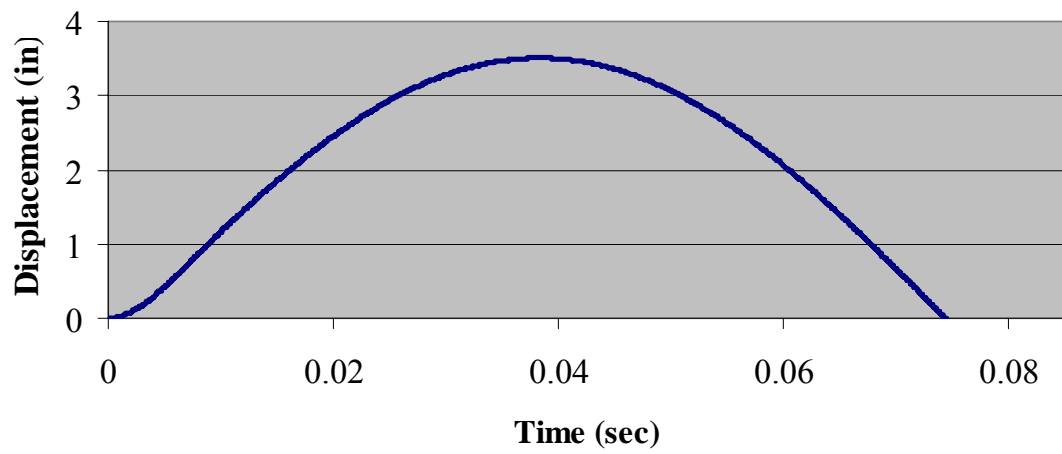


Figure 6.2-3. Displacement with Reflected Impulse of 55.7 psi-ms

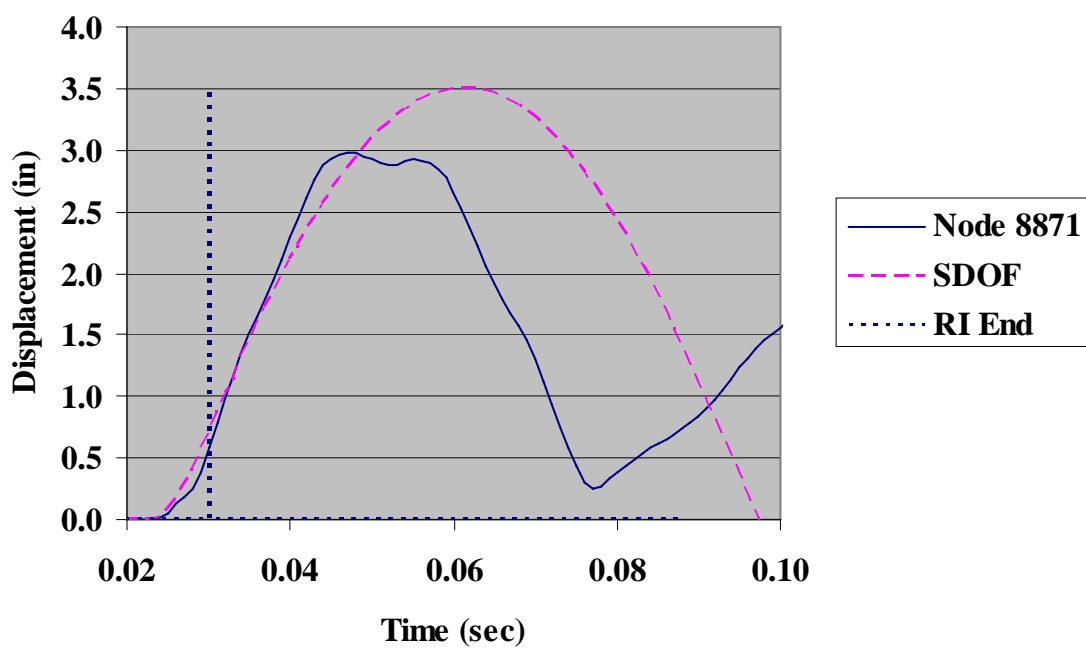


Figure 6.2-4 SDOF/LS-DYNA Model Displacement Comparison

6.3 30.5 psi-ms

Initial Conditions	
Area Exposed (in²)	696.8
Reflected Impulse (psi-ms)	30.5
Delta t (sec)	0.0001
Mt (lb.sec²/in)	0.32
KLMe	0.47
KLMp	0.47
Reflected Pressure (psi)	6.0
F₀ (lb)	4,181.00
Adjusted Time (sec)	0.01
K elastic (lb/in)	552
K plastic (lb/in)	485
K plastic (lb/in)	387
y elastic limit (in)	2.32
yp plastic (in)	4.63

Figure 6.3-1. Initial Conditions

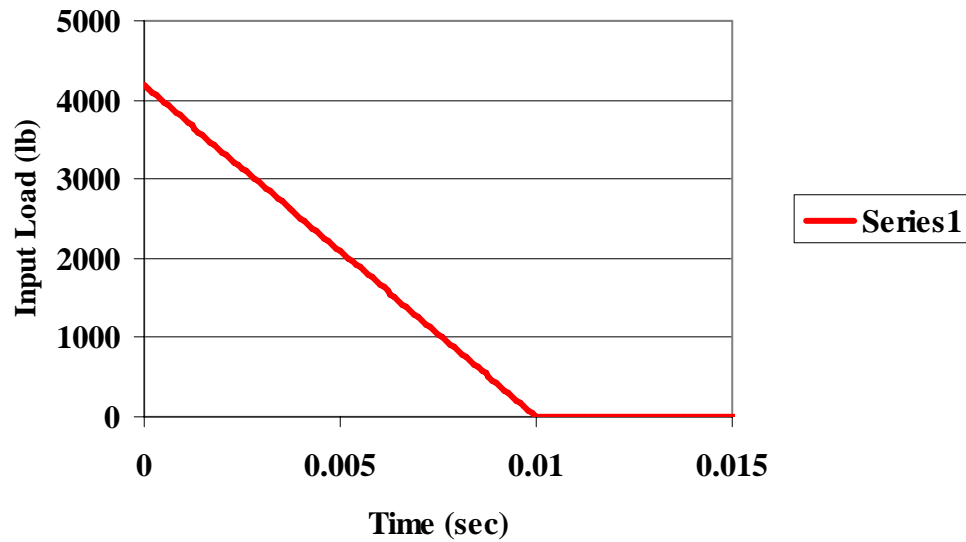


Figure 6.3-2. Load Distribution

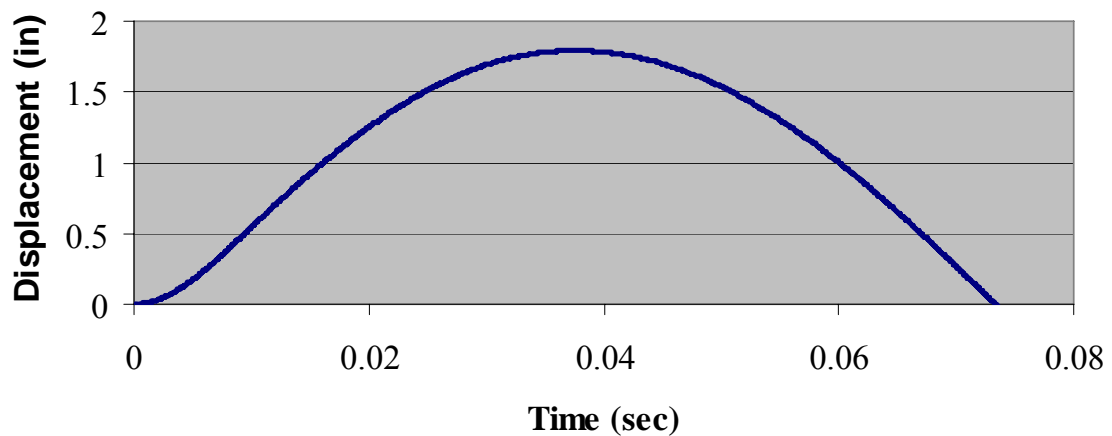


Figure 6.3-3. Displacement with Reflected Impulse of 30.5 psi-ms

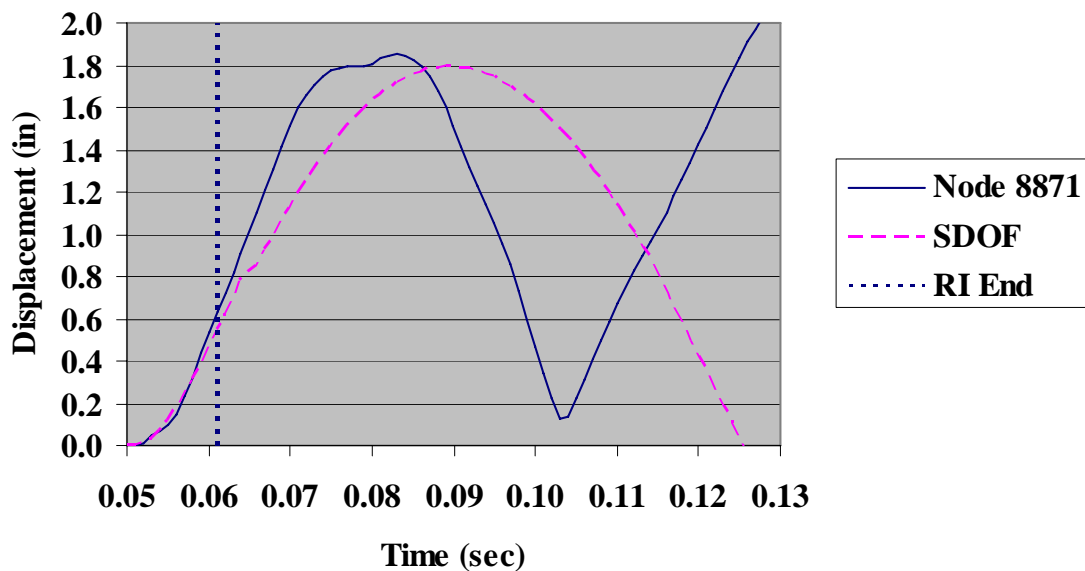


Figure 6.3-4 SDOF/LS-DYNA Model Displacement Comparison

6.4 94.8 psi-ms

Initial Conditions	
Area Exposed	696.8
Reflected Impulse (psi-ms)	94.8
Delta t (sec)	0.0001
Mt (lb.sec ² /in)	0.32
KLMe	0.47
KLMp	0.47
Reflected Pressure (psi)	7.7
F ₀ (lb)	5,365.00
Adjusted Time (sec)	0.025
Kelastic (lb/in)	552
K plastic (lb/in)	485
K plastic (lb/in)	387
y elastic limit (in)	2.32
y plastic (in)	4.63

Figure 6.4-1. Initial Conditions

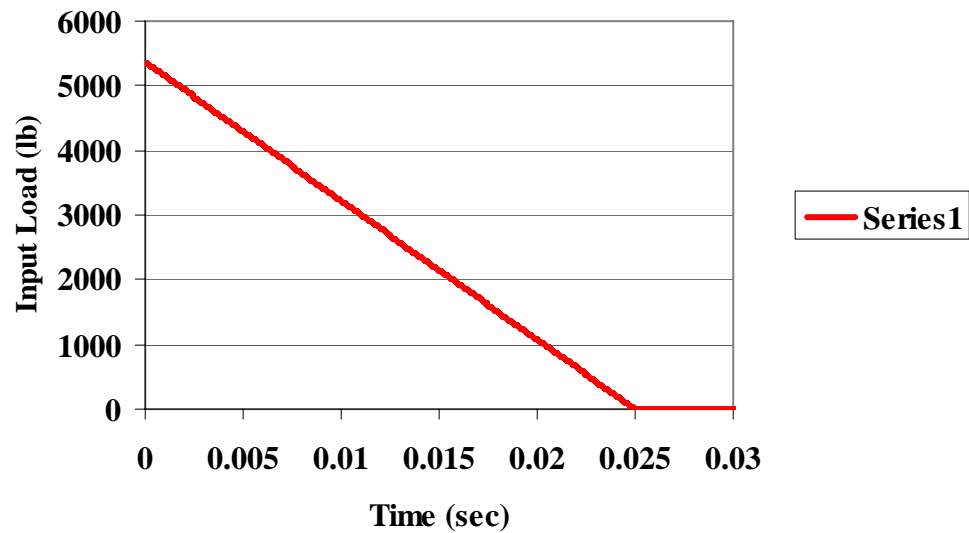


Figure 6.4-2. Load Distribution

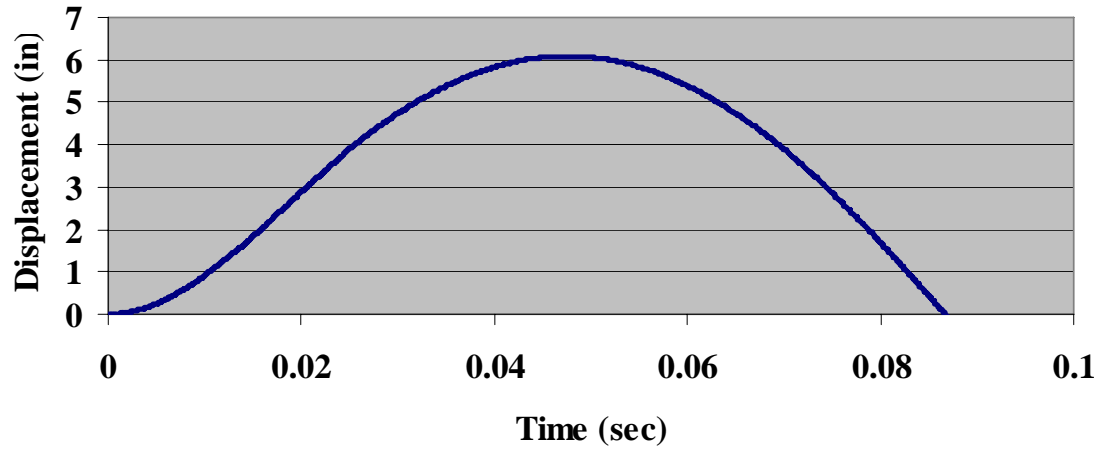


Figure 6.4-3. Displacement with Reflected Impulse of 94.8 psi-ms

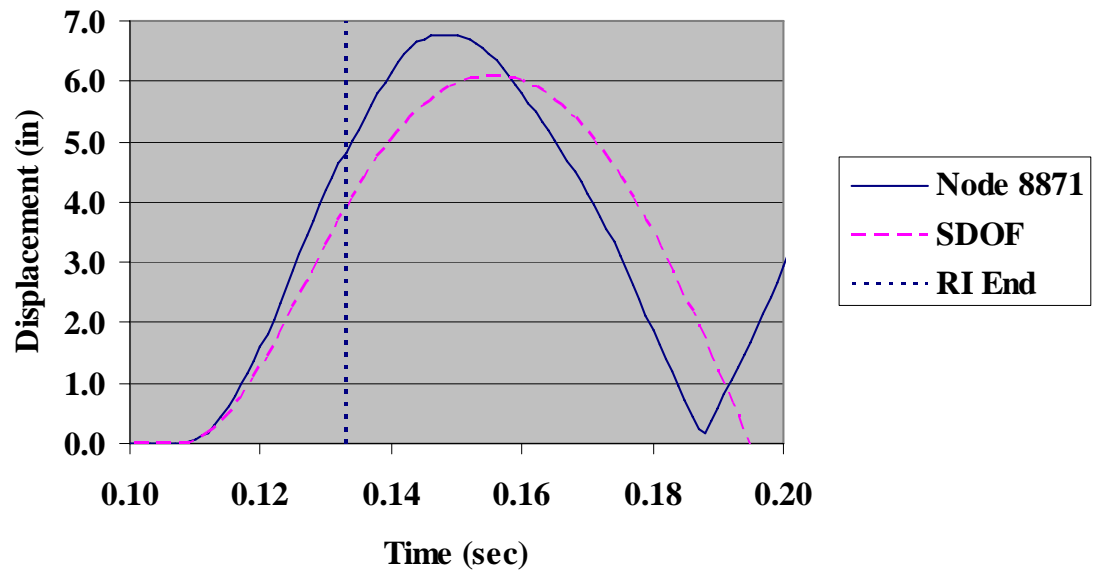


Figure 6.4-4 SDOF/LS-DYNA Model Displacement Comparison

6.5 76.4 psi-ms

Initial Conditions	
Area Exposed (in ²)	696.8
Reflected Impulse (psi-ms)	76.4
Delta t (sec)	0.0001
Mt (lb.sec ² /in)	0.32
KLMe	0.47
KLMP	0.47
Reflected Pressure (psi)	5.6
F ₀ (lb)	3,903.00
Adjusted Time (sec)	0.027
K elastic (lb/in)	552
K plastic (lb/in)	485
K plastic (lb/in)	387
y elastic limit (in)	2.32
y plastic (in)	4.63

Figure 6.5-1. Initial Conditions

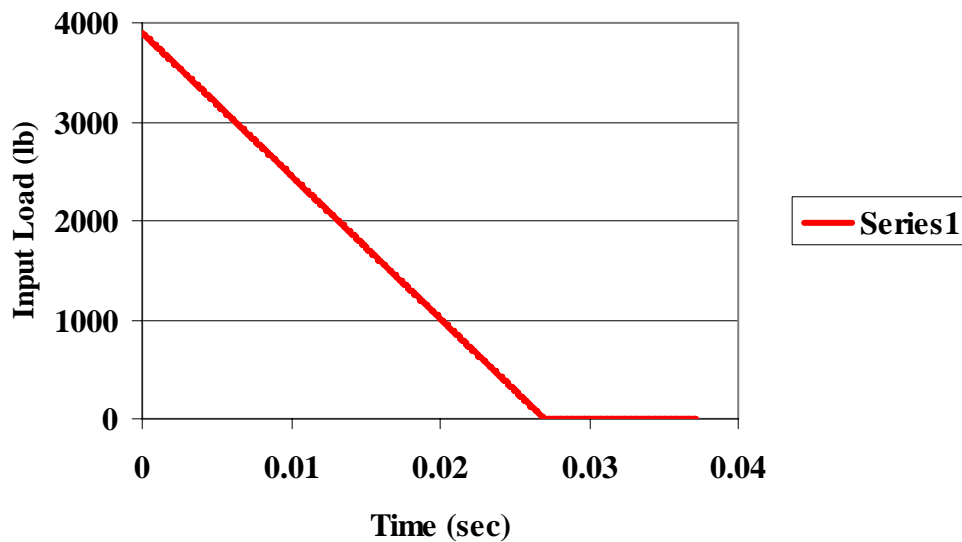


Figure 6.5-2. Load Distribution

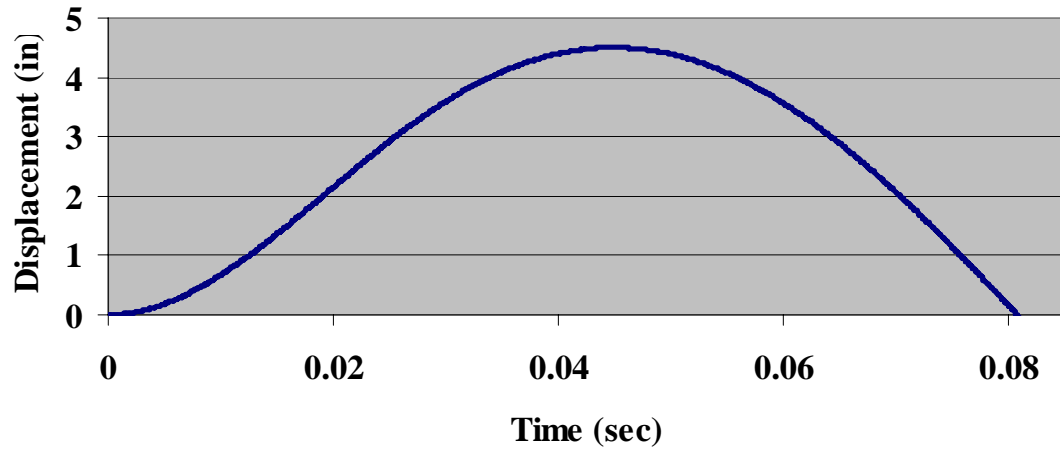


Figure 6.5-3. Displacement with Reflected Impulse of 76.4 psi-ms

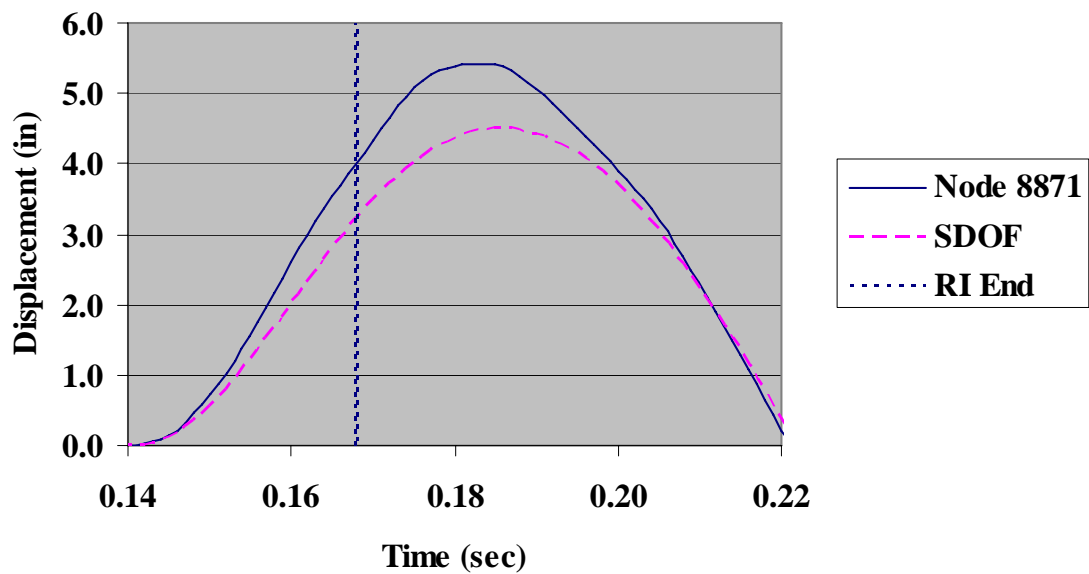


Figure 6.5-4 SDOF/LS-DYNA Model Displacement Comparison

6.6 55.0 psi-ms

Initial Conditions	
Area Exposed (in²)	696.8
Reflected Impulse (psi-ms)	55.0
Delta t (sec)	0.0001
Mt (lb.sec²/in)	0.32
KLMe	0.47
KLMp	0.47
Reflected Pressure (psi)	3.6
F₀ (lb)	2,508.00
Adjusted Time	0.031
Kelastic (lb/in)	552
K plastic (lb/in)	485
K plastic (lb/in)	387
y elastic limit (in)	2.32
y plastic (in)	4.63

Figure 6.6-1. Initial Conditions

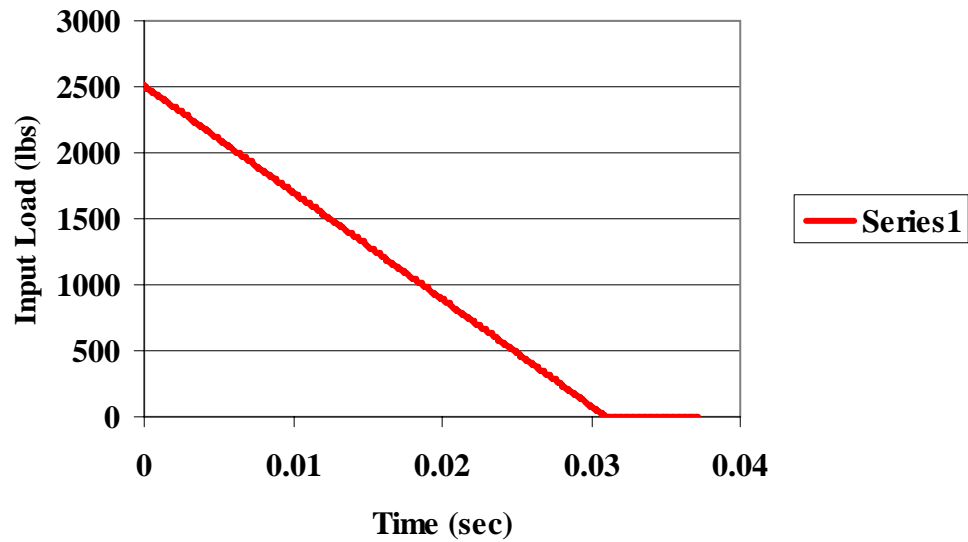


Figure 6.6-2. Load Distribution

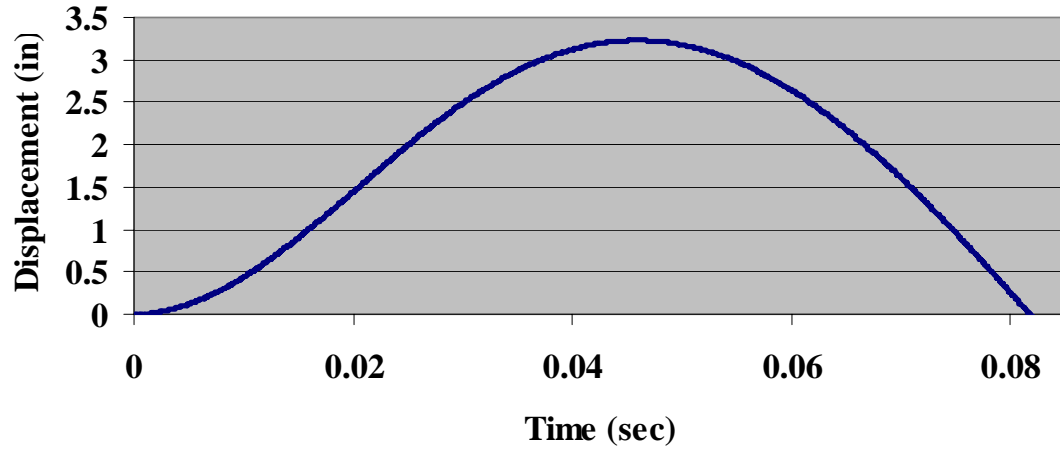


Figure 6.6-3. Displacement with Reflected Impulse of 55.0 psi-ms

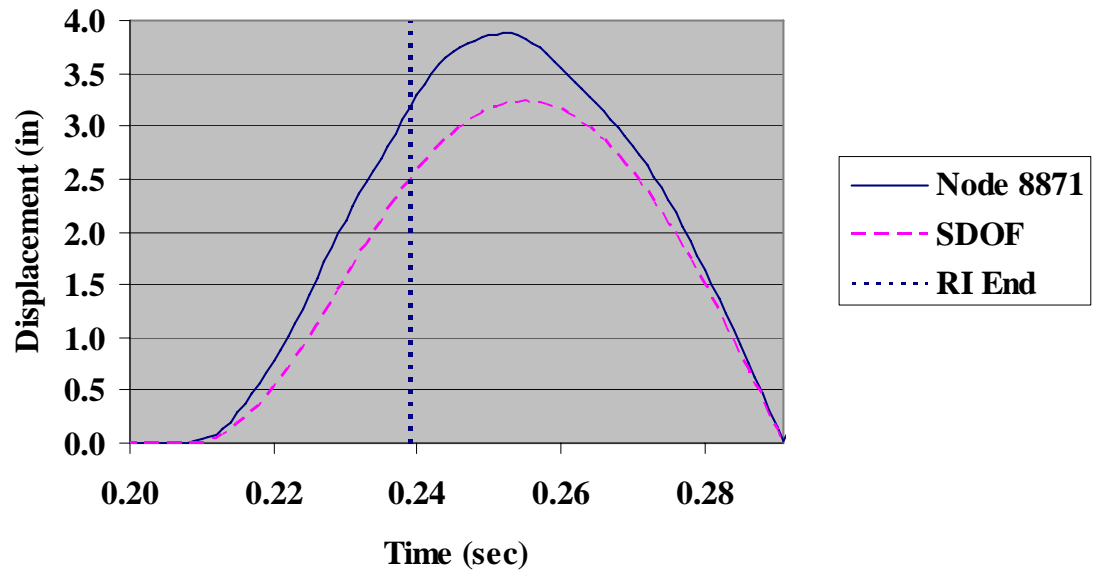


Figure 6.6-4 SDOF/LS-DYNA Model Displacement Comparison

6.7 32.2 psi-ms

Initial Conditions	
Area Exposed	696.8
Reflected Impulse (psi-ms)	32.2
Delta t (sec)	0.0001
Mt (lb.sec ² /in)	0.32
KLMe	0.47
KLMP	0.47
Reflected Pressure (psi)	1.8
F ₀ (lb)	1,524.00
Adjusted Time (sec)	0.036
K elastic (lb/in)	552
K plastic (lb/in)	485
K plastic (lb/in)	387
y elastic limit (in)	2.32
y plastic (in)	4.63

Figure 6.7-1. Initial Conditions

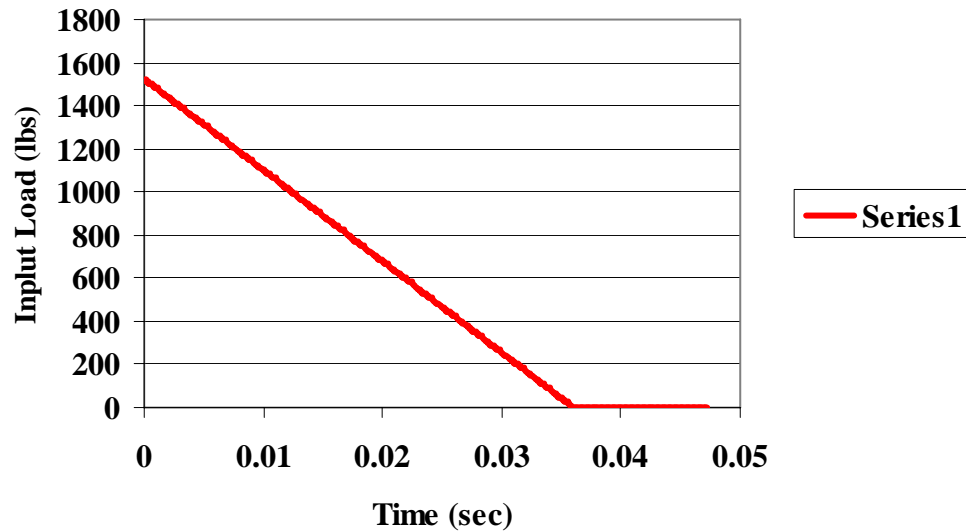


Figure 6.7-2. Load Distribution

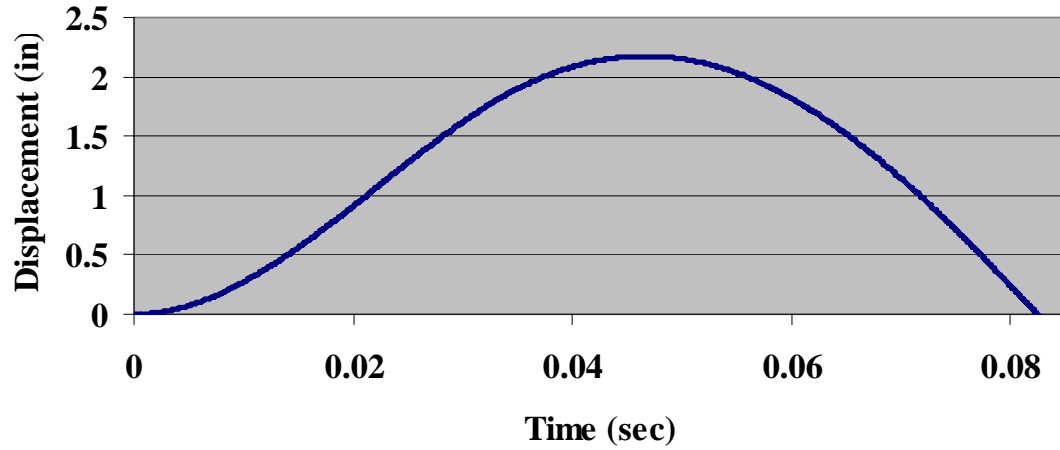


Figure 6.7-3. Displacement with Reflected Impulse of 32.2 psi-ms

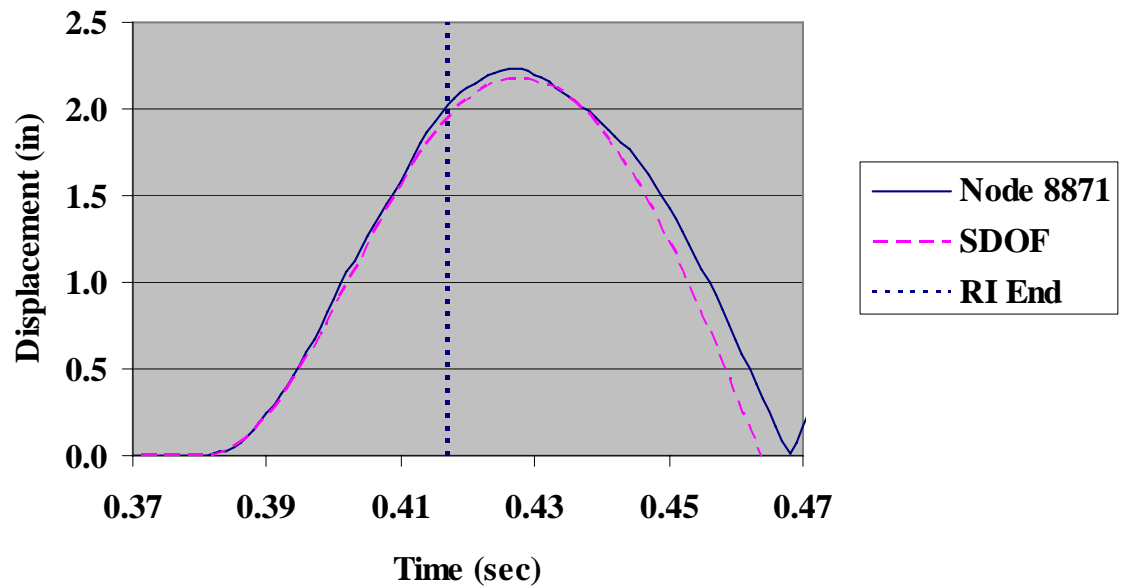


Figure 6.7-4 SDOF/LS-DYNA Model Displacement Comparison

6.8 111.0 psi-ms

Initial Conditions	
Area Exposed	696.8
Reflected Impulse (psi-ms)	111.0
Delta t (sec)	0.0001
Mt (lb.sec ² /in)	0.32
KLMe	0.47
KLMP	0.47
Reflected Pressure (psi)	30.0
F ₀ (lb)	20,904.00
Adjusted Time (sec)	0.007
K elastic (lb/in)	552
K plastic (lb/in)	485
K plastic (lb/in)	387
y elastic limit (in)	2.32
y plastic (in)	4.63

Figure 6.8-1. Initial Conditions

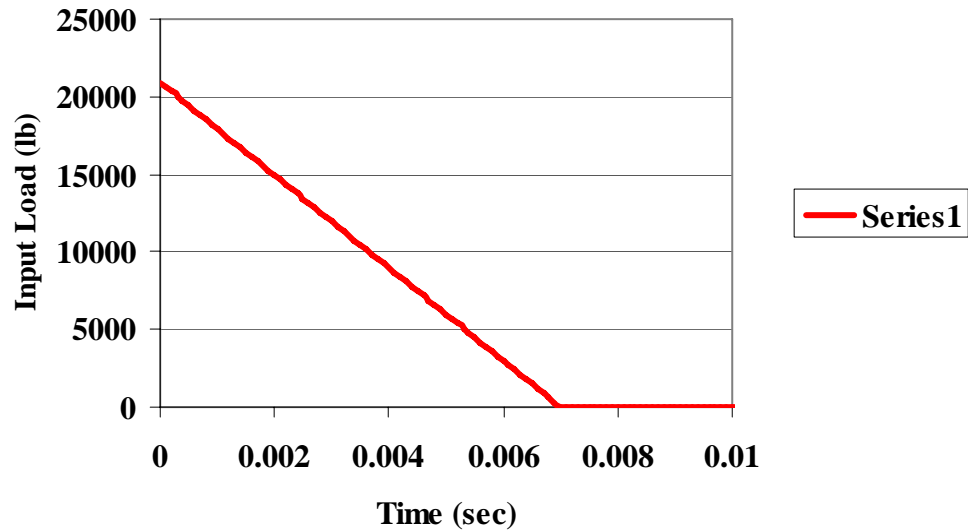


Figure 6.8-2. Load Distribution

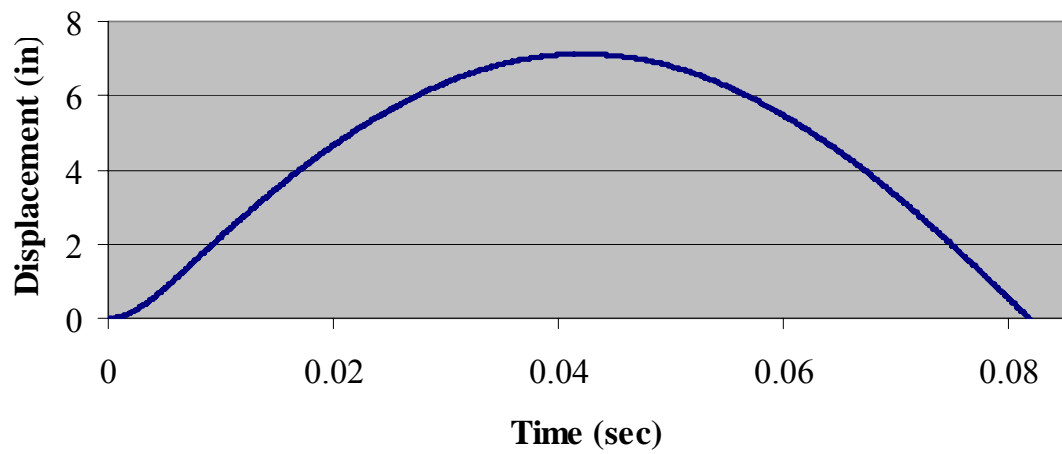


Figure 6.8-3. Displacement with Reflected Impulse of 111.0 psi-ms

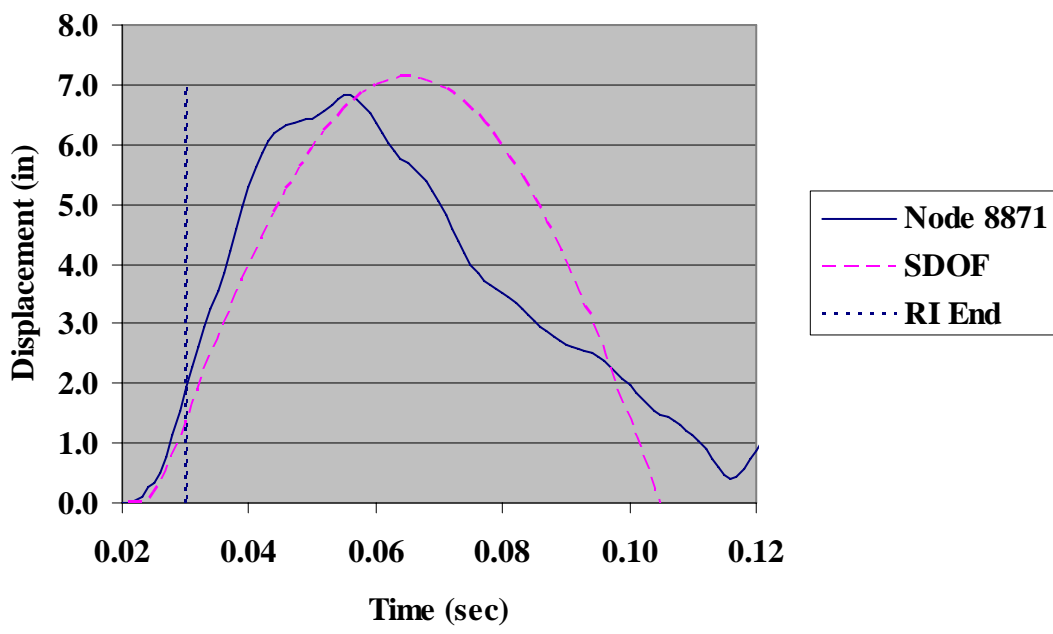


Figure 6.8-4 SDOF/LS-DYNA Model Displacement Comparison

6.9 24.7 psi-ms

Initial Conditions	
Area Exposed (in ²)	696.8
Reflected Impulse (psi-ms)	24.7
Delta t (sec)	0.0001
Mt (lb.sec ² /in)	0.32
KLMe	0.47
KLMp	0.47
Reflected Pressure (psi)	2.8
F ₀ (lb)	1,951.00
Adjusted Time (sec)	0.018
K elastic (lb/in)	552
K plastic (lb/in)	485
K plastic (lb/in)	387
y elastic limit (in)	2.32
y plastic (in)	4.63

Figure 6.9-1. Initial Conditions

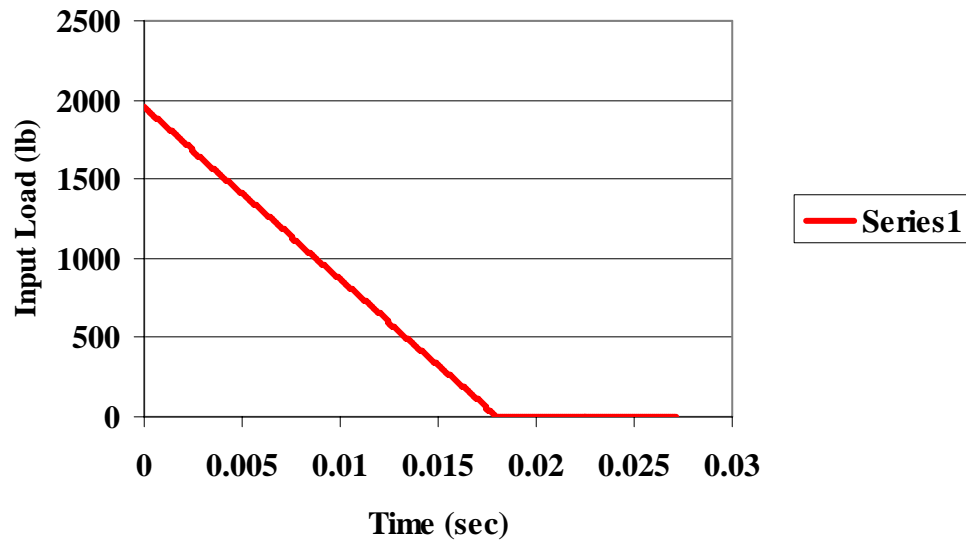


Figure 6.9-2. Load Distribution

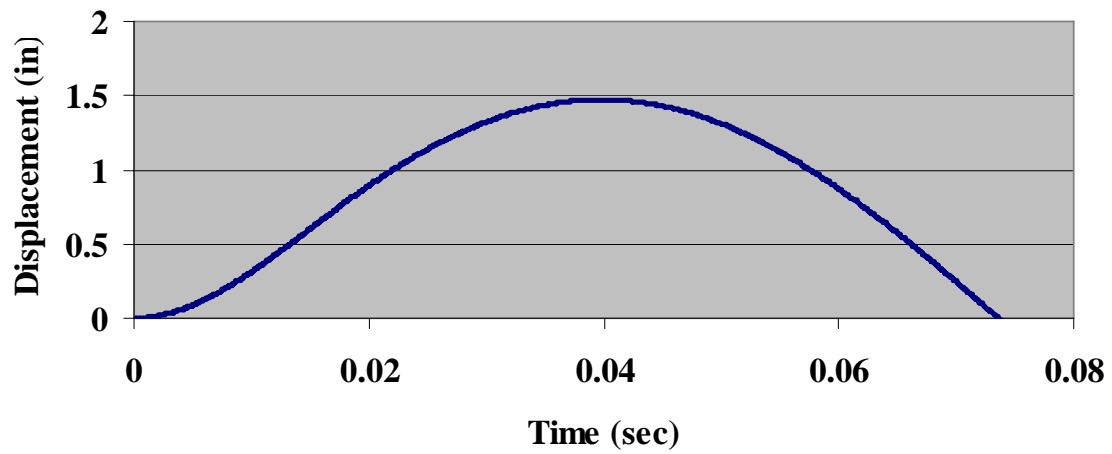


Figure 6.9-3. Displacement with Reflected Impulse of 24.7 psi-ms

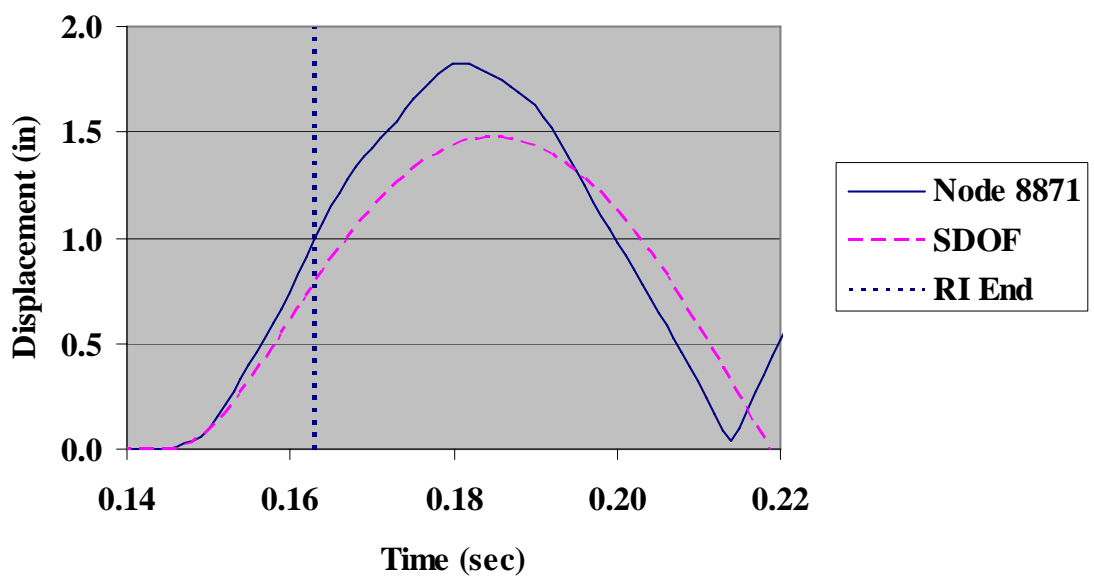


Figure 6.9-4 SDOF/LS-DYNA Model Displacement Comparison

6.10 116.8 psi-ms

Initial Conditions	
Area Exposed (in ²)	696.8
Reflected Impulse (psi-ms)	116.8
Delta t (sec)	0.0001
Mt (lb.sec ² /in)	0.32
KLMe	0.47
KLMp	0.47
Reflected Pressure (psi)	18.0
F ₀ (lb)	12,542.40
tf (sec)	0.013
K elastic (lb/in)	552
K plastic (lb/in)	485
K plastic (lb/in)	387
y elastic limit (in)	2.32
y plastic (in)	4.63

Figure 6.10-1. Initial Conditions

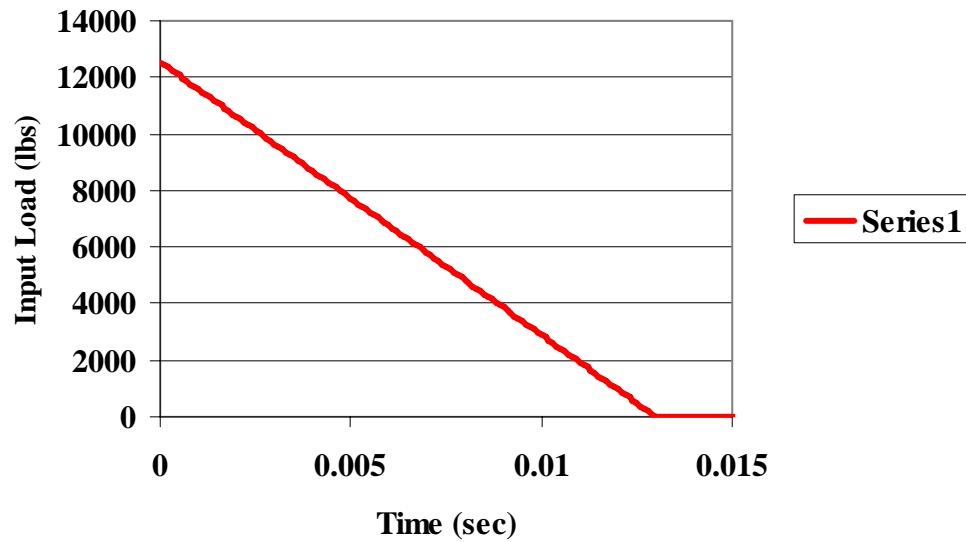


Figure 6.10-2. Load Distribution

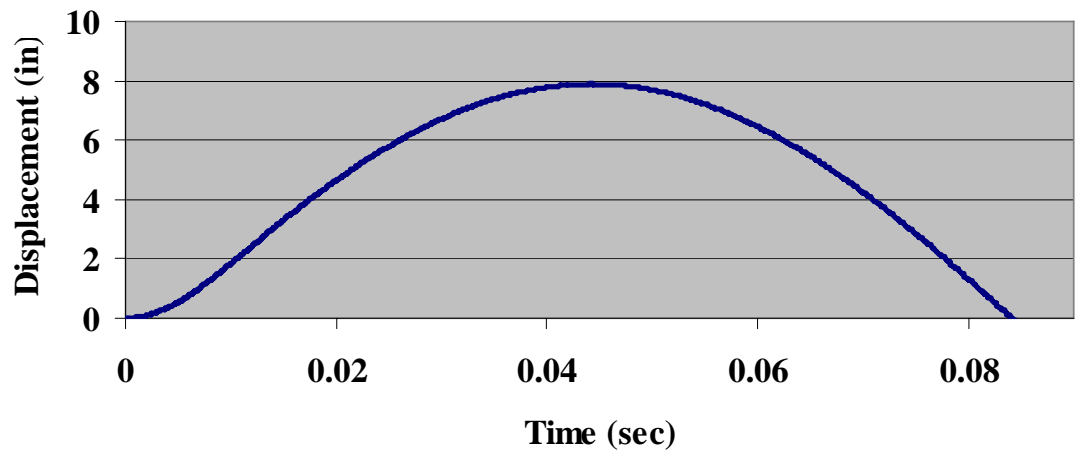


Figure 6.10-3. Displacement with Reflected Impulse of 116.8 psi-ms

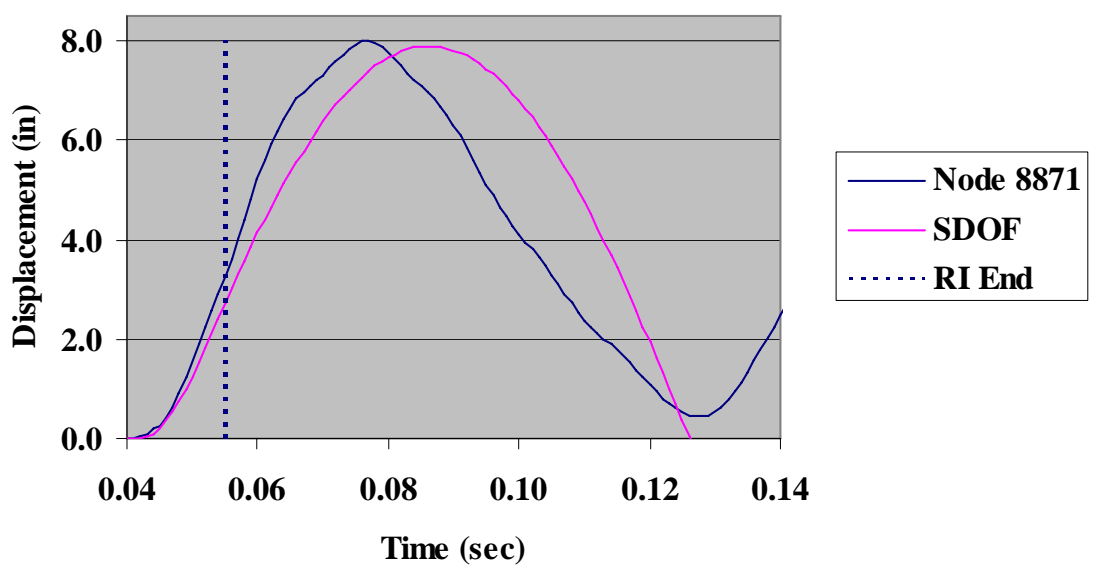


Figure 6.10-4 SDOF/LS-DYNA Model Displacement Comparison

6.11 33.1 psi-ms

Initial Conditions	
Area Exposed (in ²)	696.8
Reflected Impulse (psi-ms)	33.1
Delta t (sec)	0.0001
Mt (lb.sec ² /in)	0.32
KLMe	0.47
KLMp	0.47
Reflected Pressure (psi)	2.7
F ₀ (lb)	1,881.00
Adjusted Time (sec)	0.025
K elastic (lb/in)	552
K plastic (lb/in)	485
K plastic (lb/in)	387
y elastic limit (in)	2.32
y plastic (in)	4.63

Figure 6.11-1. Initial Conditions

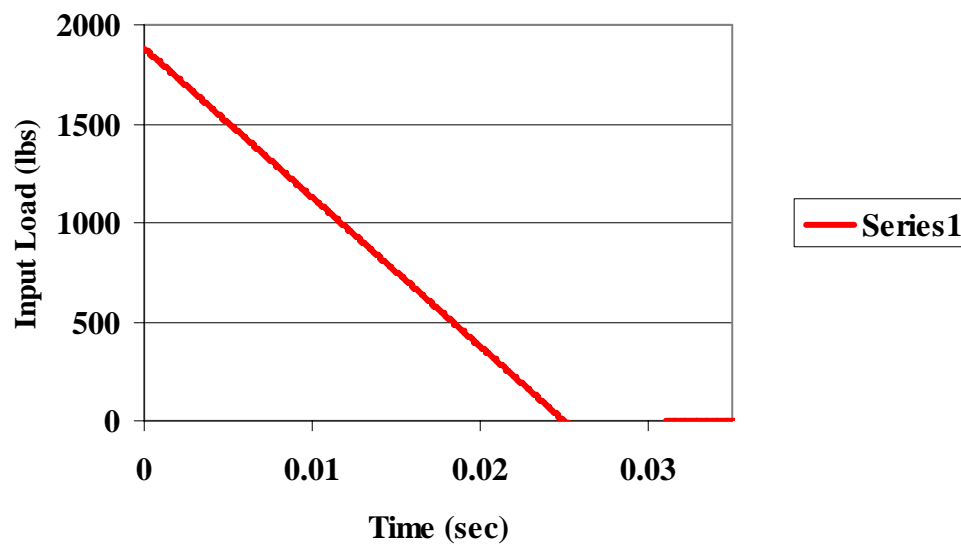


Figure 6.11-2. Load Distribution

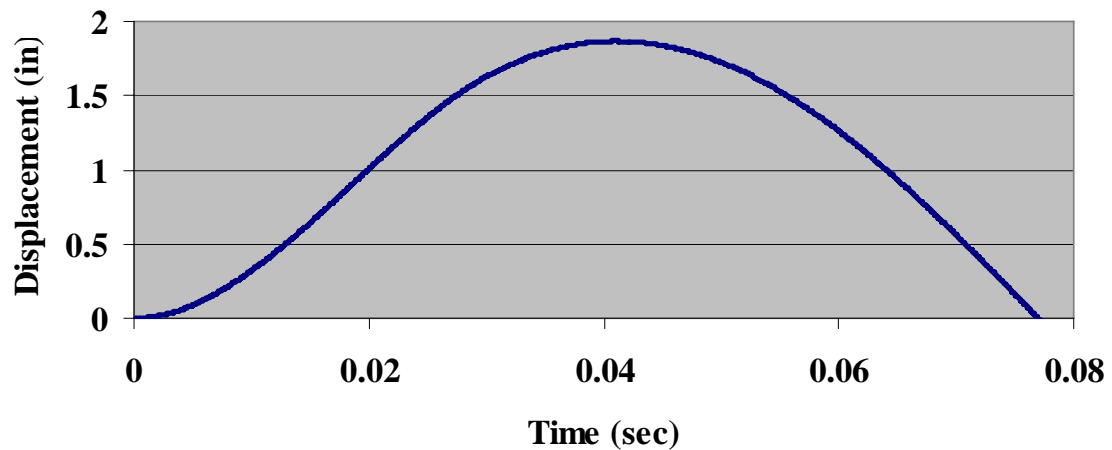


Figure 6.11-3. Displacement with Reflected Impulse of 33.1 psi-ms

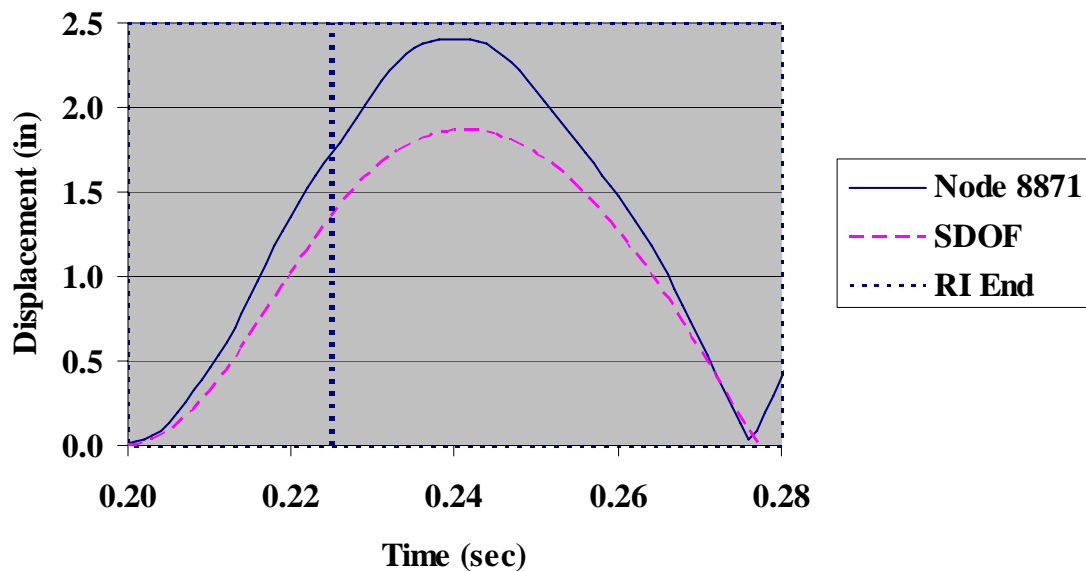


Figure 6.11-4 SDOF/LS-DYNA Model Displacement Comparison

7.0 SUMMARY AND CONCLUSIONS

The results of this effort to correlate the data generated by field testing of multiple charge sizes and stand-off distances to analytical results obtained from finite element modeling and SDOF models supports the conclusion that simple analytical tools may be developed to predict the behavior of structures. The comparison between FEM and SDOF consistently showed good correlation for the first oscillation of the frame. However, due to the differences in the overall magnitude of the deflection, more effort should be placed in the development of the resistance function. This should include a more refined load distribution as opposed to the simple parabolic distribution described in this report.

8.0 REFERENCES

- 1 Blast Response of Air Force Expeditionary Structures to Explosive Loading, Joint Soldier Protection in Contingency Environments, AFRL-ML-TY-TR-2005-4572, August 2005.
- 2 Biggs (1964), Introduction to Structural Dynamics, McGraw-Hill Book Company, New York
- 3 Metallic Materials and Elements for Flight Vehicle Structures, MIL-HDBK-5H, December 1998.

9.0 List of Acronyms

AFRL	Air Force Research Laboratory
AKSSS	Alaska Small Shelter System
ERDC	Engineer Research and Development Center
FEM	Finite Element Model
NASTRAN	NAsa STRuctural ANalysis Program
SDOF	Single Degree of Freedom
SPICE	Soldier Protection in Contingency Environments
TNT	Tri-Nitro Toluene
USAF	United States Air Force